UNIVERSIDADE DE BRASÍLIA (UNB)
INSTITUTO DE GEOCIÊNCIAS (IG)
PPG EM GEOLOGIA

MAPEAMENTO DO POTENCIAL MINERAL, TIPO IOCG, DE IDADES PALEO E NEOPROTEROZÓICAS: O EXEMPLO DOS DISTRITOS CUPRÍFEROS DO VALE DO CURAÇÁ E RIACHO DO PONTAL, BAHIA

Sérgio Roberto Bacelar Hühn

Tese de Doutorado nº152

BRASÍLIA- DF

2018

UNIVERSIDADE DE BRASÍLIA
INSTITUTO DE GEOCIÊNCIAS
PROGRAMA DE PÓS-GRADUAÇÃO EM GEOLOGIA

MAPEAMENTO DO POTENCIAL MINERAL, TIPO IOCG, DE IDADES PALEO E NEOPROTEROZÓICAS: O EXEMPLO DOS DISTRITOS CUPRÍFEROS DO VALE DO CURAÇÁ E RIACHO DO PONTAL, BAHIA

TESE DE DOUTORADO

Autor: Sérgio Roberto Bacelar Hühn
Orientadora: Profa. Dra. Adalene Moreira Silva

Brasília- DF
2018

UNIVERSIDADE DE BRASÍLIA

INSTITUTO DE GEOCIÊNCIAS

PROGRAMA DE PÓS-GRADUAÇÃO EM GEOLOGIA

MAPEAMENTO DO POTENCIAL MINERAL, TIPO IOCG, DE IDADES PALEO E NEOPROTEROZÓICAS: O EXEMPLO DOS DISTRITOS CUPRÍFEROS DO VALE DO CURAÇÁ E RIACHO DO PONTAL, BAHIA

Autor: Sérgio Roberto Bacelar Huhn

Banca Examinadora

Profa. Dra. Adalene Moreira Silva (Presidente)

Prof. Dr. Caetano Juliani (USP)

Prof. Dr. Francisco José Ferreira (UFPr)

Profa. Dra. Maria Emília S. D. Giustina (UnB)

Brasília, 18 de dezembro de 2018

AGRADECIMENTOS

A amiga e professora Adalene Moreira Silva, pela sua orientação, estimulo e excelência no direcionamento do Trabalho.

A amada esposa Marcia, minha irmã Darlene e ao meu filho Gabriel pelo apoio familiar e orações para a realização deste trabalho.

Ao instituto de Geociências da Universidade de Brasília, representados por professores e alunos que colaboraram direta ou indiretamente para a realização deste trabalho.

Ao CNPq e Vale pelo suporte nas diversas etapas de campo.

A Vale S/A em especial aos colegas de trabalho e Gerentes Fernando Matos e Fernando Greco, pelo apoio ao projeto de pesquisa, liberação de dados e discussões proveitosas.

Agradecimento especial a Raiza Toledo e Victoria Basileu, pelo substancial apoio na elaboração das ilustrações utilizadas neste trabalho.

Obrigado Pai (*In memorian* - Peter Huhn) e Mãe (Ida Carmem Bacelar Huhn) pelo crescimento proporcionado numa esfera onde sempre permeou amor, bondade, graça e o interesse por valores cristãos.

SUMÁRIO

ÍNDICE DE FIGURAS

ÍNDICE DE TABELAS

RESUMO

A tese de doutorado, em apreço, apresenta o estudo dos distritos cupríferos Riacho do Pontal e Vale do Curaçá situados nas porções sul da Província Borborema e norte do Cráton do São Francisco. A meta principal foi o mapeamento da assinatura da mineralização cuprifera, em ambas as regiões, através da integração de dados multifonte.

O Distrito Cuprífero Riacho do Pontal, de idade neoproterozóica, hospeda uma série de ocorrências que vem sendo interpretadas como depósitos IOCG, onde destacam-se os depósitos Riacho Seco e Riacho do Pontal. Os produtos derivados do processamento, interpretação e modelagem de dados geológicos, geofísicos e geoquímicos foram integrados em ambiente SIG. Posteriormente, efetuou-se a análise espacial deste dados utilizando-se a técnica de modelagem espacial intitulada lógica *fuzzy* nas escala regional e de distrito. O resultado inicial mostra áreas favoráveis com potencial de hospedar depósitos do tipo IOCG. A região considerada com maior favorabilidade foi modelada em escala 1:25.000 e, então, selecionados alvos potenciais que foram mapeados e testados através da execução de um programa de sondagem exploratória. O furo de sondagem RIA4-DH001 seccionou uma zona mineralizada de 32 m de espessura @ 1,15% de Cu.

O Distrito cuprífero do Vale do Curaçá ocupa uma área de aproximadamente 2000 km² e é considerado distritos mineiros mais importantes no Brasil. Ele abarca a mina de cobre da Caraíba Metais com reservas totais de 42,4 MT @ 1.71% Cu. A mineralização de Cu-Au vem sendo interpretada como uma mineralização ortomagmática sobreposta por um sistema hidrotermal IOCG e associada a um evento epigenético de cerca de 2,0 Ga.

Para auxiliar o entendimento da assinatura geofísica das mineralizações dos dois distritos estudados, dados magnéticos e gravimétricos foram processados, interpretados e integrados com dados geológicas e estruturais dos distritos Riacho do Pontal e Vale do Curaçá. A assinatura do Distrito Cuprífero Riacho do Pontal é caracterizada principalmente por baixos gravimétricos e magnéticos (Valores do campo magnético <24.000 nT). Já, o distrito do Cobre do Vale do Curaçá está localizado em um domínio gravimétrico anômalo coincidente com anomalias magnéticas que apresentam 110 km de comprimento por 22 km de largura e anomalia gravimétrica elevada (> -40 mGal.) As minas Caraíba, Surubim e Vermelhos e uma série de ocorrências de cobre estão situadas neste domínio com assinatura gravimétrica positiva.

Tomografia Sísmica Regional da região Centro-leste do Brasil mostra que os depósitos IOCG da Província Mineral de Carajás, do Vale do Curaçá e do Riacho do Pontal concentram-se ao longo de estruturas translitosféricas proeminentes, particularmente nas bordas de domínios positivos. Domínios de anomalia de alta velocidade podem representar blocos antigos do manto litosférico subcontinental (SLCM) flanqueado por grandes falhamentos.

ABSTRACT

The PhD thesis, presented here, deals with the study of the Riacho do Pontal and Vale do Curaçá Copper Districts located in the southern portion of the Borborema Province and north of the São Francisco Craton. The main goal was the mapping of the signature of the copper mineralization, in both copper districts, through the integration of multi-source data.

The Riacho do Pontal Copper District, of neoproterozoic age, hosts a series of occurrences that were recognized as IOCG depositis. The products derived from the processing, interpretation and modeling of geological, geophysical and geochemical data were integrated in a GIS environment. Subsequently, the spatial analysis of this data was integrated using the spatial modeling processing called fuzzy logic at regional and district scales. The initial result shows favorable areas with potential to host IOCG type deposits. The region considered with the highest favorability was modeled at a scale of 1: 25,000 and then selected potential targets that were mapped and tested through of an exploratory drilling program. The RIA4-DH001 drill hole intersected 32-m thick mineralized zone with 1.15% Cu,

The Vale do Curaçá Copper District occupies an area of approximately 2000 km² and is one of the most important mineral districts in Brazil. It host the Caraíba mine with total reserves of 96 MT @ 1.82% Cu. The copper mineralization was identified as an orthomagmatic mineralization superimposed by an IOCG hydrothermal system. The hydrothermal mineralization is associated with the epigenetic event 2.0 Ga.

To help understand the geophysical signature of the mineralizations of the two districts studied, magnetic and gravimetric data were processed, interpreted and integrated with geological and structural data from Riacho do Pontal and Vale do Curaçá Copper districts. The signature of the Riacho do Pontal Copper District is mainly characterized by gravimetric and magnetic lows (TMI <24,000 nT). However, Vale do Curaça Copper District is located in an anomalous gravimetric domain coincident with magnetic anomalies. It is 110 km in lenght by 22 km in width and shows a high gravimetric anomaly high (> -40 mGal). The Caraíba, Surubim and Vermelhos mines and a series of copper occurrences are located in this domain with positive gravimetric signature.

Regional Seismic Tomography of the central-eastern region of Brazil show that the IOCG deposits of the Carajás Mineral Province, the Vale do Curaça and Riacho do Pontal are concentrated along prominent translithospheric structures, particularly in the peak of high domains. High-speed anomaly domains may represent old blocks of the subcontinental lithospheric mantle (SLCM) flanked by major faults

INTRODUÇÃO

Depósitos de óxido de ferro, cobre-ouro (IOCG) têm sido descritos como depósitos de classe mundial que apresentam um *footprinting* que pode ser mapeado em múltiplas escalas e que mostram volumes expressivos de alteração hidrotermal em diferentes ambientes tectônicos (POLLARD et al., 2018; HITZMAN et al., 1992; BARTON, 2009, 2014; GROVES et al., 2010). Em uma escala global, os depósitos de IOCG são fortemente controlados por zonas de cisalhamento e ocorrem associados à altas concentrações de magnetita e /ou hematita. Estas concentrações, que podem ser variadas, em função da natureza do sistema são usualmente mapeadas através de anomalias magnéticas e/ou gravimétricas. Elas representam vetores que funcionam como guias exploratórios chaves para o mapeamento de novos depósitos do tipo IOCG (HAYWARD, 2014; SMITH, 2002; CLARK et al., 2003; CLARK, 2014).

Depósitos IOCG são hospedados por rochas com diferentes idades e composição, onde o fluxo de fluidos e alteração hidrotermal são canalizados principalmente ao longo das zonas de cisalhamento (GROVES et al., 2016; POLLARD et al., 2018; HUHN et al., 2014; MONTEIRO et al., 2008a, 2008b; XAVIER et al., 2010, 2012; MELO et al., 2014; HUHN et al., 2014; dentre vários). Os distritos Vale do Curaçá e Riacho do Pontal vem sendo considerados como importantes distritos mineiros para hospedar depósitos IOCG no Brasil e uma nova fronteira exploratória (TEIXEIRA et al., 2014; GARCIA et al., 2018; HUHN and SILVA, no prelo). Enquanto o distrito do Cobre do Vale do Curaçá está situado no interior do Cráton, o Distrito do Riacho do Pontal está situado na sua borda e hospedado no faixa móvel do Riacho do Pontal de idade brasiliana (LINDENMAYER, 1981; SILVA et al., 1994, TEIXEIRA et al., 2010; HUHN et al., 2014; JULIANI et al, 2017; GARCIA et al., 2018, HUHN and SILVA, no prelo). Processos de alteração hidrotermal potássica e cálci-férrica foram descritos como relacionados a zonas mineralizadas de cobre (GARCIA, 2013, HUHN et al., 2014).

Durante os últimos anos tem sido intensificado trabalhos sistemáticos e extensivos nos distritos Vale do Curaçá e Riacho do Pontal. O sucesso exploratório num distrito mineiro está diretamente relacionado ao emprego de ferramentas modernas de prospecção, que abarcam o *follow-up* geológico, estrutural e geoquímico de anomalias aliado ao emprego de técnicas e métodos geofísicos de alta resolução, estudo petrofísicos e sondagem exploratória. Inversão de dados magnéticos e gravimétricos associada ao processamento de dados de tomografia

sísmica regional foram aplicados para o rastreamento da assinatura da mineralizção de Cu-Au supra mencionada. No distrito do Vale do Curaçá, os trabalhos de integração de dados foram justapostos aos corpos mineralizados conhecidos e permitiram a caracterização da mineralização e a priorização de trends de maior potencialidade metalogenética. No distrito Riacho do Pontal, a integração de dados foi validada com execução de sondagem exploratória no prospecto Ria-4 e novos alvos foram selecionados através de processamento de dados usando lógica *fuzzy*.

A tomografia sísmica tem sido usada por vários autores para entender o arcabouço geodinâmico global (GRIFFIN et al., 2013; BEGG et al., 2012). A aplicação de imagens de tomografia sísmica revelou que os limites das zonas cratônicas e descontinuidades no manto litosférico subcontinental (SCLM) são fisicamente favoráveis para a ascensão do magma (GRIFFIN et al., 2013). Em todo o mundo, diamante, elementos do grupo da platina (PGEs), Ni-Cu- (PGE) e depósitos de pórfiro e IOCG de cobre estão situados em bordas cratônicas e podem ser relacionados à evolução tectônica do SCLM (GRIFFIN et al., 2013; BEGG et al., 2012; CZARNOTA et al., 2014). Neste trabalho, os dados de tomografia sismica foram interpretados na região da Província Mineral de Carajás, bem como nos Distritos Vale do Curaçá e Riacho do Pontal, objetivando a identificação de novos parâmetros prospectivos e/ou novos vetores exploratórios.

LOCALIZAÇÃO

A área deste trabalho de pesquisa é situada na região norte do Estado da Bahia (Fig.A). O Distrito Vale do Curaçá fica situado predominantemente nos munícipios de Jagurarari, Pinnões e Uauá (Ba). O Distrito de Riacho do Pontal engloba principalmente o município Curaçá (Ba).

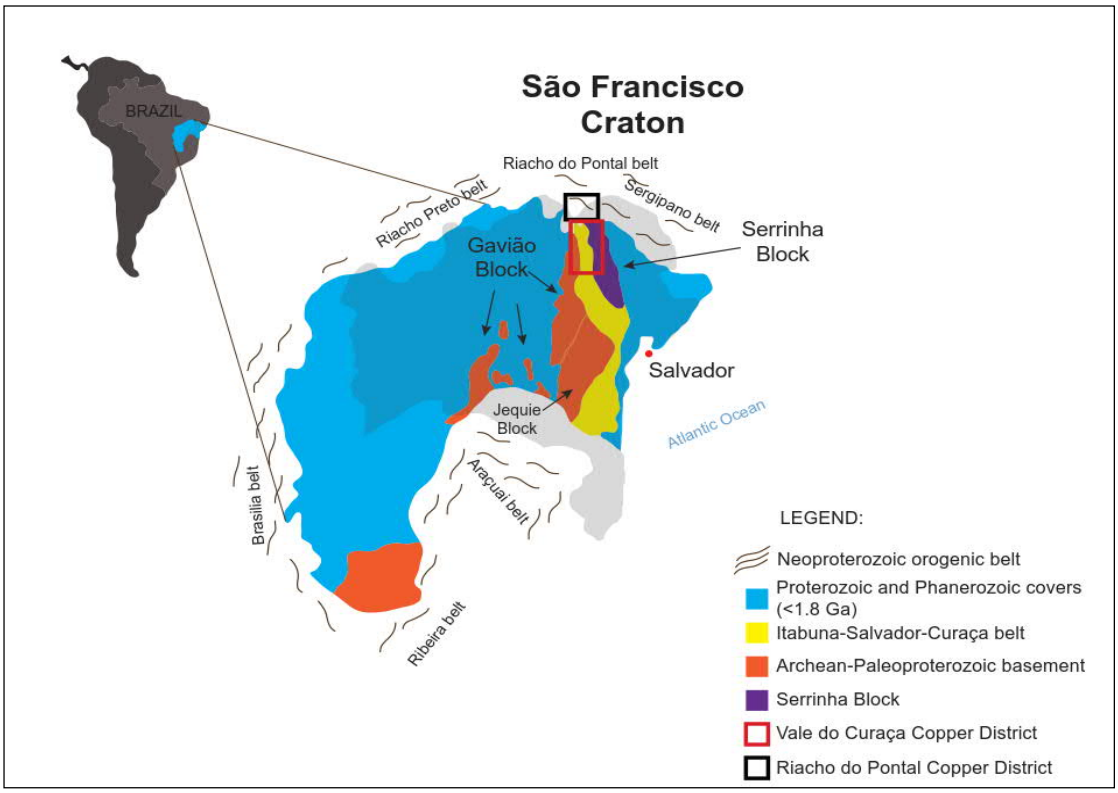

Figura A: A figura apresenta o Cráton do São Francisco e faixas móveis associadas. O polígono em cinza destaca o distrito de cobre do Vale do Curaçá, enquanto o magenta indica o posicionamento do distrito do Riacho do Pontal (Modificado de Teixeira et. al. 2010)

OBJETIVO

O objetivo principal deste trabalho é mapear o *footpriting* dos distritos cupríferos IOCG do Riacho do Pontal e Vale do Curaçá, através da análise de dados magnéticos, gravimétricos, apoiados por dados de tomografia sísmica de caráter regional, estudos geológicos, estruturais e geocronológicos. Pretende-se, ao final, contribuir para uma melhor compreensão destes importantes distritos cupríferos no Brasil.

Os objetivos específicos consistem em:

a) Mapear feições estruturais regionais e locais com o intuito de mapear os *traps* estruturais, condutos para percolação de fluidos hidrotermais através de produtos derivados de dados magnéticos, gravimétricos e de sensores remotos;
b) Inversão de dados gravimétricos e magnéticos com o intuito de caracterizar o padrão dos ambientes mineralizados em Riacho do Pontal e no Vale do Curaçá;
c) Gerar mapas de favorabilidade mineral, por meio da aplicação de métodos de análise espacial como lógica fuzzy e com objetivo de gerar alvos potenciais

para pesquisa de cobre em *brownfield* e *greenfield* no Distrito Riacho do Pontal;

d) Através dos dados de tomografia sísmica regionais selecionar novos ambientes tectônicos a serem pesquisados nas regiões que abrangem a Província Mineral de Carajás (Pa), bem como os Distritos Riacho do Pontal e Vale de Curaçá (Ba).

Metodologia e Escopo do Estudo

Os materiais utilizados nesta Tese de Doutorado compreendem dados geofísicos, de sensores remotos, um acervo de dados geofísicos, geoquímicos e de sondagem. O conjunto dos materiais e métodos utilizandos é apresentado abaixo de forma sucinta e foi abordado de forma mais robusta nos artigos gerados que compõem este manuscrito.

Dados Magnetométricos, Gamaespectométricos, Gravimétricos e de Tomografia Sísmica

Os dados gravimétricos fazem parte do banco de dados terrestre fornecido Serviço Geológico do Brasil (CPRM), obtidos a partir da utilizanão de um gravímetro LaCoste & Romberg (Modelo G-939), com espaçamento de 5 a 10 km entre as estações. O trabalho foi realizado entre 2005 e 2007, onde um total de 130 pontos foi utilizado no presente estudo.

Os dados magnéticas e radiométricas foram adquiridos do projeto Riacho Seco e Andorinhas da CBPM (2001). Os dados possuem um espaçamento entre linhas de voo e controle de 500m a 10.000 m nas direções NS e EW, respectivamente. Eles foram adquiridos a uma altura constante de 100 m e correspondem a um total de 48.641 quilômetros lineares.

O processamento dos dados geofísicos foi efetuado utilizando técnicas qualitativas de pré-processamento, interpolação em malhas regulares e geração de produtos relevantes na interpretação e, posteriormente, técnicas de modelagem e inversão. Adicionalmente, foram coletados dados de propriedades físicas de rocha em testemunhos de sondagem com o objetivo de auxiliar a modelagem e a inversão de dados em ambiente 3D.

A base de dados de tomografia sísmica, bem como os mapas gerados a partir deles e utilizados no presente trabalho são de propriedade da *Minerals Targeting International Pty Ltd* (“MTI”) e compreendem o produto GLAM (*Global lithosphere architeture mapping*). O

GLAM é o resultado de uma compilação global de dados que compreende muitos conjuntos de dados geocientíficos, incluindo gravidade, magnetismo, tomografia sísmica, perfis sísmicos crustais, magnetotelúricos, geologia, geoquímica de isótopos e geocronologia. O produto é uma das primeiras tentativas sistemáticas de mapear o manto litosférico sub-continental (SCLM), incluindo detalhes sobre a evolução do manto e a sua arquitetura trans-litosférica (GRIFFIN et al., 2013; GRIFFIN et al., 2016).

Dados de Sensores Remotos

Neste trabalho, foram utilizados os conjuntos de dados do mosaico ALOS / PALSAR e ALOS 2 / PALSAR-2 para interpretação estrutural das regiões que abrangem os Distritos cupríferos Vale do Curaçá e Riacho do Pontal. As imagens usadas são de 2015, com resolução espacial de 25 m. Esta informação foi integrada nos dados gamaespectrométricos e magnéticos, com o intuito de refinar a interpretação estrutural dos distritos estudados.

Dados Geológicos

Foram coletados dados geológicos e estruturais, em etapas de campo que totalizaram 120 dias cujos objetivos foram: a) caracterizar a assinatura hidrotermal das ocorrências estudadas; b) entender o relacionamento entre a zona colisional com as diversas ocorrências de cobre; c) determinar controles regionais e locais da mineralização.

Foram efetuados perfis geológicos e *follow-up* dos alvos selecionados, possibilitando o balizamento das interpretações geológicas e geofísicas.

Seis furos de sondagem foram executados, no Distrito Riacho do Pontal, totalizando 1800 m. Os furos foram direcionados para validar os modelos prospecctivos obtidos, onde regiões com ocorrencias associadas a anomalias geoquímicas de cobre em solo.

Dados de Geoquímicos

Os estudos geoquímicos foram focados em análises a partir de amostras de solo e testemunho de sondagem. Amostras de rocha (*chip sample*), sedimento de corrente, solo e

aquelas derivadas de furos de sondagem exploratórias foram coletadas em regiões chaves nos alvos estudados. As amostras foram analisadas por Screen Fire Assay e ICP-mass spectometry (ICP-MS) e foram realizadas pelos laboratórios ALS Minerals, Intertek, SGS Minerals Services e ACME Analytical Laboratories LTD. Os dados geoquímicos referentes a amostras de solo e de rocha foram tratados utilizando o *software* Geosoft *Oasis Montaj 8.5.1*. Foram feitas análises geoquímicas com 31 elementos para as amostras coletadas.

Dados Geocronológicos U/Pb em zircões detriticos e ^{40}Ar-^{39}Ar

Considerando a escassez de dados geocronológicos robustos para a região de estudo, efetuou-se algumas análises U/Pb em zircão (LA-ICPMS) e ^{40}Ar-^{39}Ar (biotita) de amostras associadas às zonas mineralizadas. As informações sobre a idade dos depósitos tipo IOCG Riacho do Pontal e Vale do Curaçá auxiliam no mapeamento das idades dos dois sistemas e dos eventos hidrotermais. A integração com os modelos gerados na inversão dos dados geofísicos e propriedades físicas indicaram o caminho para subsidiar a análise do sistema mineral dos dois distritos (Apêndice 1, Figura B).

Datação U-PB

Três amostras foram selecionadas para a datação U-Pb a partir de de zircões detríticos obtidos a partir de um granada-biotita paragneisse (Amostra DH001-003) e um biotita paragneisse (Amostra DH002-009). Sessenta e três (63) pontos da amostra DH-001-003 e 10 pontos da amostra DH-002-009 foram analisados (Apêndice 1, Figura B).

Duas amostras de afloramentos foram selecionadas para obtenção de idades Ar-Ar em testemunhos de sondagem (PCB-SRB-01 e PCB-SRB-02). Foram amostrados biotita milonitos relacionados a processos de alteração hidrotermal. Foram analisados 2 grãos de cada amostra para obtenção de idades ^{40}Ar-^{39}Ar (Apêndice 1).

As amostras foram tratadas em um disco de alumínio de 21 cavidades juntamente com o monitor de fluência de nêutrons Fish Canyon Sanidine (idade 28,201 ± 0,046 Ma; KUIPER et al., 2008), Os discos de irradiação foram fechados com tampas de alumínio, envoltos em papel alumínio e selados a vácuo em frascos de quartzo. Todas as amostras foram irradiadas por 14 horas durante o período de 8 de junho de 2016 a 10 de junho de 2016 na instalação B-1 CLICIT revestida com cádmio, um reator tipo TRIGA, Oregon State University, EUA.

A sensibilidade do espectrômetro de massas foi calculada com base na análise de uma pipeta de ar (1,634 x 10-13 moles ^{40}Ar) no detector de Faraday (4.257 mV) equipado com um resistor de 1 x 1011 Ohms, produzindo uma sensibilidade de Faraday de 3,84 x 10-9 moles / nA. A sensibilidade atual do multiplicador medida em um Multiplicador de elétrons Balzers 217, operado com um ganho de ~ 145.000 é de aproximadamente 4,5 x 10-14 moles / nA.

As idades de platô de aquecimento incremental estão de acordo com a definição de Fleck (1977): "uma seqüência de dois ou mais passos correspondendo a pelo menos 50% do total ^{39}Ar liberado, os valores de idade estão dentro de 2σ do valor médio calculado pela ponderação com variância inversa". Os erros de idade do platô são relatados no nível de confiança de 95% (2σ) e incluem os erros nos fatores de correção da irradiação e o erro em J, mas não incluem a incerteza nas constantes de decaimento do potássio (Apêndice 1).

Petrofísica

Os dados petrofísicos foram obtidos a partir de 33 amostras derivadas dos furos de sondagem PCB-RIA4-DH001 (14 amostras) e PCB-RIA4-DH-002 (19 amostras) efetuados no alvo Riacho do Pontal, tais como: a) biotita-quartzo-milonito; b) quartzo-anfibólio-biotita-milonito; c) quartzo-magnetita-biotita-milonita; e d) milonito de biotita. Adicionalmente, foram analisadas 10 amostras de biotita-magnetita-calcopirita das minas da Caraíba e Surubim.

Os dados de susceptibilidade magnética foram coletados utilizando-se um suscetibilimetro KT10 PLUS S/C (Terraplus), onde os dados obtidos são apresentados em $SIx10^{-3}$. Dados de densidade volumétrica de rocha (g/cm³) foram obtidos por meio de medida por saturação a vácuo das amostras. A resistividade elétrica foi medida em amostras com água sob vácuo e deixada em repouso por 24 horas usando analisador de freqüência

Inversão de Dados Magnéticos e Gravimétricos

Dados magnéticos e gravimétricos, foram gridados usando os algoritmos de curvatura mínima do Geosoft Oasis Montaj, com celula de 125 metros. O processamento dos dados foi apresentado anteriormente e com maior detalhe dentro do capítulo 03.

A plataforma Oasis Montaj e o pacote de inversão VOXI MVI foram usados para a inversão 3 D de dados magnéticos e gravimétricos. A interpretação dos dados de campo em potencial é chave para prospectar depósitos de IOCG. Os corpos de minério do sistema mineral IOCG são geralmente relacionados a rochas magnéticas e densas.

Para inversão dos dados magnéticos foram processados usando o módulo VOXI-MVI. A inversão dos dados magnéticos, pelo vetor de magnetização MVI, possibilita a recuperação da direção de magnetização e amplitude de cada domínio magnético na área de levantamento (ELLIS et al., 2012). Processamento foi realizado em grids do campo magnético total, onde é possível ilustrar a geometria das anomalias magnéticas e destacar os caminhos magnéticos ao longo das zonas de cisalhamento.

Para a elaboração da modelagem gravimétrica, foram utilizados mapas topográficos com o mesmo tamanho de célula (125 m). No entanto, as informações geológicas, incluindo propriedades petrofísicas, geologia de superfície, interpretação estrutural e interpretação geofísica em grade, foram utilizadas qualitativamente na modelagem 3

Análise Espacial e Integração dos Dados Multifonte

Diferentes técnicas de análise espacial têm sido utilizadas na integração de dados (BONHAM-CARTER et al., 1994). Vários autores usam métodos de SIG nas avaliações do potencial mineral com objetivos diferenciados (CARRANZA et al., 2003; NYKANEN 2008; SILVA, 1999, SILVA et al., 2012).

Existem basicamente dois tipos de modelos utilizados para a previsão do potencial mineral de uma área: modelos guiados pelos dados (*data-driven*) – pesos de evidência, regressão logística e redes neurais artificiais – e modelos guiados pelo conhecimento (*knowledge driven*) – lógica boleana, lógica *fuzzy*, *index overlay*). Na modelagem dirigida pelo conhecimento, geralmente utiliza-se a lógica *fuzzy* na qual o *expert* exerce uma influência maior na modelagem dos dados e no cruzamento das diferentes informações (BONHAM-CARTER, 1994).

Na modelagem dirigida pelos dados é mapeada a associação espacial entre ocorrências minerais conhecidas e o conjunto de dados estudados, que resulta no grau de favorabilidade de cada um dos conjuntos. A metodologia é fundamentada na relação estatística entre os vários planos de informação e as características relacionadas às ocorrências minerais (BONHAM-CARTER, 1994; SILVA et al., 1999; SILVA et al., 2000).

Neste trabalho foi empregada a lógica *fuzzy,* que representa um avanço em relação a lógica booleana. Na lógica booleana, aos conjuntos de dados de cada plano de informação como mapas geológico, estrutural, geofísicos ou geoquímicos, é associado pelo especialista um peso com valor binário de 0 ou 1, ou seja: para a ausência ou presença de potencial mineral de dada substância (BONHAM-CARTER, 1994).

A teoria da lógica *fuzzy* (BONHAM-CARTER, 1994) consegue comportar uma escala contínua de pertinência aos conjuntos, variando de um (pertinência total) até zero (não pertinência total). Desta maneira, medições individuais de um elemento químico, por exemplo, podem ser classificadas de acordo com o grau de pertinência ao conjunto "Anomalia" (BONHAM-CARTER, 1994). Valores muito altos serão certamente anômalos, possuindo uma pertinência *fuzzy* (*fuzzy membership)* "1", enquanto valores muito baixos ou abaixo do *background* terão pertinência *fuzzy* "zero". Entre estes dois extremos existem toda uma faixa de possíveis valores de pertinência.

A classificação do mapa evidencial em *fuzzy memberships* pode ser definida: (i) em termos de um julgamento subjetivo do especialista (BONHAM-CARTER, 1994), no caso de informações categóricas como em um mapa geológico; (ii) ou através de uma função de pertinência fuzzy para informações ordinais ou por intervalos, como no caso da distribuição de elementos químicos em solo. Os limiares desta função de pertinência podem ser definidos com base em critérios estatísticos.

Estrutura da Tese

Este doutorado está estruturado em dois capítulos na forma de artigos direcionados para publicação em periódicos científicos especializados sobre os temas abordados.

Os artigos contemplam tópicos propostos conforme os objetivos e respondem a importantes questões relacionadas à tipologia, evolução estrututural e o "footprint" das mineralizações IOCG situadas nos Distritos cupríferos Vale do Curaçá e Riacho do Pontal. No Distrito Riacho do Pontal foi feita integragão de dados usando lógica fuzzy para a seleção de prospectos favoráveis para hospedar depósitos do tipo IOCG. O detalhamento de cada tópico proposto, com metodologias utilizadas e resultados obtidos encontram-se presentes em cada um dos capítulos abaixo.

Capitulo 1

Este Capítulo apresenta o artigo denominado ¨ **Favorability potential for IOCG type deposits in the Riacho do Pontal Belt: new insights for identifying prospects of IOCG‑type deposits in NE Brazil"** que foi submetido e aceito no "Brazilian Journal of Geology".

Este artigo usa uma abordagem de "lógica Fuzzy" para criar modelos preditivos de exploração em escala regional a de distrito mineiro. Especificamente, dados geológicos, geoquímicos, de sensoriamento remoto e geofísicos aéreos foram utilizados em modelos regionais e locais objetivando identificar novas áreas com potencial para novas descobertas de depósitos IOCG na província de Borborema. Na escala de distrito mineiro, dados geológicos, geoquímicos do solo e geofísicos aéreos de maior resolução que cobrem o Prospecto Riacho do Pontal , foram integrados. Um programa de exploração usando sondagem exploratória implementado no alvo RIA4 que validou os resultados do modelo utilizado, visto que o Furo de sondagem RIA4-DH0001 recortou uma zona mineralizada com 32 m @ 1,15% de cobre.

Capitulo 2

Este Capítulo apresenta o artigo denominado "**Mapping New IOCG Mineral Systems in Brazil: The Vale do Curaçá and Riacho do Pontal Copper Districts"** e foi submetido ao periódico "Ore Geology Reviews". O manuscrito, figuras e legendas do artigo encontram-se em anexo neste volume. Este artigo tem por finalidade apresentar as principais características geológicas, estruturais e geofísicas dos depósitos IOCG situados nos Distritos Vale do Curaçá e Riacho do Pontal. Foram gerados modelos prospectivos 2D e 3D, com inversão de dados magnéticos e gravimétricos, nos Distrítos cupríferos Vale do Curaçá e Riacho do Pontal, com intuito de mapear o "footprint" da mineralização cuprífera nos distritos supracitados.

CAPITULO 1

“FAVORABILITY POTENTIAL FOR IOCG TYPE DEPOSITS IN THE RIACHO DO PONTAL BELT: NEW INSIGHTS FOR IDENTIFYING PROSPECTS OF IOCG‑TYPE DEPOSITS IN NE BRAZIL”

SÉRGIO ROBERTO BACELAR HUHN & ADALENE MOREIRA SILVA

Aceito para publicação no periódico “*Brazilian Journal of Geology*”

(DOI: 10.1590/2317-4889201820180029)

FAVORABILITY POTENTIAL FOR IOCG TYPE DEPOSITS IN THE RIACHO DO PONTAL BELT: NEW INSIGHTS FOR IDENTIFYING PROSPECTS OF IOCG-TYPE DEPOSITS IN NE BRAZIL

Sérgio Roberto Bacelar huhn[12]* and Adalene Moreira Silva[1]

1 - Instituto de Geociências, Universidade de Brasília, Brasília, DF, 70910-900, Brazil

2 - VALE S/A, Rodovia BR-381/km 450, 33040-900, Santa Luzia, MG, Brazil
*Corresponding author

Abstract

Archean iron oxide-copper-cobalt-gold (IOCG) deposits have been systematically described in the world class Carajás IOCG district, Amazonian region of Brazil. More recently, several Neoproterozoic (ca 1.13 to 0.96 Ga) IOCG deposits have been identified in the Riacho do Pontal mobile belt situated in the Borborema Province on the northern border of the São Francisco Craton, but have not been as thoroughly characterized.

In these Neoproterozoic deposits, several copper occurrences have been mapped along secondary shear zones where the gneissic host rocks show evidence for intense hydrothermal alteration. The primary hydrothermal mineral associations resulted in sodic-calcic, calcic-potassic and calcic-ferric alteration. The copper grades of the main prospects range between 0.5 and 0.8 wt% with an average of ~0.7 wt%, while the gold grade is about 0.15 grams per tonne.

This study uses a fuzzy logic approach to create regional to district scale predictive exploration models. Specifically, multi-parameter geologic, geochemical, remote sensing, and airborne geophysical data incorporated into regional and local models predict known copper mineralization and, importantly, highlight prospective areas for new IOCG targets in the Borborema Province. At district scale, multiple higher resolution geological, soil

geochemical, remote sensing, and airborne geophysical data that cover the Riacho do Pontal belt, were analyzed.

Aster and airborne magnetic derivative products significantly improved the understanding of the structural setting. Additionally, airborne gamma-ray spectrometry data mapped potassium enrichments related to copper mineralization. A drilling exploration program implemented on target RIA4 validated these model results. Drill hole RIA4-DH0001 crosscuts a mineralized zone with 32 m of 1.15 wt% copper.

Keywords: Copper. IOCG. Shear Zones. Hydrothermal Alteration. Fuzzy Logic. Borborema Province.

Resumo

Dados geológicos, geoquímicos, geofísicos e de sensoriamento remoto foram integrados em modelos regionais e locais objetivando a parametrização de feições prospectivos de depósitos e zonas mineralizadas da tipologia IOCG conhecidas no cinturão do Riacho do Pontal. Assim como, selecionar novas áreas prospectivas para hospedar mineralização IOCG nesta região da província de Borborema, nordeste do Brasil.

Depósitos IOCG, arqueanos, de classe mundial tem sido descritos sistematicamente no norte do Brasil, Provincia Mineral de Carajás. Mais recentemente, uma serie de depósitos IOCG neoproterozóicos mais jovens (cerca 1.13 a 0,96 Ga) tem sido identificados no cinturão móvel Riacho do Pontal, situado na borda norte do Craton do São Francisco, Várias ocorrências de cobre tem sido mapeadas ao longo de zonas de cisalhamento associados a processos de alteração hidrotérmical pervassivos.

As principais zonas de alteração hidrotermal são: sódico-calcica, calcica-potássica e cálcica-férrica. Os teores das principais zonas mineralizadas variam entre 0,5 e 0,8% Cu, com teor medio de 0,7% cobre. Os teores de ouro são da ordem de 0,15 g/t; Este estudo usa abordagem de lógica fuzzyana para criar modelos de favorabilidade em escala local e regional. Os resultados obtidos do processamento de dados regionais mapearam os alvos mais potenciais. Um programa de exploração de perfuração validou esses resultados do modelo no alvo RIA4. Furo desondagem RIA4-DH0001 interceptou uma zona mineralizada com 32 m @ 1,15% cobre.

Na escala local foram integrados vários dados de maior resolução, incluindo dados geológicos, de geoquímica do solo,de sensoriamento remoto e dados geofísicos aéreos. A interpretação dos dados Aster aos produtos derivados magnéticos aéreos melhoraram significativamente a compreensão estrutural da área. Além disso, os dados de espectrometria de raios gama transportados por via aérea mapearam potenciais de potássio e urânio relacionados à mineralização de cobre.

Palavras chaves: Cobre. IOCG. Zonas de Cisalhamento. Alteração Hidrotermal. Lógica Fuzzy. Província Borborema.

Introduction

Iron Oxide-Copper-Gold (IOCG) deposits include a wide spectrum of copper deposits types showing high content of magnetite and/or hematite with low titanium content (HITZMAN et al., 1992). Their age of formation range from Archean to Phanerozoic.

The mineralizations are frequently associated with intrusive magmatic bodies (HITZMAN, 2000; POLLARD, 2001; WILLIAMS et al., 2005; XAVIER et al., 2010) and are commonly found in breccias, veins, stockworks or lenses with polymetallic enrichments (Cu, Au, Ag, P, U and REE) that are tectonically-controlled along shear zones. Interest in IOCG deposits was boosted after the discovery in 1975 of the Olympic Dam deposit and the consolidation of the mineral potential of the Gawler range region in South Australia.

In the late 1990s, reinterpretation of the typology of Archean copper deposits of the Carajás Mineral Province such as Salobo, Sossego, Cristalino and Igarapé Bahia-Alemão deposits (HUHN; NASCIMENTO, 1997; LINDENMAYER, 2003; TALLARICO et al., 2005; MONTEIRO et al., 2008; GRAINGER et al., 2008; GROVES et al., 2010; JULIANI; MONTEIRO; FERNANDES, 2016), which show many similarities with other IOCG deposits (HITZMAN et al., 1992; HITZMAN, 2000), led to a boom in exploratory activity in Brazil.

The significance of the Neoproterozoic copper deposits of the Borborema Province as potential IOCG deposits was first emphasized by Maas et al (2003), Machado (2006) and Huhn et al (2011). These authors interpreted the geological and geochemical signature of copper occurences associated with quartz-hematite breccias in the region of Mandacaru, São Julião, Fronteiras and Pio IX, Campos Sales and Aurora as a succession of IOCG mineralizations formed as a response of intensive hydrothermal alteration in km-scale shear zones (HUHN et al., 2014). The most important deposit is the Riacho Seco Copper Project (5 Mt @ 0.8% Cu), which is part of the Riacho do Pontal Fold Belt (RPFB) and was discovered by Companhia Baiana de Pesquisa Mineral (CBPM) in 1974. The mineral potential of the RPFB is still unknown due to a lack of systematic exploration activities and elaborate academic studies.

The main objective of this paper is to integrate an extensive geophysical, geological and geochemical dataset using a fuzzy modeling approach in order to build a robust and rigorous protocol adapted for exploration of the Riacho do Pontal IOCG district. The data integration revealed new high-quality targets of potential interest for mining exploration. The economic interest of one of these targets was validated by a drill core campaign.

The RPFB is part of the Borborema Province located in the northern part of the São Francisco Craton (BRITO-NEVES, 1975,1983; ALMEIDA et al., 1976) in northeast Brazil (Fig. 1.1). It represents Meso to Neoproterozoic sequences that were deformed during the Brazilian orogeny (FUCK et al., 1993). The Borborema Province is limited to the south by the São Francisco Craton, to the west by the Parnaíba Basin and to the north and east by the sedimentary basins of the coastal margin (Fig.1.1).

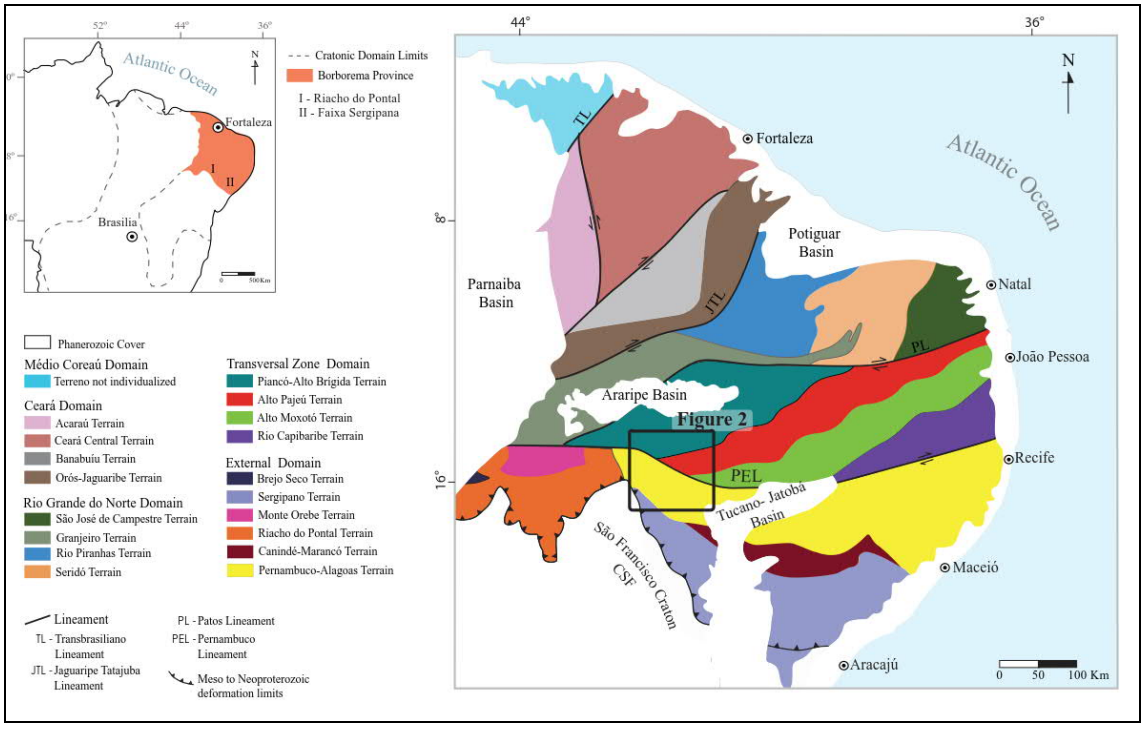

Figure 1.1 a) Tectonic positioning of the regional geology of Northeast Brazil in relation to Craton São Francisco and Borborema Province; b) Simplified tectonic map of São Francisco Craton and regional geological map of Borborema Province (BP) showing the Riacho do Pontal Belt (GOMES, 1998; OLIVEIRA; MEDEIROS, 2000).

Using gravimetric and magnetic data, Oliveira e Medeiros (2000) subdivided the Borborema Province into five major tectonic blocks. These are: 1) Médio Coreaú, 2) Ceará (or Cearense), 3) Rio Grande do Norte, 4) the Transverse or Central zone, and 5) the South or External zone (Fig. 1.1). On the basis of geological and structural studies, Sá, Macedo e Fuck (1992) proposed that the Borborema Province is composed of different domains that experienced distinct tectono-metamorphic evolutions, i.e., a gneissic-migmatitic basement and different supracrustal units showing differents tectonic-stratigraphic evolution. Santos (1996),

using a lithostratigraphic approach, identified a variety of sedimentary terrains, which were grouped into three main belts defined as the northern, transverse and southern (external), belts (e.g., SANTOS et al., 1997); Sá (1994); Brito-Neves et al. (2000); Brito-Neves et al. (2005).

Detrital zircons collected in the meta-sedimentary rocks forming the Borborema Province show a range of U-Pb ages between 980 and 1199 Ma, which were interpreted to reflect a maximum depositional age related to Brazilian orogen (OLIVEIRA et al., 2006). Granite zircon U-Pb ages show the occurrence of two main types of intrusive bodies: pre-collisional granitoids such as the 628 ± 12 Ma old Camará tonalite and 571 to 584 Ma old syn-collisional granites (e.g., Angico and Pedra Furada granites; BUENO et al., 2009).

The limit of the Borborema Province with the northern border of the São Francisco Craton (Fig. 1.1) has been mapped by thrust shear zones and is interpreted as a Brazilian collisional zone that developed during a convergence episode of Neo to Mesoproterozoic age (ALKMIM et al., 1993).

Exploration activities conducted during the 1970s, which were focused on volcanogenic massive sulfide mineralization (FRANKLIN et al., 1981; LINDENMAYER, 1981), led to the discovery of the Caraíba mine (24 MT@ 1,8 % Cu). The Caraíba mine occurs on the north portion of São Francisco Craton and is part of the Vale do Curaçá district. It has been described as having a magmatic origin in several studies (DELGADO; SOUSA, 1975; LINDENMAYER, 1981; OLIVEIRA; TARNEY, 1995). According to Garcia (2013), the formation of the Vale do Curaçá district is characterized by a multiphase evolutionary history, which includes (i) a primary magmatic mineralization stage at ca. 2.6 Ga, (ii) development of the Itabuna-Salvador-Curaçá metamorphic zone at ca. 2.08 Ga, (iii) remobilization during orogenic collapse and emplacement of an IOCG system at ca. 2.04 Ga associated with mineralization epigenetics (TEIXEIRA et al., 2010; FRAGUAS, 2012; GARCIA, 2013), and (iv) uplift of the orogen and late stage metasomatism at ca. 1.92 Ga.

The Riacho do Pontal Prospect

According to Bueno et al (2009) and Huhn et al (2014), the central portion of the Riacho do Pontal prospect is mainly composed by gneisses and tonalites of the Sobradinho Remanso Complex (Fig. 1.2). This geological unit lays in contact to the South with dolomitic marble and subordinated quartzites of the Macururé Group and is intruded by syn-collisional

granites towards the south. The rocks of the Macururé Group are thrusted over the São Francisco Craton.

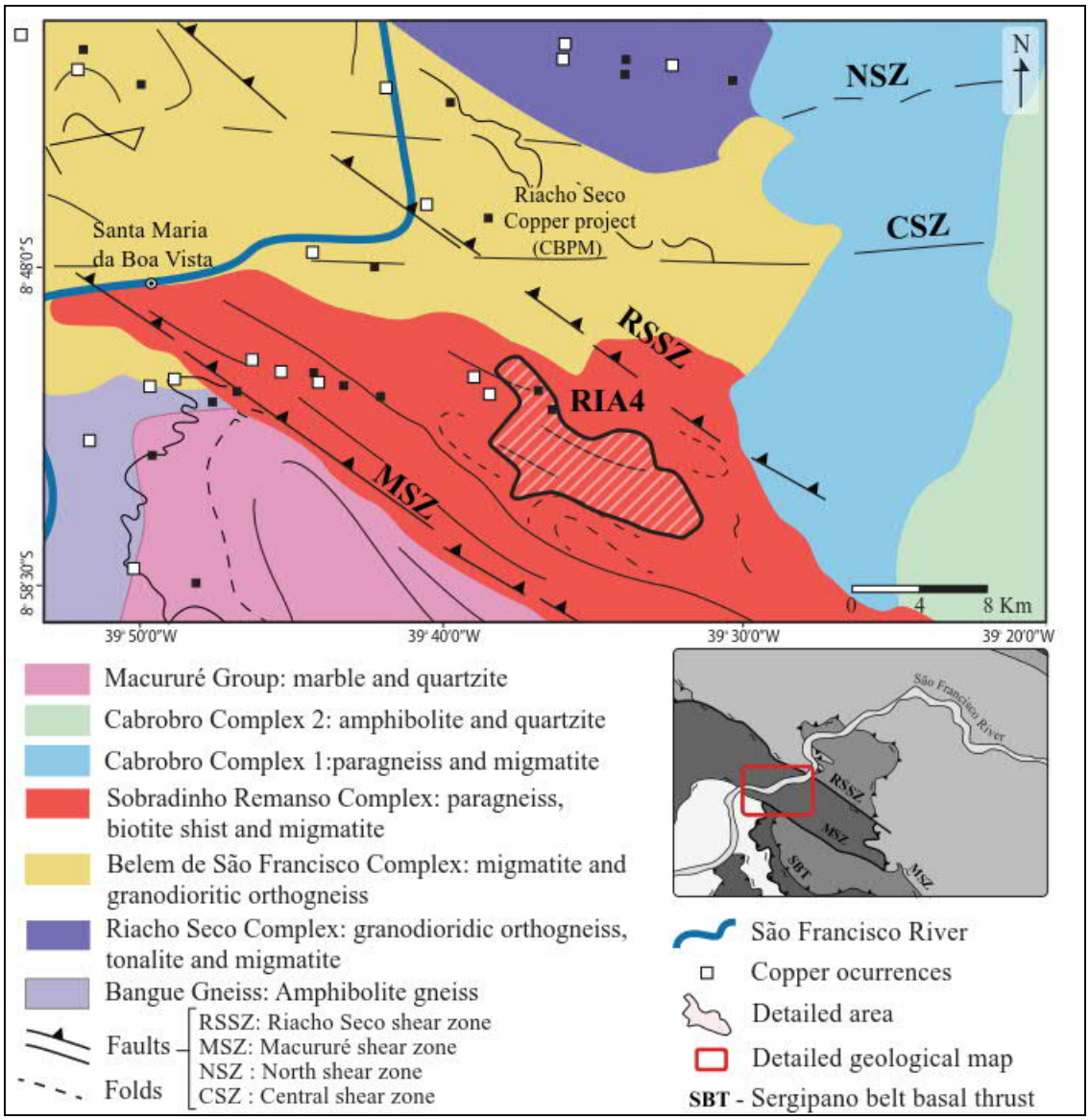

Figure 1.2 Simplified local geological map of the Riacho do Pontal prospect (after BUENO et al., 2009). The red dashed polygon Ria4 is detailed in validation of the potential targets.

Several main shear zones-oriented NW-SE occur cut across by late NE-SW faults. These major shears include the Riacho Seco, Macururé, North and Central shear zones. Riacho Seco (RSSZ) and Macururé (MSZ) correspond to thrust faults, while the North (NSZ) and Central (CSZ) are clockwise strike-slip shear zones.

Geophysical, Geochemical and Geological Constraints

Airborne Geophysical Survey

Airborne magnetic and gamma-ray survey was flown in 2005 over the Pernanbuco-Piauí area using 500-m-spaced north-south-oriented flight lines, with tie lines flown every 250 m at a nominal altitude of 100 m above ground. The Pernanbuco-Piauí survey consisted of 104,120 km of high-resolution magnetic gamaespectrometric profiles oriented N-S. Details of the data acquisition protocol, the aircraft used, and the geophysical sensors utilized can be foe und at the Brazil Geological Survey (CPRM, 2006).

The flight line magnetic data were corrected for the International Geomagnetic Reference Field (IGRF) and interpolated onto a 125 m grid using a bidirectional gridding method. Using the appropriate algorithms to preserve data fidelity at the original sample location, this method enhances magnetic features perpendicular to the flight line direction. The algorithm was based on linear interpolation along the direction of the flight lines and on Akima spline interpolation perpendicular to the flight lines. Microleveling and decorrugation techniques were also applied to the data. The magnetic anomaly data were reduced-to-the-magnetic-north pole (RTP) assuming an inclination of -20° and a declination of -22.31°. The results were compared with the calculation of the amplitude of the analytic signal (ASA). The ASA is of central interest to locate the spatial distribution of magnetic sources (NAGHIBIAN, 1972; LI, 2006; ROEST et al., 1992) and evaluate the best solution in accordance with geological data and interpretation.

In the Riacho do Pontal prospect, a total of 18 copper occurrences located on low magnetic anomalies lining shear zones were identified using this protocol. These shear zones show intense hydrothermal alteration overprint. To identify the different rocks types affected by these hydrothermal processes, ratios between gamma-spectrometric channels were used (OSTROVSKY, 1975; PIRES, 1985). Specifically, the parameter F = K x (eU/eTh) (EFIMOV, 1978) which establishes to co-evolution of the abundance of K and the eU/eTh ratio, have been widely used. Additionally, because of the relative less mobile character of Th, Saunders, Terry e Thompson (1987) and Pires (1985) used the normalization of K and U by Th to evaluate K anomalies along shear zones.

According to Oliveira (2008) it is possible to observe, on a regional scale, that the supracrustal sequence of the Riacho do Pontal and Sergipana bands were placed aloctone with displacements of the order of 30 to 60 km (SÁ et al., 1992) and Oliveira (2008) showed that the region of the Riacho do Pontal Fold Belt has a regional positive gravimetric anomaly with a wavelength of 200 km and an amplitude of 60 mGal. The region has an aeromagnetic

pattern characterized by dominant shallow sources defined by positive E-W linear axis with amplitudes less than 100 nT and short wavelengths (10 km). The anomaly is interpreted as the result of a crustal shortening related to a neoproterozoic collisional process (Fig. 1.3).

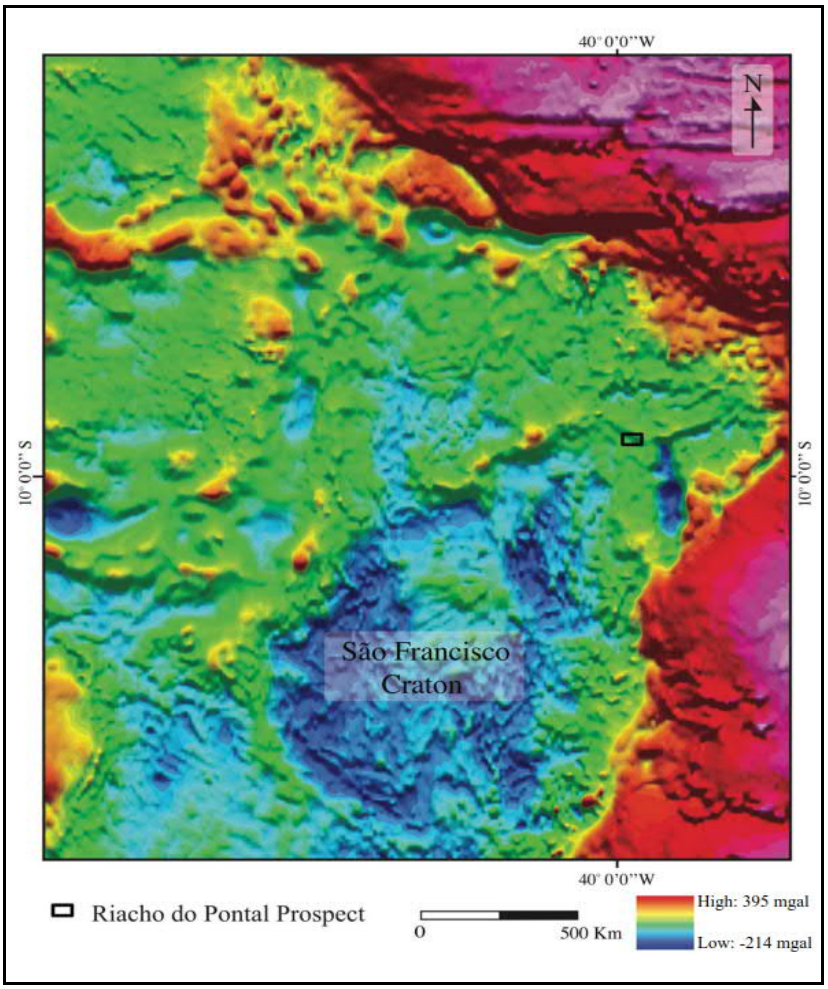

Figure 1.3. Regional Bouguer anomaly map showing the signature of the São Francisco Craton and surrounding Brazilian fold belt. The black polygon outline the Riacho do Pontal prospect studied here (after OLIVEIRA, 2008)

Stream Sediment and Soil Geochemistry

The stream and soil sediments geochemical data were used in the data integration to identify new exploration targets. The geochemical data available for the Riacho do Pontal project include major and trace element compositions of both stream and soil sediments. Stream sediments were collected in active river beds and analyzed by the Brazil Geological Survey. A total of 194 stream sediments were obtained over an area of 1816 km^2. Each sample represents the sum of different fractions of sediments collected over an area of about

5000 to 10000 m^2. The samples were dried at 60°C, sieved to a fraction of <80 mesh, and sprayed to a fraction of <150 mesh. The samples were dissolved using *aqua regia* (3:1 HCl:HNO_3). The chemical analyses were performed using a combination of ICP-AES and ICP-MS.

Using a digital terrain model (DTM), sediment geochemical data were processed at a sub-basin scale according to the following protocol (BUARQUE, 2007, Fig.1.4): i) extraction of drainage effect without generating depressions, ii) generation of a matrix file with the direction of flow for each cell, iii) generation of a cumulative flow matrix file for each cell, iv) extraction of drainage network, v) conversion to vector file, vi) delimitation of watershed areas, with the definition of values corresponding to the direction of flow in the basin, for each drainage section and vii) generation of the map of sub-basins (CARRANZA; HALE, 1997). The samples were interpolated in a grid using barriers for each catchment basin, using a minimum curvature spline technique. Figure 1.4 shows the geochemical stream sediment samples and catchment basin maps that were generated. Stream sediment grid data were interpreted and integrated with geophysical and geological data.

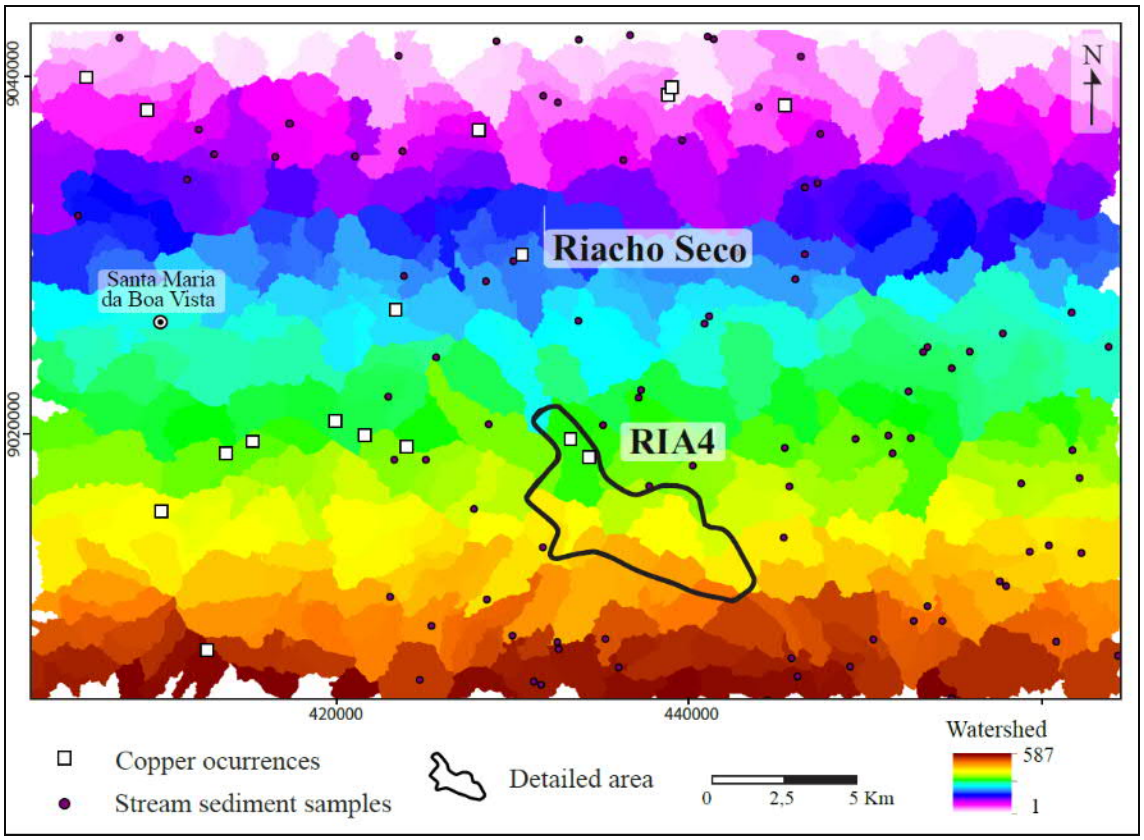

Figure 1.4 Stream sediment samples and catchment basins processing used at the Riacho do Pontal prospect. The black polygon RIA4 is detailed in validation of the potential targets.

Soils are poorly developed in the Riacho do Pontal prospect as weathering is limited in this arid climate with no apparent laterite profile. The collected samples are mainly composed of siltstones and sandstones containing abundant angular fragments, hence arguing for limited transport. These sediments may therefore reflect the nature of the immediately underlying host rock. However, due to high grade metamorphism and, potentially, hydrothermal alteration, the protoliths are seldom recognizable. A total of 1494 soil samples were collected along NW-SE trending line profiles up to 1.6 km in length, which were obtained throughout the area labeled RIA4 in Figure 1.3. Samples were analysed by AR/ICP-OES (ME-ICP41) for 33 elements and by FA-ICP (PGM-ICP23) for Au, Pt and Pd. The chemical soil data were interpolated in a grid using kriging data processing.

Geological and Drill Core Geochemical Data

The geological map of the Riacho do Pontal prospect was constructed using regional maps available at CPRM and data obtained from Vale exploration (VALE, 2009). The structural interpretation was performed using Aster images and airborne magnetic derivative products. In addition, four drill holes representing 1295.30 m of cores were performed during the exploration campaign. Among these, only three holes were analysed for their major and trace element compositions. The fourth drill hole RCB-RIA4-DH00001 was analysed down to 63m depth only. All samples were digested by *Agua Regia* techniqueand analysed by ICP-OES (ME-ICP41) for 33 elements and FA/ICP-OES for Au (SHIVER, 2009).

Results

Geological and Structural Data

The Riacho do Pontal prospect has a strong NW-oriented structural fabric that is represented by major shear zones. The mainly units of the Riacho do Pontal prospect are characterized by rocks composed of gneiss and migmatites. The metasedimentary cover is composed of quartzite and schists. Petrographic studies using Energy Dispersive X-ray Spectrometry coupled with Scanning Electron Microscope allowed the characterization of hydrothermal mineral signature (HUHN et al., 2014). Hydrothermal alteration led to a pervasive calcic and calcic-ferric overprint of the host gneisses and migmatites. Early stage

sodic-calcic hydrothermal alteration is distal in relation with areas of higher strain rate. The hydrothermal alteration process led to replacement of metamorphic minerals of banded gneiss by hydrothermal assemblages (Table 1).

Table 1. Hydrothermal alteration and mineralogical assemblages related to copper mineralization zones in the Riacho do Pontal prospect.

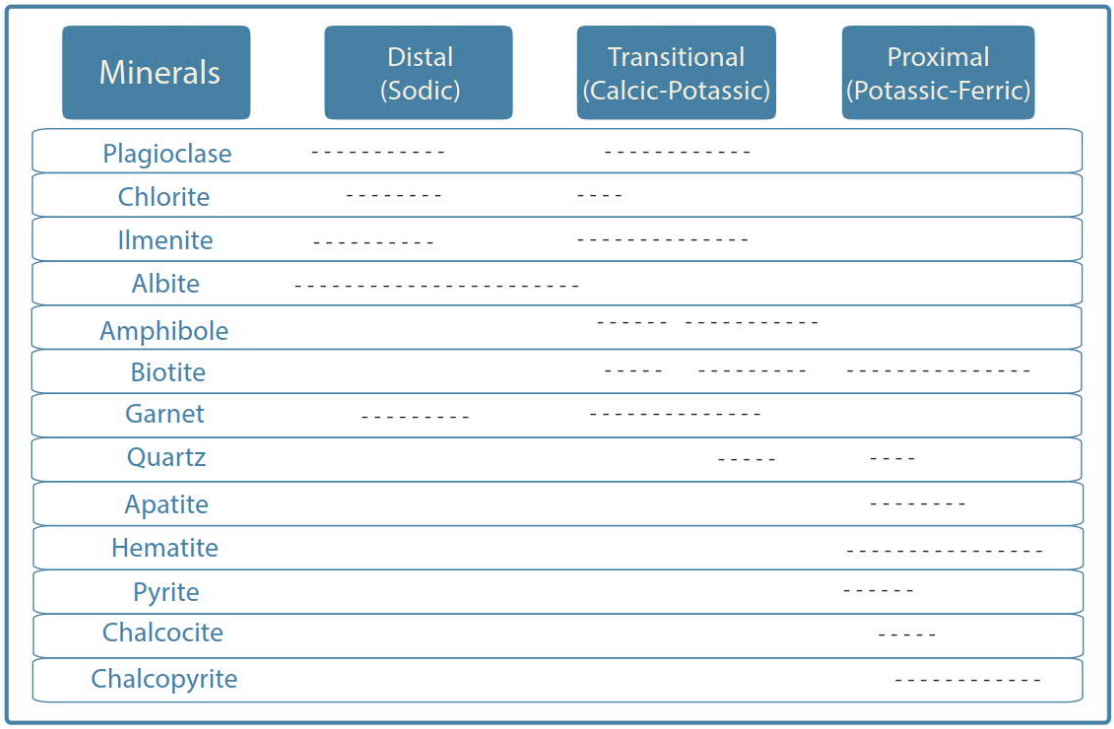

Riacho do Pontal prospect has a strong NW-SE oriented structural fabric that is represented by shear zones identified in figure 1.4. Locally, strongly mylonitized rocks along shear zones defines a L-S tectonite fabric. Ore zones are strongly controlled by restraining bends of shear zones and late breccia zones along the bends (Fig. 1.5). Secondary ore zones are subparallel to these major lineaments. Late faults oriented NE-SW representing a late stage of brittle extensional deformation are frequent in the region.

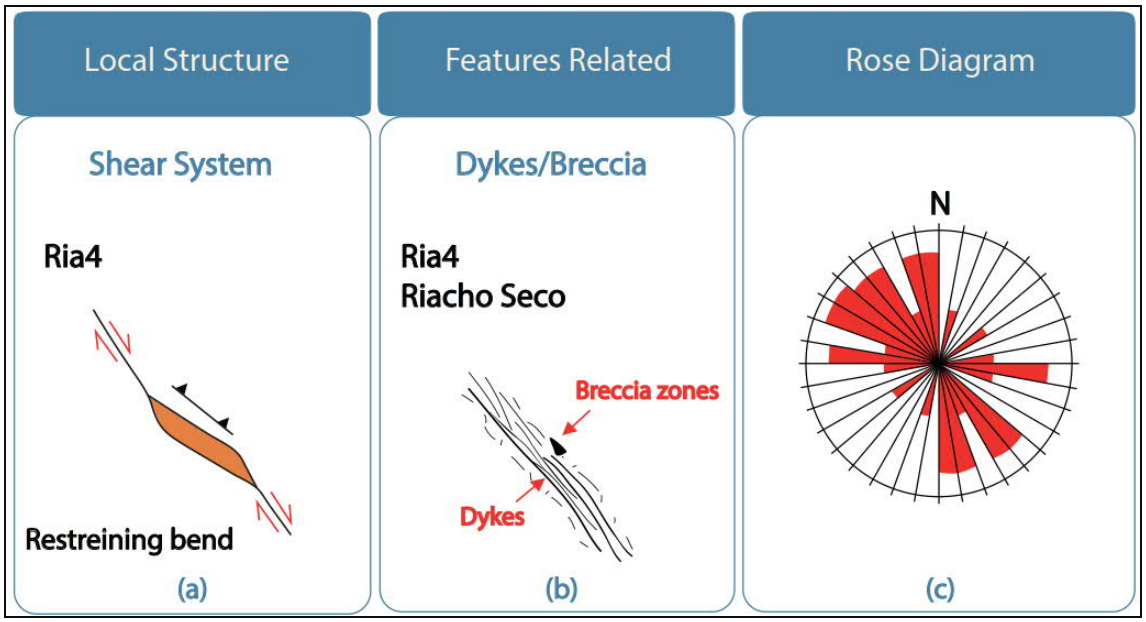

Figure 1.5 Map showing the local geologic structures at Riacho do Pontal prospect (a); features related to copper occurrences at the Riacho do Pontal and Riacho Seco prospect (b) and (c) Rose diagram showing major NW and NE shear.

Geophysical Data

Gamma-ray spectrometric data have been very useful for mapping of geological units and hydrothermal zones of Riacho do Pontal prospect (HÜHN et al., 2014). The ternary image of Figure 1.6 (RGB colors) represents a compositional map of U, Th and K. Different subdomains can be recognized. In the central portion of the area, where orthogneiss rocks of the Sobradinho Remanso Complex outcrops, intense potassic hydrothermal alteration can be recognized in the Riaco Secho Shear Zone (RSSZ) and the Macururé Shear Zone (MSZ). This potassic alteration occurs locally associated with strong enrichments in hematite and/or magnetite (Table 1). Specifically, magnetite bodies were identified along the North Shear Zone (NSZ), which cut across the gneisses of the Complexo Belém do São Francisco. The white areas in the central part of the ternary map along the RSSZ, the MSZ and the Central Shear Zone (CSZ) corresponds to intense siliceous alteration zones.

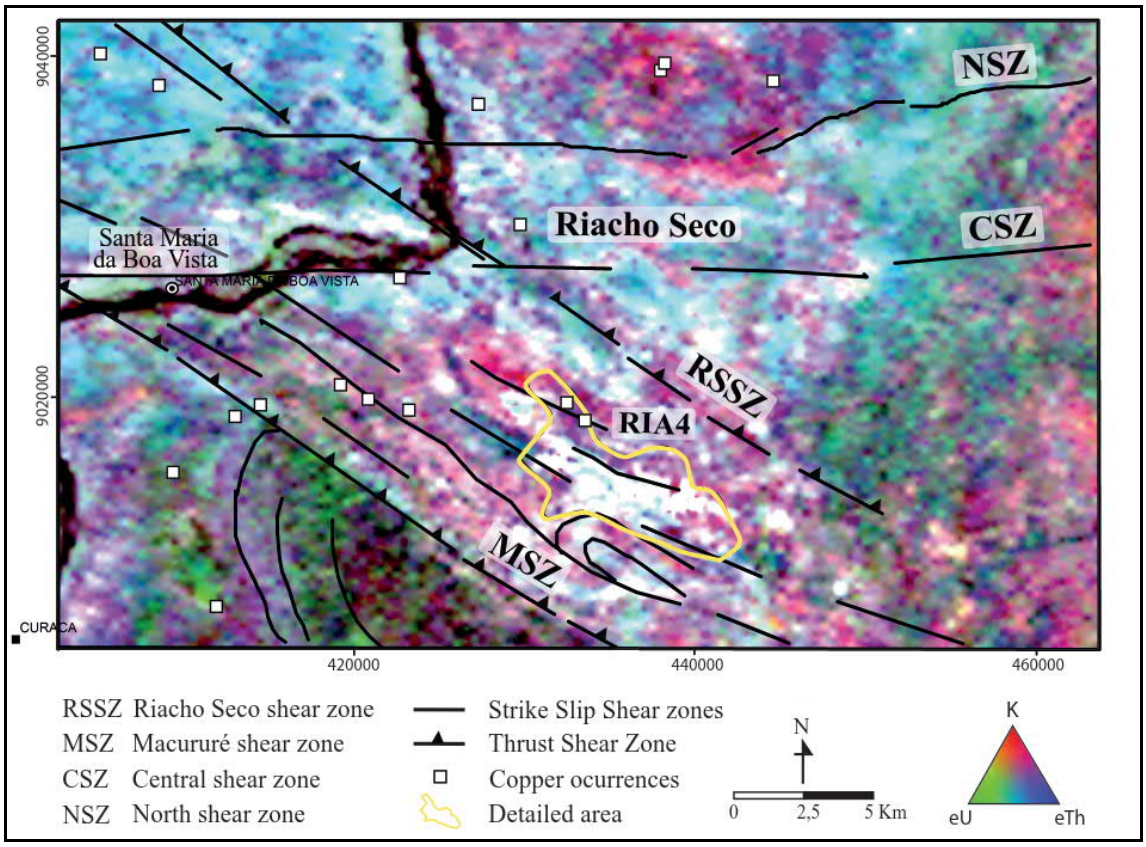

Figure 1.6 Ternary image of the Riacho do Pontal prospect area showing the distribution of potassium (K, red), thorium (Th, blue) and uranium (U, green). The yellow polygon RIA4 is detailed in validation of the potential targets.

Figure 1.6 shows a flowchart that summarizes the enhancement techniques applied to magnetic data of the studied area. Results generated from the magnetic data includea) a map of the total magnetic intensity (TMI), b) the first order derivatives along two horizontal components (Dx, Dy) and one vertical component (DZ) and c) the 3D analytic signal amplitude (ASA) calculated from the TMI (ROEST et al., 1992). These data were used to delineate the boundaries of the sources and assist with the magnetic and structural interpretations of the studied area (Fig. 1.6), including the amplitude of the analytical signal and the "worm" method (WM, see below. (ARCHIBALD et al.,1999).

Multi-scale Edge Mapping (MED or Worm (WM)) is a process of highlight edges in potential field data **(**ARCHIBALD et al., 1999). MED processing involves upward continuation processing to separate the potential field data into shallow high frequencies associated with short wavelength responses, in contrast with deeper low frequencies related to long wavelength responses. The MED processing seeks to decrease the ambiguity in potential field interpretation and provides useful information about the general shape and relative depth of edges, such as faults and geological contacts (ARCHIBALD et al., 1999). In the studied

area, the worm linear features represent irregularities of potential field data, corresponding to major geological contacts and shear zones (Figures 1.7 and 1.8).

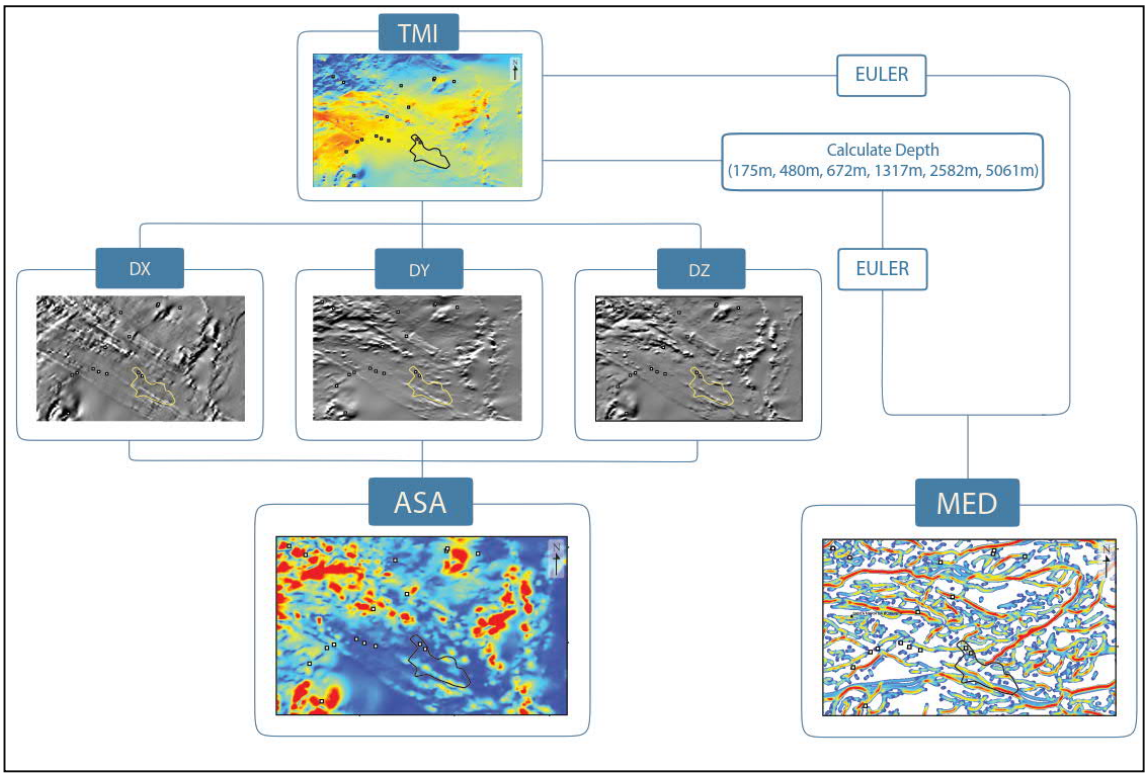

Figure 1.7 Flowchart of operations illustrating the processing of magnetometric data and the transformations of linear relations in a 3 components space domain including, het anomalous magnetic field (CMA), vertical and horizontal derivatives DZ, DX and DY , and the analytical signal amplitude (ASA). MED is a process of highlight edges in potential field data (ARCHIBALD et al., 1999; HORNBY et al., 1999;).

With the exception of the Riacho Seco Shear Zone (RSSZ), figure 1.7 shows that the major shear zones mapped on the surface which show a dominant NW trend dipping50 degrees to the NE, overlap relatively well with the WM (MED) structures. In addition, the two main strike-slip shear zones (CSZ and NSZ) displaying a subvertical EW trend are strongly underlined by the WM structures, which indicates that they represent deeply rooted features. The absence of a clear overlap with the Riacho Seco Shear Zone (RSSZ) argues for a shallow structure (Fig. 1.8). Between the MSZ and RSSZ structures, second order thrust structures are also quite concordant with the WM data. Note that he RIa4 target is bounded to the south by a secondary NW-SE trending shear zone (Fig.1.8).

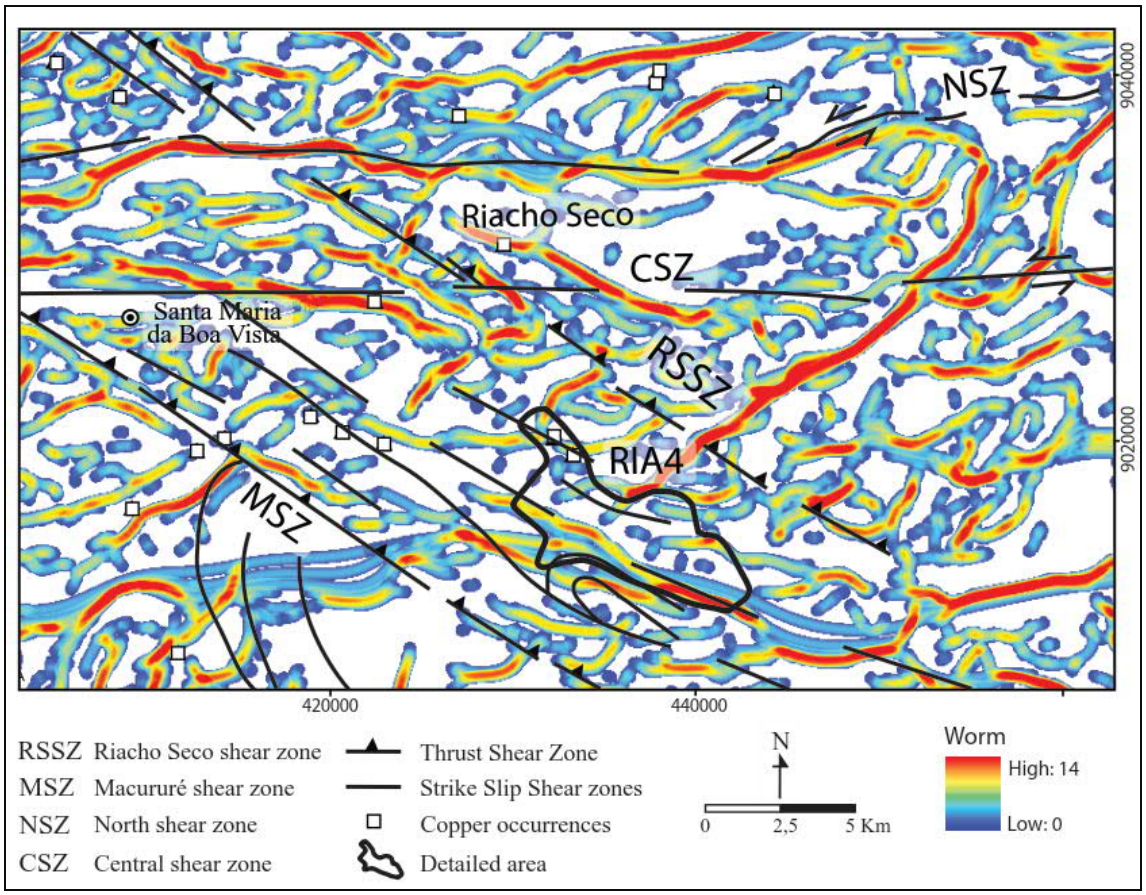

Figure 1.8. Aeromagnetic worms lineaments with major shear zones and copper occurrences at the Riacho do Pontal prospect. Worming processing highlights the major and secondary structures. The black polygon RIA4 is detailed in validation of the potential targets .

Stream Sediment and Soil Geochemistry

Principal component analysis was applied to seven multi-element associations (Cu, Ni, Fe, P, La, Cr and Zn) that characterize the known copper occurrences in the Riacho do Pontal prospect. (The Riacho Seco copper Project is situated on the NW worm structure parallel to RSSZ in Figure 1.8). Analyzing that the geostatistical behavior of the stream sediment geochemical data according to the matrix of self-vectors of table 2 , it is verified that Cu, Ni, Fe and La shows anomalies from the principal component (PC) 6 and have spatial associations with known copper-gold occurrences (Table 1). The sixth principal component (PC6) has high positive loadings for Cu, Ni, Fe, and La. This multi-element geochemical map was used to validate the results of the predictive mineral potential of the Riacho do Pontal prospect (Fig 1.9).

Table 2. Principal component analyses of stream sediment data from the Riacho do Pontal prospect.

Principal Components Eigenvectors	Cu	Ni	Fe	P	La	Cr	Zn
1	0,1916204	0,2054073	0,1578991	0,33218070	-0,2501926	0,8951185	-0,01005916
2	0,2473167	0,03362516	0,2337775	0,43689220	-0,7604466	-0,4169447	0,02467909
3	0,0409507	0,02415018	0,0407080	-0,0800833	0,319028	0,157858	0,99849340
4	0,9917154	-0,8331272	-0,965052	0,1239673	0,085005	-0,451941	-0,00032030
5	0,07891539	0,99940824	-0,0541230	-0,05125238	-0,0015744	0,003615	-0,09393550
6	0,9566740	0,2465354	0,424739	-0,35370430	0,893393	-0,099972	-0,04368640
7	0,1118552	0,5189384	0,2266562	0,77555328	0,0591650	-0,1566430	-0,01977967

The soil sampling at the RIA4 target were projected along profiles oriented sub-perpendicular to the main NW-SE structural/geological trend. The soil geochemical results from the main trend include up to 613 ppm Cu, 23 ppb Au, 162 ppm Zn, 547 ppm Ni, 8.94% Fe and 1945 ppm Cr (SHRIVER, 2009). The northern and central-northern portion of the area show a positive correlation between Cu and Au, with anomalous values of Cu. A contour map of the Cu concentrations shows a cluster of anomalous samples near the gossanic outcrops.

Data Integration and Prospectivity Map

One of the most important decision-making in mineral exploration is the selection of prospects in a given geological environment. Conceptual mineral exploration models based on geology are currently less commonly used than those based on geophysical and geochemical data. Thus, extensive geological knowledge of the exploration model combined with the predictability of integrating multi-source data can increase the exploration success rate. This success rate is closely related to management, and continuous improvement of the database will allow the exploratory model to evolve. Persistence and agility in making “stop and go” decisions are critical for high-potential projects to advance. The approach used in this paper is the knowledge-driven models for data integration and target selection (BONHAM-CARTER, 1994; FORD; HART, 2013).

Knowledge-based prospectivity mapping was performed by extracting the spatial relationships from exploration datasets based on an exploration model, quantifying these spatial relationships and integrating them using mathematical operators chosen by the user. The lower potential areas that do not show evidence of mineralization are assigned very low

potentials that are close to, but not exactly, zero. The mathematical operators, fuzzy algebraic product, fuzzy algebraic sum and fuzzy gamma are commonly used in fuzzy data integration (BONHAM-CARTER, 1994; FORD; HART, 2013; PORWAL; CARRANZA; HALE, 2003; SILVA et al., 2000).

Application of a Fuzzy Model tothe Study Area

The parameters were integrated into a prospectivity map using the fuzzy-logic method first developed by Bonham-Carter (1994). In the fuzzy theory, the members of a fuzzy set is expressed on a continuous scale from 0 to 1. Values were selected to reflect the degree of membership of a database that has been analyzed based on expert judgment. The various classes of layers of a set of maps can be expressed in terms of fuzzy memberships of different sets and can be stored as an attribute table of a map (BONHAM-CARTER, 1994).

The spatial association between the copper occurrences and structural features can be analyzed using fuzzy logic to determine whether potential IOCG targets are located in connectionwith geologic structures. The geochemical, structural, magnetic and potassium anomalous maps, after being fuzzified, were combined using fuzzy operators, in order to generate the final model. Frequently used operators are: "Fuzzy-AND", "Fuzzy-OR", "Fuzzy-Soma", "Fuzzy-Product" and "Fuzzy-Gamma" (BONHAN-CARTER, 1994; CARRANZA; HALE, 2001; LEE, 2007).

The structural prediction map integrated a high density of worm features (density of linear features in the neighborhood of each output raster cell) and buffer (200 m) around mapped linear features. A fuzzy gamma operator of 0.9 was used to combine different maps in order to highlight the potential connectivity between the deep and shallow structures. Such structures have the potential to represent preferential conduits for hydrothermal fluid circulation. The geochemical PC6 prediction map is represented by Cu, Fe, Ni and La catchment basin anomalous maps.

The geophysical prediction map it was selected areas with magnetic low signature looking for copper occurrences related to hematite zones along fault zones. Aiming to map areas with potassic hydrothermal alterations it was used the processing of anomalous potassium (OSTROVSKY, 1975; PIRES, 1985). The operator fuzzy sum was performed to integrate the geochemical, structural, magnetic and hydrothermal data. The final predictor map is shown in figure 1.9.

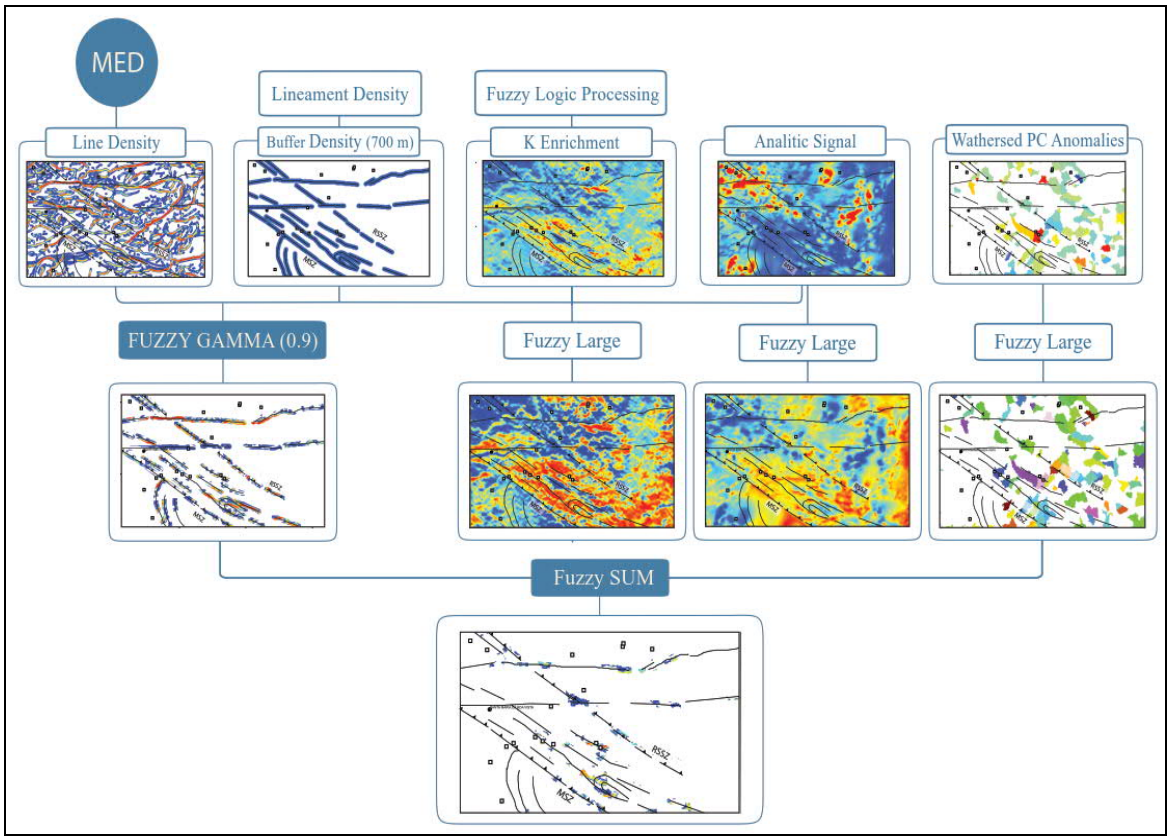

Figure 1.9. General flow chart of fuzzy data integration modeling using sets of geological, geochemical, structural, magnetic and **anomalous** potassium maps to select favorable targets for copper deposits.

The data integration using fuzzy operators was described by Raines et al. (2000), Raines et al. (2010) and Nykänen et al (2008). The Arc-SDM arctoolbox can be downloaded from http://www.ige.unicamp.br/sdm (SAWATZKY et al., 2004). The detail prospective favorability maps of the area are shown in figures 1.10 and 1.11

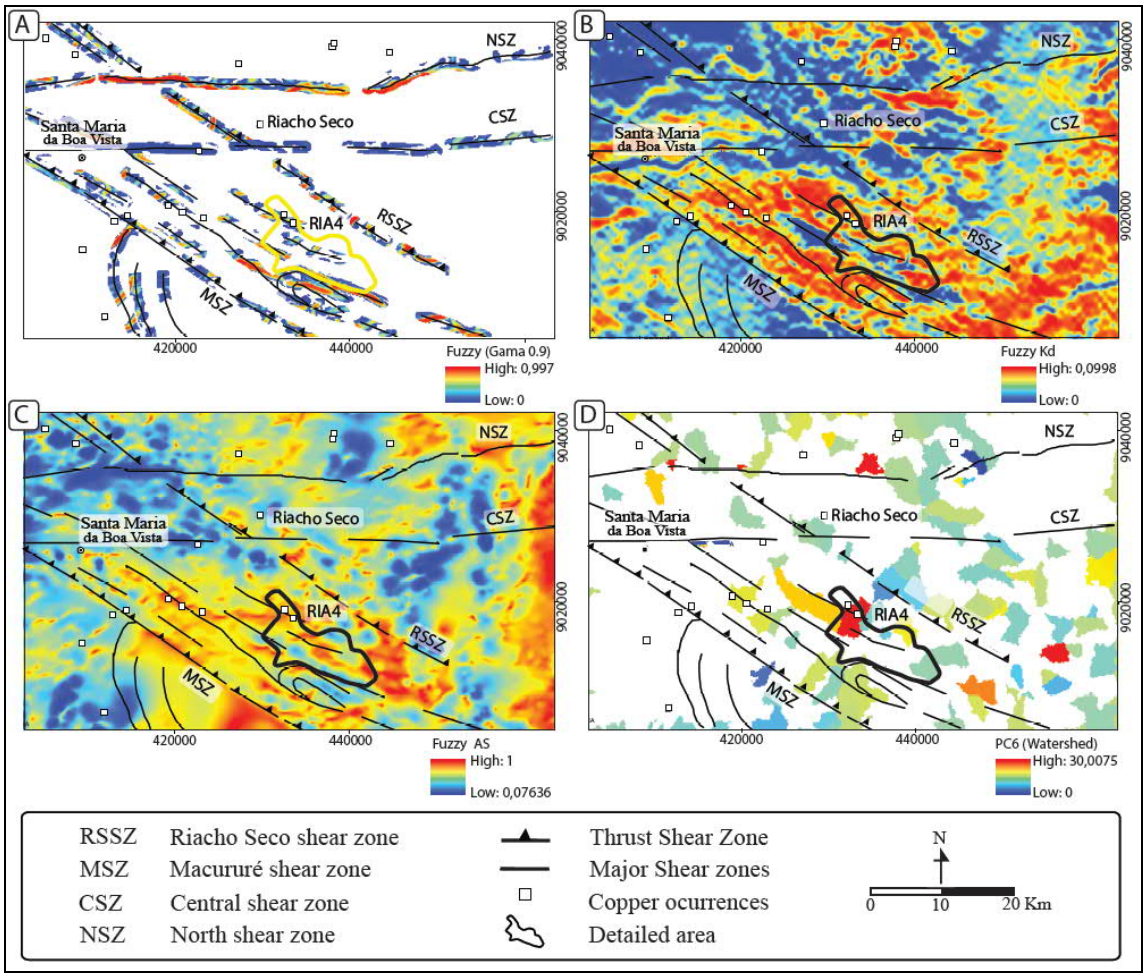

Figure 1.10. The figure shows set of intermediate layers maps used in fuzzy data integration modeling reclassified using the fuzzy membership tools: (a) the relevant intersecting structures, b) high **anomalous potassium values ,** c) high analytical signal amplitude values, d) High positive loadings for Cu, Ni, Fe, and La in the PC6 stream sediment. The black polygon is described in the second part of this paper.

In the final favorability model of figure 1.11, approximately 10% of the zones with high potential were identified to host copper mineralization. In particular, special attention should be given to the high score areas in the fuzzy classification, such as the area located between the shear zones RSSZ and MSZ (including target RIA4) and the targets along the NSZ and CSZ.

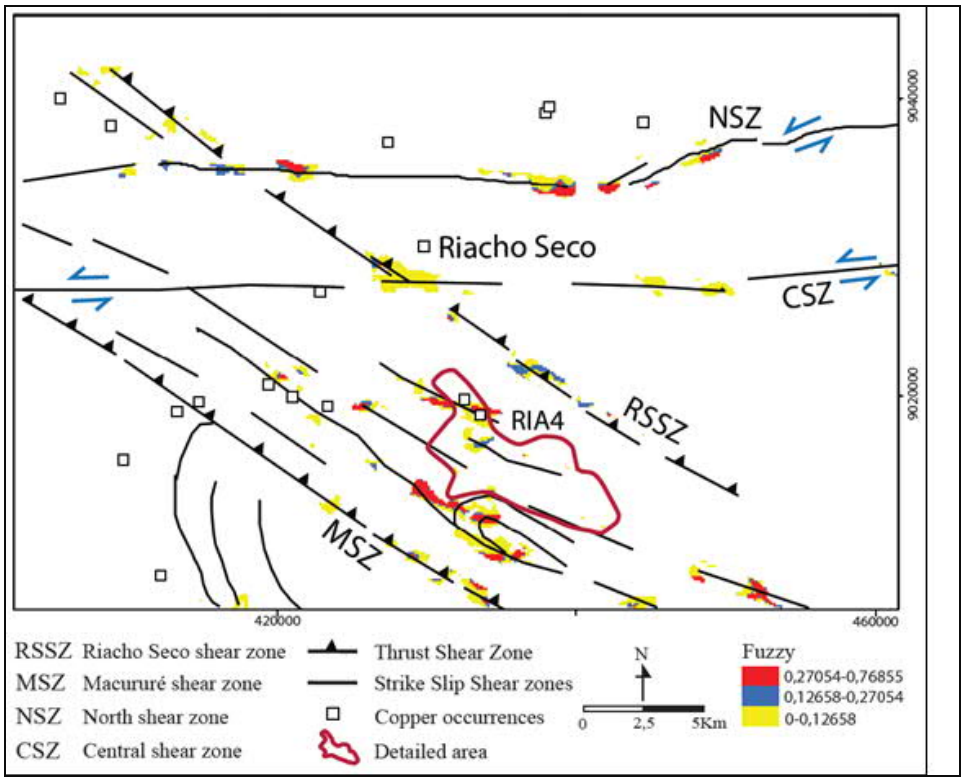

Figure 1.11 Final classified fuzzy favorability map showing higher-potential areas. The central portion of the area was selected for more detailed exploration activities. The red polygon is approached in validation of the potential targets.

Validation and Assessment of the Best Targets Using a Drilling Program

Validation of the potential targets of economic interest represents an important aspect of prospectivity mapping analysis. In this study, the RIA4 target is one of the best potential prospects identified by the regional approach. RIA4 target was selected to validate the exploration model . Figure 1.12 shows the flow chart for the fuzzy modeling at the scale of RIA4. As for regional scale modeling, different components (structural, soil geochemistry, magnetic, and hydrothermal maps) were selected for data integration and were gridded to RIA4 prospect area. Different from the regional scale modeling is that the soil geochemistry instead of stream sediment geochemistry was used as the geochemical component..

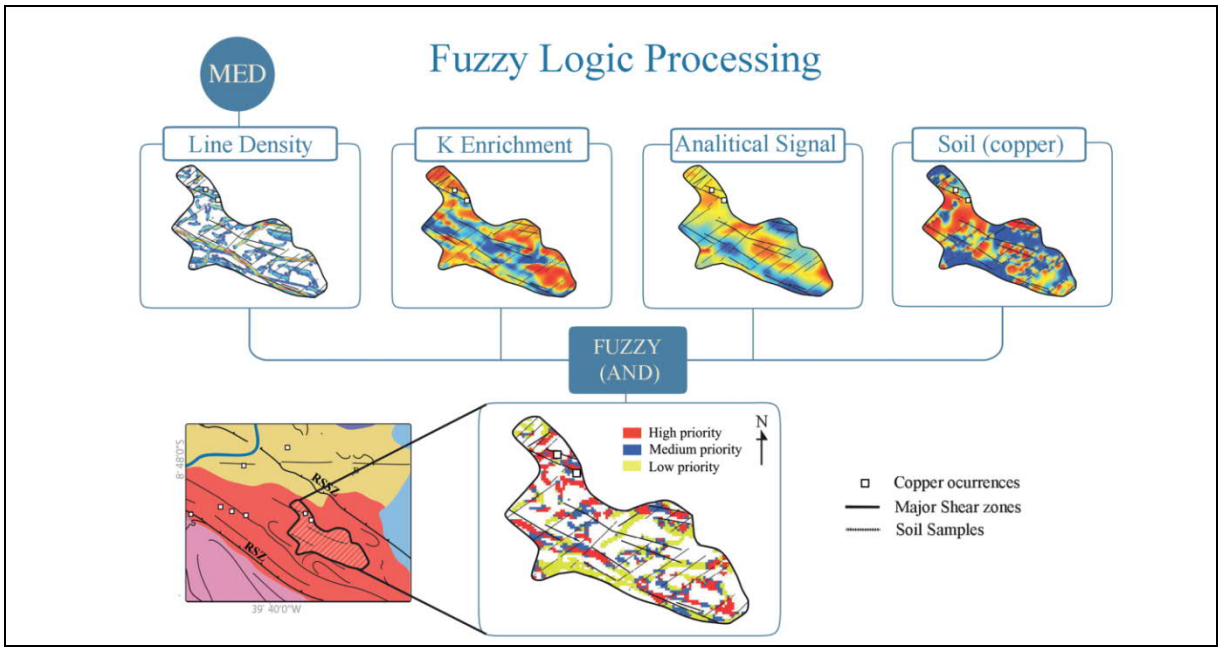

Figure 1.12 Maps of the fuzzy set of evidence layers. Structure, K enrichment, analytical signal and soil geochemistry were assigned using fuzzy logic weight and the fuzzy logic AND operator. The medium- and/or high-priority areas account for over 22% of the study area.

The prospective maps were integrated using fuzzy AND operator to generate the integrated fuzzy favorability mapfor IOCG mineralization in the RIA4 target. The potential areas for host copper mineralization at the RIA4 target are shown in the fuzzy favorability map of figure 1.13. The medium- and/or high-priority fuzzy areas account for over 22% of the study area. From the exploration point of view only the north central portion of the area was partially tested by exploratory drilling.

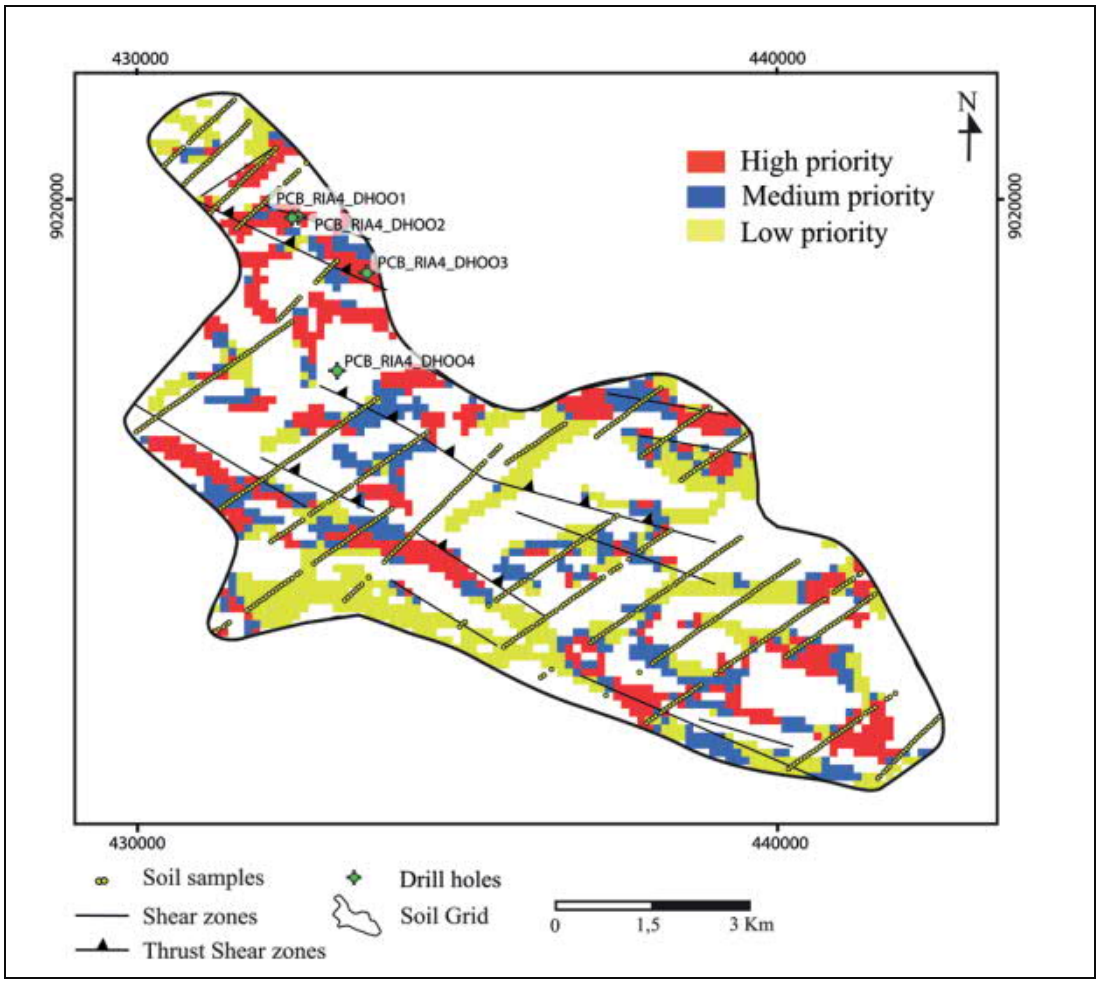

Figure: 1.13 Fuzzy favorability map, showing areas of medium and/or high priority that have greater potential to find copper mineralization at the RIA-4 target. Four drill holes were obtained to validate the exploration favorability model.

Two drill holes were located in area of high-priority of the fuzzy favorability map (Fig. 1.13). Geologically the two drill cores were obtained at the site where malachite is hosted in sheared hematite-biotite-rich rocks. RIA4-DH00001 crosscut the ore zone, which is characterized by pyrite-chalcopyrite-bornite with a 32-m thick zone of 1.15% Cu. The geochemical results from drill hole RIA4-DH00001 show high values for Au (243 ppb), Ni (1675 ppm), Cr (4020 ppm) and Zn (390 ppm; SHRIVER, 2009).

Drill hole RIA4-DH00002 intersected banded leucogneiss with silicified zones and several biotite- and amphibole-rich intervals, some of which contained trace chalcopyrite and pyrite. This low-grade mineralization zone is interpreted as a zone of trans-tensional deformation (Figure 1.14). Drill hole RIA4-DH003 was drilled 1.3 km southeast of RIA4-DH001. The hole was positioned on the edge of the high-priority anomaly, crosscutting intense biotite-hematite hydrothermal zones with discontinuous mineralized intervals with

low grade copper (0.2 wt%). Drill hole RIA4-DH00004 was drilled 2.5 km southeast of RIA4-DH0001 in an area with malachite occurrences and intersected biotitic leucogneiss, with few and discontinuous garnet-biotite rich intervals and a very low grade of copper. RIA4-DH00004 was located in low-potential areas, as illustrated on the fuzzy favorability map (Figure 1.14). The results obtained in the drill holes reported above validate the exploration used in this work. From an exploratory point of view, additional probing is recommended in areas of high potentiality in the fuzzy favorability map. A geological cross section showing drill holes PCB-RIA4-DH-01 and DH-02 in the recognized mineralized zone of the Riacho do Pontal prospect is illustrated in figure 1.14.

Finally, figure 1.14 provides an overview of the data integration, including the outcrop mapping, drilling, model validation, features of the ore zone and the style of mineralization. In the fuzzy analysis of the Riacho do Pontal Belt, the moderately and highly score fuzzy favorable. The high priority targets should be investigated by additional exploration activities.

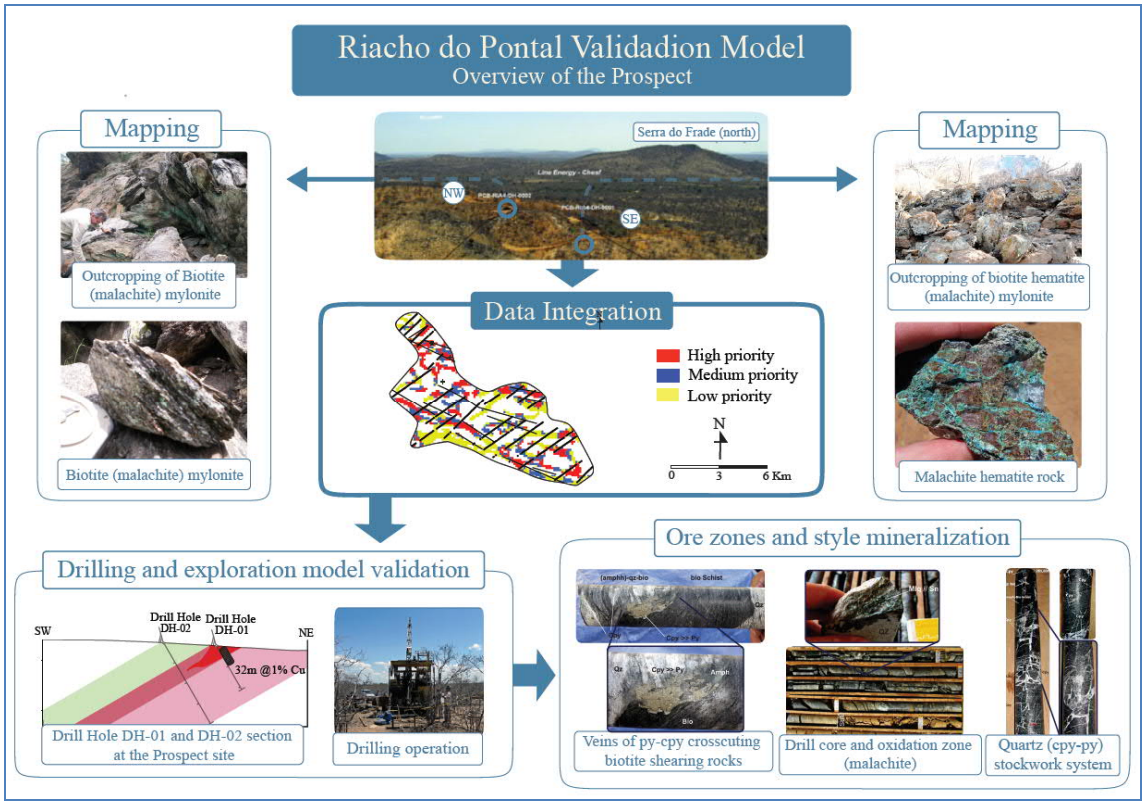

Figure 1.14 Overview of data integration of the Riacho do Pontal project showing outcrop mapping, drilling, model validation, features of the ore zone and mineralization style. high-priority targets should be investigated by additional exploration activities.

Conclusions

This study used a knowledge-driven fuzzy method to produce a prospectivity map of the area of the Riacho do Pontal prospect. Comparative evaluation of the results was performed using drill holes in the study area. The results indicate that the fuzzy method can be used to prioritize a prospect area. The proposed method can be applied as a reliable knowledge-based tool for prospective areas of the Riacho do Pontal belt.

Regional and district-scale fuzzy models were implemented using prediction maps by processing the following exploration datasets: structure density (lineaments and worms), soil and stream sediment geochemistry data, and airborne magnetic and gamma ray data.

The fuzzy analysis that was used to assess the Riacho do Pontal Belt at the regional scale indicated that moderately and highly favorable areas have the potential to host IOCG deposits. The modeling was validated with a drilling exploration program for the target RIA4. Drill hole RIA4-DH001 intersected a 32-m thick mineralized zone that contained 1.15% Cu.

Finally, on a broader exploration perspective, mineralization along the Brazilian fold belts that surround the São Francisco Craton could be evaluated as potential tectonic settings for IOCG deposits.

Acknowledgments

The authors gratefully acknowledge Vale S. A. for their support of this study. We would like to thank Fernando Greco, F. Matos and the Vale exploration team for extensive discussions. A.M. Silva gratefully acknowledges the National Council for Scientific and Technological Development (CNPq) for the research grant (307177/2014-9). We would also like to thank Raiza Toledo Rodrigues Toledo and Victoria Basileu for their special support in developing the figures and Pascal Philippot for his constructive comments on different versions of the manuscript.

References

ALKMIM, F.F.; BRITO-NEVES, B.; CASTRO, J.Alves. Arcabouço tectônico do Cráton São Francisco: uma revisão. In: DOMINGUES, J.M. L.; MISI (eds). **O Cráton do São Francisco**. Salvador. SBG/SGM/CNPq, 1993. p. 45-62.

ALMEIDA, F.F.M.; HASUI, Y.; BRITO-NEVES, B. The Upper Precambrian of South América. **Boletin IG**, Universidade de São Paulo, n.7, p. 45-80,1976.

ARCHIBALD, N.; GOW, P.; BOSCHETTI, F. Multiscale edge analysis of potential field data. **Exploration Geophysics**, n.30, p.38-44, 1999.

BONHAM-CARTER, G.F. **Geographic information systems for Geoscientists**: Modelling with GIS: Oxford, Pergamon, 1994. 398 p.

BRITO-NEVES BB. et al. A Zona Tectônica Teixeira Terra Nova- ZTTTN - Fundamentos da Geologia Regional e Isotópica. **Geologia USP Série Científica**, n.5, p.57-80, 2005.

BRITO-NEVES, B.B. **O mapa geológico do nordeste Oriental do Brasil**: escala 1:1.000.000. Full Professor. 1983. 177f. Thesis - Instituto de Geociências, Universidade de São Paulo, São Paulo, 1983.

BRITO-NEVES, B.B. **Regionalização geotectônica do Pré-cambriano nordestino**. 1975. 198f. Tese (Doutoramento) - Instituto de Geociências, Universidade de São Paulo, São Paulo, 1975.

BRITO-NEVES, B.B.; SANTOS, E.J.; VAN SCHMUS, W.R. Tectonic history of the Borborema province. In: CORDANI, U.G. et al (eds.). **Tectonic Evolution of the South America. Tectonic Evolution of the South America**. 31st International Geological Congress, 2000, Rio de Janeiro, Brasil, p. 151-182.

BUARQUE, D. C. **Extração automática de parâmetros físicos de bacias hidrográficas a partir do MNT para utilização em modelos hidrológicos**. 2007. Disponível em: <http: //galileu. iph.ufrgs.br /collischonn/HIDP 23/HIDP 23.html>. Acesso em: 25/10/2012

BUENO, J.F. et al. U–Pb dating of granites in the Neoproterozoic Sergipano Belt, NE-Brazil: Implications for the timing and duration of continental collision and extrusion tectonics in the Borborema Province. **Gondwana Research**, n.15, p. 86-97, 2009.

CARRANZA, E. J. M.; HALE, M. A catchment basin approach to the analysis of reconnaissance geochemical-geological data from Albay Province, Philippines. **Journal of Geochemical Exploration**, n.60, p.157 – 171, 1997.

CARRANZA, E.J.M.; HALE, M. 2001. Geologically constrained fuzzy mapping of goldmineralization potential, Baguio district, Philippines**. Natural Resources Research,** n.2, v. 10, p. 125-136, 2001.

COMPANHIA DE PESQUISA DE RECURSOS MINERAIS – CPRM. **Projeto Aerogeofísico Pernambuco – Piauí**. Relatório Final do Levantamento e Processamento dos Dados Magnetométricos e Gamaespectométricos. CPRM, 2006.v. 1. 268p.

DELGADO, L.M.; SOUZA, J.D. **Projeto Cobre Curaçá.** Gologia Econômica do Distrito Cuprífero do Rio Curaçá, Bahia, Brasil. Relatório Final. CPRM. 1975. V I A. DNPM/CPRM.

EFIMOV, A.V. Multiplikativnyj pokazatel dlja vydelenija endogennych rud poaerogamma-spektrometriceskim dannym. In: Metody rudnoj geofiziki, edited by: Naucno-proizvodstvennoje objedinenie **"Geofizika"** Leningrad. 1978.

FORD, A.; HART, C.J.R. Mineral potential mapping in frontier regions: a Mongoliancase study. **Ore Geol. Rev**. n.51, p.15–26, 2013.

FRAGUAS, S. 2012. Evolução da Mina Caraíba, Bahia. In: **Simexmin:** novos casos de sucesso em exploração mineral e desenvolvimento de minas no Brasil. 2012. CD-ROM.

FRANKLIN, J.M.; LYDON, J.W.; SANGSTER, D.F. Volcanicassociated massive sulfide deposits. In: SKINNER B.J. (ed.). **Economic Geology**, 75th Anniversary Volume, Denver, Society of Economic Geologists, 1981. p. 485-627.

FUCK, R.A. et al. 1993. As faixas de dobramentos marginais do Cráton do São Francisco: síntese do conhecimento. In: DOMINGUEZ, J.M.L.; MISI, A. (eds). **O Cráton do São Francisco**. SBG/SGM/CNPq, Salvador, 1993. p.121-146.

GARCIA, P.M.P. **Metalogênese dos Depósitos Cupriferos de Caraíba, Surubim, Vermelhos e Sussuarana, Vale do Curaçá , Bahia, Brasil**. 2013. 223f. Tese (Mestrado) – UFBa, Salvador, 2013.

GOMES, H.A. **Programa de Levantamentos Geológicos Básicos do Brasil**. Serra Talhada, Folha SC.24-Z-C. Brasília,CPRM, Mapa geológico, escala 1:250.000. 198. 1 CD-ROM.

GRAINGER, C.J. et al. Metallogenesis of the Carajás mineral province, southern Amazon craton, Brazil: varying styles of Archean through Paleoproterozoic to Neoproterozoic base- and precious-metal mineralization. **Ore Geology Reviews**, n.33, p.451-489, 2008.

GROVES D.I. et al. Iron Oxide Copper-Gold (IOCG) deposits through Earth history: implications for origin, lithospheric setting and distribition from other epigenetic iron oxide deposit. **Economic Geology,** n.105, p. 61-656, 2010.

HITZMAN, M.W., 2000. Iron oxide-Cu-Au deposits: what, where, when, and why. In: PORTER, T.M. (ed.). **Hydrothermal iron oxide copper-gold and related deposits**: a global perspective, Adelaide, Australian Mineral Foundation, 2000. p. 9-25.

HITZMAN, M.W.; ORESKES, N.; EINAUDI, M.T. Geological characteristics and tectonic setting of Proterozoic iron oxide (Cu-U-Au-REE) deposits. **Precambrian Res**, 58:241–287, 1992.

HORNBY, P.; BOSCHETTI, F.; HOROWITZ, F. G. Analysis of potential field data in the wavelet domain. **Geophysical Journal International,** n.137, v.1, p.175-196, 1999.

HÜHN, S. R. B. et al. Geology of the Riacho do Pontal iron oxide copper-gold (IOCG) prospect, Bahia, Brazil: hydrothermal alteration approached via hierarchical cluster analysis. **Brazilian Journal of Geology**, n.44, v.2, p. 309-324, June 2014.

HÜHN, S.R.B. et al. Caracterização geológica do prospecto de óxido de ferro-cobre-ouro (IOCG) Aurora, Ceará, Brasil. **Revista Brasileira de Geociências**, n.41, v.3, p. 525-538, 2011.

HÜHN, S.R.B.; NASCIMENTO, J.A.S. São os depósitos cupríferos de Carajás do Tipo Cu-Au-U-ETR?. In COSTA M.L., ANGÉLICA R.S. (Coords). **Contribuições a Geologia da Amazônia**. Belém. FINEP.SBG-NO. 1997. p.143-160.

JULIANI, C.; MONTEIRO, L.V.; FERNANDES, C.M.D. Potencial mineral: cobre. In **Recursos Mineral do Brasil**: problemas e desafios. 2016. 134-153p.

LEE, S. Application and verification of fuzzy algebraic operators to landslide susceptibility mapping. **Environmental Geology**, n.52, v.4, p. 615 – 623, 2007.

LI, J.Y. et al. Crustal tectonic frame work of northern Xinjiang and adjacent regions and its formation. **Acta Geologica Sinica**, n.80, p. 148-168, 2006.

LINDENMAYER Z.G. Depósito de Cu-Au do Salobo,Serra dos Carajás: Uma revisão. In: RONCHI, L.H.; ALTHOFF, F.J. (eds.). **Caracterização e modelamento de depósitos minerais.** Ed. Unisinos, 2003. p. 69-98.

LINDENMAYER, Z.G. **Evolução geológica do Vale do Curaçá e dos corpos máfico-ultramáficos mineralizados a cobre**. 1981. 140f. Dissertação (Mestrado) - UFBA, Salvador, 1981.

MAAS, M.V.R. et al. Aplicação da geofísica aérea na exploração mineral e mapeamento geológico do setor sudoeste do Cinturão Cuprífero Orós-Jaguaribe. **Revista Brasileira de Geociências**, n.33, v.3, p.279-288, 2003.

MACHADO, M.A. **Caracterização Descritiva e Genética de Ocorrências Cupro-Hematíticas no Setor Sudoeste do Sistema Orós-Jaguaribe Província Borborema**. 2006. 100f. Dissertação (Mestrado) - Universidade de Brasília, Brasilia, 2006.

MONTEIRO, L.V.S. et al. Spatial and temporal zoning of hydrothermal alteration and mineralization in the Sossego iron oxide–copper–gold deposit, Carajás Mineral Province, Brazil: Paragenesis and stable isotope constraints. **Mineralium Deposita**, n.43, p.129-159, 2008.

NAGHIBIAN, M. N. The analytic signal of two-dimensional magnetic bodies with polygonal cross-section: Its properties and use for automated anomaly interpretation. **Geophysics**, v.37, p.507-517, 1972.

NYKÄNEN, V. et al. Reconnaissance-scale conceptual fuzzy-logic prospectivity modelling for iron oxidecopper – gold deposits in the northern Fennoscandian Shield, Finland. **Australian Journal of Earth Sciences**, n.55, v.1, p.25-38, 2008.

OLIVEIRA, E.P. et al. Geologic correlation between the Neoproterozoic Sergipano Belt (NE Brazil) and the Yaoundé Belt (Cameroon Africa). **Journal of African Earth Sciences,** n.44, p. 470-778, 2006.

OLIVEIRA, E.P; TARNEY, J. Genesis of the copper-rich Caraiba norite – Hypersthenite Complex. Brasil. **Mineralium Deposita**, n.30, p.351-373, 1995.

OLIVEIRA, R.G. **Arcabouço Geofísico, Isostasia e Causas do Magmatismo Cenozóico da Província Borborema e de sua margem Continental (Nordeste do Brasil).** 2008. 411f. Tese (Doutorado) – UFRN, Natal, 2008.

OLIVEIRA, R.G.; MEDEIROS, V.C. Contrastes geofísicos e heterogeneidade crustal do terreno Pernambuco-Alagoas, Província Borborema, NE Brasil. In: SBG-Núcleo Nordeste, Simpósio de Geologia do Nordeste. 17. Recife. **Resumos...** Boletim 16. 2000. p 176.

OSTROVSKY, E.A. Antagonism of radioactive elements in wallrock alteration fields and its use in aerogamma spectrometric prospescting. **International Geology Review,** n.17, p. 461-468, 1975.

PIRES, A.C.B. Identificação geofísica de áreas de alteração hidrotermal, Crixás-Guarinos, Goiás. **Revista Brasileira de Geociências**, v. 25, p. 61−68, 1985.

POLLARD, P.J. Sodic–(calcic) alteration in Fe-oxide–Cu–Au districts: an origin via unmixing of magmatic H2O-CO2-NaCl + CaCl2-KCl fluids. **Miner. Depos**., n.36, p.93-100, 2001.

PORWAL, A.; CARRANZA, E.J.M.; HALE, M. Knowledge-driven and data-driven fuzzy models for predictive mineral potential mapping. **Nat. Resour. Res**., n.12, p.1, p.1–25, 2003.

RAINES, G.L.; BONHAM-CARTER, G.F.; KEMP, L.D. **Weights of evidence:** an arcview extension for predictive probabilistic modeling: ArcUser, ESRI, 2000.

RAINES, G.L.; SAWATZKY, D.L.; BONHAM-CARTER, G.F. **New fuzzy logic tools in ArcGis 10**: ArcUser, ESRI, 2010. 13 p.

ROEST, W. R.; VERHOEF, J.; PILKINGTON, M. Magnetic interpretation using the 3-D analytic signal. **Geophysics**, n.57, v.1, p. 116–125, 1992.

SÁ, E.F Jardim de. **A Faixa Seridó (Província Borborema, NE do Brasil) e o seu significado geodinâmico na Cadeia Brasiliana/Pan-Africana.** 1994. 803f. PhD (Thesis) - Brasília, Instituto de Geociências,Universidade de Brasília, Brasília, 1994.

SÁ, E.F Jardim de; MACEDO, M.H.F.; FUCK, R.A. Terrenos Proterozóicos na Província Borborema e a margem norte do Cráton São Francisco. **Rev. Bras. Geoc**., n.22, p.472-480, 1992.

SANTOS E.J. Ensaio preliminar sobre terrenos e tectônica acrescionária na Província Borborema. In: SBG. 39º Congresso Brasileiro de Geologia. 39.,199l. Salvador. **Anais...,** 1996. p. 47-50.

SANTOS, E.J.; OLIVEIRA, R.G.; PAIVA, I.P. Terrenos do Domínio Transversal da Província Borborema: controles sobre acresção e retrabalhamento crustais ao sul do Lineamento Patos. In: SBG, Simp. Geol. Nord., 17**, Resumo…** 1997. p. 11-14.

SAUNDERS, D.F.; TERRY, S.A.; THOMPSON, C.K. Test of National Uranium Resource Evaluation gamma-ray spectral data in petroleum reconnaissance. **Geophysics**, n.52, v.11, p. 1547-1556, 1987.

SAWATZKY, D. L. et al.. **ARCSDM3.1**: ArcMAP extension for spatial data modelling using weights of evidence, logistic regression, fuzzy logic and neural network analysis. 2004. Disponível em: <http://www.ige.unicamp.br/sdm/ArcSDM3.1.>. Acesso em: 10/11/2015

SHRIVER, A. N. Vale S.A. Internal report. Riacho do Pontal, Bahia. **Geochemistry Review**, 2009. 11p.

SILVA, A.M. et al. Predictive Geophysical Model for Gold mineralization in the Quadrilátero Ferrífero, Brazil: the case of Cuiabá **Revista Brasileira Geociências**, Brasília, n.30, v.3, p.539-542, 2000.

TALLARICO, F.H.B. et al. Geology and SHRIMP U–Pb geochronology of the Igarapé Bahia deposit, Carajás copper–gold belt, Brazil: an Archean (2.57 Ga) example of iron–oxideCu–Au–(U– REE) mineralization. **Economic Geology**, n.100, p.7–28, 2005.

TEIXEIRA, J.B.G. et al. Depósitos de cobre do Vale do Rio Curaçá, Bahia. In: BRITO, R.S.C.; SILVA, M.G.; KUYUMJIAN, R.M. (eds.). **Modelos de depósitos de cobre do Brasil e sua resposta ao intemperismo**. Brasília: CPRM, 2010. 190 p.

VALE S.A., 2009. GANFK – Programa Cu-Ni Brasil, Alvo Riacho do Pontal – Ba, Informe Executivo, Vale, Relatório interno. Agosto de 2009. 15p.

WILLIAMS, P.J. et al. Iron oxide-copper-gold deposits: Geology, spacetime distribution, and possible modes of origin. In: J.W. Hedenquist, J.F.H. Thompson, R.J. Goldfarb, J.P.Richards (eds.) **100th Anniv**. Vol. Econ. Geol., SEG, p. 371-405, 2005.

WILLIANS, P. J. 'Magnetite-Group' IOCGs with Special Reference to Cloncurry (NW Queensland) and Northern Sweden: Settings, Alteration, Deposit Characteristics. **Fluid Sources and Their Relationship to Apatite-Rich Iron Ores. Short Course Notes**, v. 20, p. 23-38, 2010. Canada: Geological Association of Canada.

XAVIER, R. P. et al. The iron oxide copper-gold deposits of the Carajas mineral province, Brazil: An updated and critical review. In: Porter TM (ed.) Hydrothermal Iron Oxide Copper–Gold and Related Deposits. **A Global Perspective**, v. 3, p. 285-306, 2010. Adelaide: PGC Publishing.

XAVIER, R.P. et al. Tourmaline B-isotopes fingerprint marine evaporates as the source of highsalinity ore fluids in iron oxide-copper-gold deposits, Carajás Mineral Province (Brazil). **Geology,** n.36, p.743-746, 2008.

CAPITULO 2

"MAPPING NEW IOCG MINERAL SYSTEMS IN BRAZIL: THE VALE DO CURAÇÁ AND RIACHO DO PONTAL COPPER DISTRICTS"

SÉRGIO ROBERTO BACELAR HUHN & ADALENE MOREIRA SILVA

Submetido *ao periódico "ORE GEOLOGY REVIEWS".*

MAPPING NEW IOCG MINERAL SYSTEMS IN BRAZIL: THE VALE DO CURAÇÁ AND RIACHO DO PONTAL COPPER DISTRICTS

Sérgio Roberto Bacelar Huhn [1,2]*, Adalene Moreira Silva[1] and Francisco José Fonseca Ferreira [3].

1 - Instituto de Geociências, Universidade de Brasília, Brasília, DF, 70910-900, Brazil.

2 - VALE S/A, Rodovia BR-381/km 450, 33040-900, Santa Luzia, MG, Brazil.

3 - Universidade Federal do Paraná, Laboratório de Geofísica Aplicada. PO Box 19045, 81531-980. Curitibá- PR, Brazil.

*Corresponding author

Abstract

Integration of geophysical and geologic data identify important geological, structural and metallogenetic characteristics related to the Proterozoic Riacho do Pontal and Vale do Curaçá iron-oxide copper gold (IOCG) mineral systems in northeast Brazil. The Vale do Curaçá and the Riacho do Pontal Copper Districts are located within the northern part of the Archean São Francisco Craton and represent two pulses of mineralization. An older magmatic event associated with the Caraíba Cu deposit, which is located within the Vale do Curaçá District, is related to Paleoproterozoic (ca 2 to 2.2 Ma) hydrothermal processes. A younger, Neoproterozoic (ca 750 to 570 Ma) episode of volcanism and associated plutonism, is represented by the Riacho do Pontal mineral district. Seismic tomography data across east-central Brazil shows the multi-age Carajás Province, Vale do Curaçá and Riacho do Pontal IOCG districts, sit along either side of a prominent northwest-trending upper lithospheric high velocity zone. The edges of the high velocity zone point to long-lived subparallel trans-crustal structures that have been the focus of multiple reactivations and IOCG mineralization events. Regional gravity and magnetic maps show the Vale do Curaçá Copper District is located in an area of increased gravity over a 110 by 22 km area and includes a high amplitude -34 mGal gravity anomaly associated with the Caraiba IOCG deposit, which has an average of density of 3.13 g/cm^3 in contrast with the lower density (2.98 g/cm^3) non-mineralized host rocks. The gravity anomaly signature over the Riacho do Pontal Copper District is characterized by a 40 km long NW-SE trending Bouguer anomaly low. Geologically, the district contains low density gneiss outcrops of Sobradinho Remanso and the southern portion of the Riacho Seco

Complex. The Ria4 occurrences of the Riacho do Pontal Copper District are located on these regional low-gravity domains. Data from regional airborne magnetic and ground gravity surveys were inverted to magnetic susceptibility and density, respectively, over the known districts. Results show that the Caraiba deposit is characterized by a coincident dense and magnetic source that dips at a low angle to depths approximately 1,5 km with structural control due to a shear fault. The 3D models show two main NNW prospective trends. Trends I and II have a sigmoidal shear shape and are positioned in the contact zone between domains with high magnetic susceptibility (SI >0.005) and density (> 3,4g/cm^3). Trend I is 60 by 7 km and hosts the Caraíba, Surubim and Vermelho copper mines and other minor deposits. Results obtained from the 3D magnetic inversion model in the region of the Riacho do Pontal district show weak magnetic anomaly highs that extend along a NW-SE gradient trend. The magnetic gradient is related to mapped shear zones that overprint older and deeper NE-SW features of the São Francisco cratonic root.

Introduction

Magnetic and gravity anomaly signatures related to magnetite and hematite-rich Cu ore zones have led the mining community and other researchers to use these data as an effective exploration tool to find new IOCG deposits (HAYWARD et al., 2016; SMITH, 2002; CLARK et al., 2013; CLARK, 2014). World-class iron oxide copper-gold (IOCG) deposits express their metallogenic footprint in different tectonic settings geophysically with variable volumes of associated alteration and metal endowments Pollard et al. (2018; HITZMAN et al, 1992; BARTON, 2014; GROVES et al., 2010). IOCG mineralization is often controlled by shear system zones and with high concentrations of magnetite and/or hematite. Frequently, the geometry and structural control of mineralized trends are related to secondary structures, transpression sites and orebody plunges along stretching lineations (O'DRISCOLL, 1985; HITZMAN, 2000; GROVES et al., 2016). These important geologic features of IOCG mineralization are often expressed in physical property changes related to density, magnetization, and seismic velocities at a wide range of scales.

Geologic characteristics of world-class Brazilian IOCG deposits are distinct and show the complex interplay between geologic structure, fluid flow and hydrothermal alteration types (LINDENMAYER, 1981; LINDENMAYER, 1982; HUHN; NASCIMENTO, 1997;

REQUIA et al., 2003; TALLARICO et al., 2005; DREHER et al., 2008; MONTEIRO et al., 2008a, 2008b; TEIXEIRA et al., 2010b; XAVIER et al., 2010, 2012; MELO et al., 2016; HUHN and SILVA, 2018). For example, the flow of mineralized fluids along regional shear zones is responsible for the sigmoidal "sigmoidal-shape" structural pattern/magnetic signature of the Carajás Province and of the Vale do Curaçá District (HOLDSWORTH; PINHEIRO, 2000; LINDENMAYER, 1982).

The Vale do Curaçá (VC) and Riacho do Pontal (RP) Cu districts host Cu as the primary commodity along with Au, Fe and Cr and other metals (TEIXEIRA et al., 2010a, JULIANI et al. 2016; Fig.2.1) Previous studies characterized the Cu deposits as magmatic. According Lindenmayer (1981) the mineralization is exclusively hosted in orthopyroxenite. High concentrations of sulfides, however, can also occur in norite, biotitite as well as in calcsilicate rock. Recently, new geologic (TEIXEIRA et al., 2010a, HUHN et al., 2014, HUHN & SILVA, 2018, JULIANI et al. 2016, GARCIA et al., 2018), tectonic (Silva et. al. 1996, TEIXEIRA et al., 2010a) , isotopic and geochemical (GARCIA et al., 2018) studies have shown evidence that the copper mineralization is related to the diverse family of IOCG deposits. In the last 10 years, high-resolution airborne geophysical surveys have been completed. The geophysical effort has motivated new exploratory campaigns in both districts. However, despite the increase in modern airborne geophysical coverage and geologic mapping, there remains a low discovery rate that identifies new IOCG deposits. The low discovery rate is partly due to the absence of a modern mineral systems approach followed by a systematic exploration program that includes higher density exploration drilling. Additional challenges exist in that the shallower deposits have been discovered and the major efforts are focused on exploration under cover.

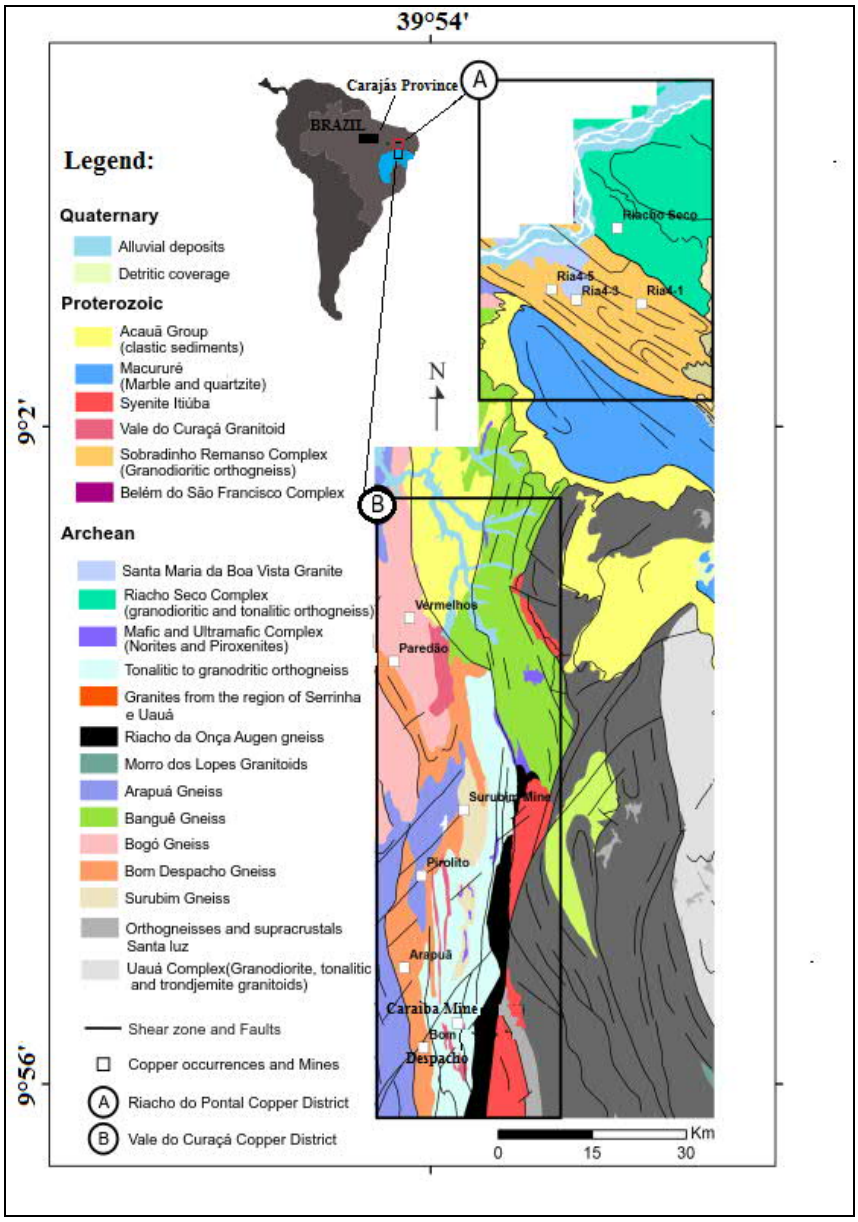

Figure 2.1. Geologic map showing the study location and (A) the Riacho do Pontal and (B) the Vale do Curaça copper districts. Major Cu mines and occurrences are shown. (Modified after Teixeira et. al. 2010a).

Both the Vale do Curaçá and Riacho do Pontal Copper Districts can be considered one of the most important areas for IOCG prospectivity in Brazil. Globally, IOCG deposits are a significant source of base and precious metal wealth that is key to supporting and expanding economic growth. In particular, the Vale do Curaçá Copper District, which occupies an area of approximately 2000 km^2, is the one of the most significant mining district in Brazil, having produced in 2018 30KT of copper contained. Approximately 300 Cu occurrences and prospects have been mapped. The District includes total resources of 42.4 MT @ 1.71% Cu

(MENDONCA et al., 2018). The most productive Cu deposits at Vale do Curaçá are: Caraíba-Pilar (24,8 Mt @ 1.9% Cu), Vermelhos (4,52 @ 3,4 % Cu - underground), Surubim (4,5 MT@ 1,04% Cu), R22 W (283.000 T @ 0,54% Cu; MENDONCA et.al. 2018).

Even with these large metal endowments, there is a lack of knowledge that provides broad insight into the how the deposits formed and the larger mineral systems that were active during their emplacement. In a previous study, Huhn and Silva (2018) used multi-parameter geologic, geochemical, remote sensing, and airborne geophysical data to statistically identify new areas of IOCG prospectivity related to shallow mineralization along the northern border of the São Francisco Craton (Fig.2.1). Areas of known mineralization and areas of new prospectivity were identified in map form. The study presented here expands on this previous work in three ways. First, magnetic and gravity maps are interpreted, in concert with new geologic information, to map the deep crustal and lithospheric controls on Cu mineralization. Secondly, regional magnetic and gravity data are inverted to 3D models of magnetic susceptibility and density, respectively, to understand the concealed geology related to physical property distributions and geometries underlying the districts. Third, seismic tomography data are analyzed to place the Vale do Curaçá and Riacho do Pontal IOCG districts in a tectonic and cratonic framework and to characterize potential lithospheric controls of the mineral provinces. Our objective is that these approaches will lead to an advanced understanding of the mineral system(s) that controlled the emplacement of the northeast Brazil IOCG mineral districts.

Purpose and Scope

The purpose of our study is to synthesize available regional magnetic, gravity, and seismic tomography data with geologic information to evaluate the two- and three-dimensional geologic and tectonic setting of the Curaçá and Riacho do Pontal IOCG Districts. An overarching goal of our study is to develop a better understanding of the deep crustal and lithospheric structural controls that provided controls for the Paleoproterozoic and Neoproterozoic mineralization events. Fundamental questions we hope to address are (1) Did IOCG mineralization occur at similar crustal levels for both districts?; (2) What are the deposits main structural controls?; (3) Can we extend our findings to map other areas of IOCG prospectivity within mobile belts situated along the border of São Francisco Craton?

Geologic Setting and Mineralization

Classification as IOCG Deposits

Pioneering studies on the Caraíba Cu deposit within the Vale do Curaçá Mining District emphasized orthomagmatic processes as responsible for the genesis of Cu mineralization (LINDENMAYER, 1981; LINDENMAYER, 1982; SILVA et al., 1996). Maier and Barnes (1999) noted the unusual aspects of the Caraíba deposit shared similarities with other Cu deposits of magmatic origin that include a) the presence of primary sulfides including bornite and chalcopyrite; b) the presence of large amounts (> 50 wt %) magnetite; c) high Cu/Ni ratio (~ 40); and d) orthopyroxenites with abundant biotite related to shear zones. The importance of metasomatic processes in the genesis of the Caraíba deposit was initially suggested by Rocha (1999) and more recently confirmed by Teixeira et al (2010b), who proposed the style of mineralization of deposits in the Vale do Curaçá Copper District is analogous to other IOCG deposits worldwide.

Early studies of Cu deposits in the Riacho do Pontal District has been characterized, in the region of Riacho Seco, as type VMS by several authors (CPRM 2001, GARCIA, 2017). Huhn et. al. (2014) and Huhn and Silva (2018) have used the following criteria to associate the mineralizations of the Riacho do Pontal copper occurrences as IOCG deposits: a) it is strongly associated with potassic and albite alteration, b) copper ore is hydrothermal and epigenetic, closely associated with shear zones; c) presence of hydrothermal iron oxides spatially and temporally related to copper orebodies; d) mineralization that is not spatially related to proximal granites.

Paleoproterozoic Vale do Curaçá copper District

Since the beginning of the last century, the Vale do Curaçá Copper District (‘B’ in Fig. 2.1) has been the focus of intense geologic mapping and exploration activity. During the 1970’s, a mineral exploration boom occurred in this region. The focus of the exploration program was Cu in volcanic-hosted massive sulfide mineralization (VMS) (FRANKLIN et. al., 1981; BARRIE; HANNINGTON, 1999) in greenstone belts and Cu mineralization hosted in mafic-ultramafic layered complexes (DELGADO; SOUSA, 1975; LINDENMAYER,

1982). The exploration activities led to the discovery of the Caraíba mine, which is the largest mine in the district. In addition, a series of copper deposits and occurrences in the Vale do Curaçá District were discovered. Approximately 300,000 meters of drilling has occurred in the mining district (FRÁGUAS, 2013).

The geology of the Vale do Curaçá copper district (B, in Fig. 2.1) consists mainly of rocks belonging to the Itabuna-Salvador-Curaçá Orogen (ISCO, ca 2 to 2.2 G.a). The ISCO is located east of the Gavião and Jequié blocks and west of the Serrinha Block (Fig. 2,2) and represents an 800 km-long belt of Archean to Paleoproterozoic high metamorphic grade granulitic rocks (BARBOSA; SABATÉ, 2004; TEIXEIRA et al., 2010a). These rocks were deformed and metamorphosed due to the collision of the Gavião, Jequié and Serrinha blocks (PADILHA; MELO, 1991; BARBOSA; 1990; BARBOSA; DOMINGUEZ, 1996; TEIXEIRA et al., 2010b) and present high metamorphic grade and syntectonic granites (OLIVEIRA et al., 2004). Shrimp U/Pb ages of 2,695 ±12 Ma were obtained in granulitic rocks at the Caraíba Complex (TEIXEIRA et al., 2010b) and 2,072 Ma for the metamorphic event (OLIVEIRA et al., 2004).

The detailed geology of the Curaçá copper District comprises Tanque Novo and Caraíba Complexes. The Tanque Novo Complex consists of Bom Despacho, Arapuá, Surubim and Bogó Gneissic rocks (LINDENMAYER, 1981) consisting mainly of feldspathic quartz gneiss, cordierite-garnet-biotite gneiss, amphibolite, and magnetite (quartzite)-rich rocks (LINDENMAYER, 1981; TEIXEIRA et al., 2010b). The Caraíba Complex contains tonalite to granodiorite bodies. A series of mafic-ultramafic bodies were individually intruded into the supracrustal rocks. These rocks have undergone episodes of deformation, metamorphism and related granitic intrusion. Uranium-lead SHRIMP dates of ultramafic rocks within the Caraíba mine show the rocks formed at ca 2,580 ± 10 Ma (OLIVEIRA et al., 2004).

Shear zones have been mapped along the Vale do Curaçá District and are often marked by intense biotite-rich rocks related to mylonitic rocks. These zones are characterized by two phases of progressive deformation (ROCHA, 1999; SILVA et al., 2007): a) The first phase (D1) represents transpressive thrust structures showing convergence to the west. The associated metamorphism was in the amphibolite to granulite facies. b) The D2 phase was related to directional shear zones with closed N-S isoclinal folds and penetrative vertical shearing structures. Kinematic studies indicate that D1 was overprinted by sinistral strike-slip shear zones (SILVA et al., 1996; TEIXEIRA et al., 2010a). These shear zones were

responsible for the positioning of mylonitized granites and the intense fluid flux. The shearing process destroyed the preexisting fabric. The main mineralization event in the Vale do Curaçá District occurred between ca 2,050 and 2,010 Ma (TEIXEIRA et al., 2010a; GARCIA et al., 2018).

Geology of the Caraiba Mine

The geology of the Caraíba Mine is well marked by the contact between the orthogneiss (G2) and mafic-ultramafic rocks. Frequently, biotite has been mapped along north-south trending geologic contacts. The supracrustal rocks include banded gneiss, diopsidite, forsterite marbles, granitiferous mafic granulite, biotite-schist and iron formations (LINDENMAYER, 1982).

The Caraíba orebody is hosted mainly in mafic-ultramafic complexes. Rocha (1999) and (TEIXEIRA et al., 2010b) recognized hydrothermal calcic-ferric alteration related to Cu-ore zones. More recent work shows an early (2580±10 Ma; Oliveira et. al. 2004) orthomagmatic mineralization overprinted by a later event that produced the IOCG mineralization at ca 2 Ga (GARCIA, 2013;GARCIA et al., 2018, TEIXEIRA et al., 2010b). Studies conducted by Silva et al (1985, 1996, 2007) found evidence for structural control at the Caraíba mine.

Ore minerals at Caraíba include chalcopyrite, bornite and chalcocite usually associated with magnetite. Intercumulus crystals of disseminated chalcopyrite, bornite and magnetite, grown in the interstices of pyroxenes and amphiboles constitute the primary (magmatic) mineralization. Minerals associated with hydrothermal alteration include biotite, microcline, epidote, chlorite, magnetite and quartz (GARCIA, 2013). The Cu ore occurs within veins, hydrothermal breccia, or within breccia with “jaguar” texture. Magnetite occurs commonly in equilibrium with spinel and ilmenite and exhibits replacement by chalcopyrite, bornite and ilmenite, especially when the host is biotite mylonite.

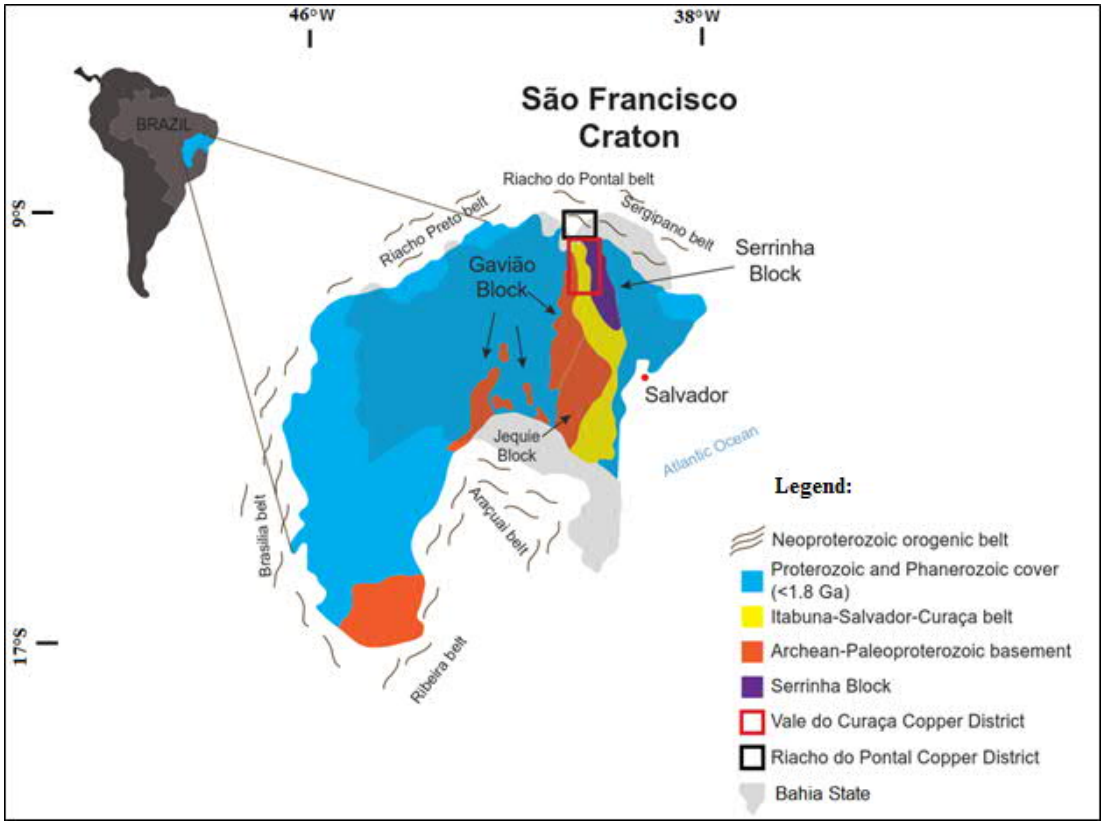

Figure: 2.2 Simplified geologic map of the São Francisco Craton (SFC) showing the locations of the Vale do Curaçá and Riacho do Pontal Copper Districts. Both districts are situated on the northern edge of the SFC in contact with Borborema Province. (Modified from Teixeira et al. (2010a).

Geology of the Neoproterozoic Riacho do Pontal Copper District

More than twenty copper occurrences have been described in the Riacho do Pontal region ("A' in Fig. 2.1; Teixeira et al. 2010a). Geologically, these occurrences are mostly located in the contact zone between the Borborema Province and the San Francisco craton (Figs. 2, 3). This area is a small slab of the ca 750 to 570 Ma Brasiliano collisional zone, which developed during the convergence of Neo- to Mesoproterozoic terrains with the São Francisco Craton (ALKMIN et al., 1993). Copper occurrences are structurally controlled by shear zones (Fig. 2.1). The Ria4 occurrences and Riacho Seco Deposit (Fig. 2.1) are the main Cu occurrences in the district.

Several alteration types related to hydrothermal processes have been identified in the Riacho do Pontal District (HUHN et al., 2014). Hydrothermal alteration has led to a pervasive calcic-potassic and calcic-ferric overprint of the host gneisses and migmatites. Early stage sodic hydrothermal is distal in relation to areas with calcic-potassic and potassic-ferric alteration with higher strain rate. Hydrothermal alteration processes led to a replacement of metamorphic minerals within banded gneiss to a suite of minerals including albite, biotite, hematite and amphibole. The replacement minerals are spatially connected to penetrative shear deformation and ore plunge along stretching lineations (HUHN and SILVA, 2018). Pyrite, hematite, chalcopyrite and chalcocite are related to the ore zones. Magnetite typically occurs in association with the Cu-ore minerals and constitutes less than 1% of the paragenesis (GARCIA et al., 2018).

The Riacho do Pontal Belt was overprinted by two main shearing events: a) D1-thrust shear zones with convergence towards the north, representing a series of northwest-trending parallel structures related to hydrothermal alteration and mineralization; and b) D2-dextral strike slip shear zones related to multiple reactivation that are responsible for strong shearing of paragneissic and orthogranitic rocks. Both events were related to transpressive structural regimes.

The Riacho do Pontal Copper District, is located at the apex of three orogenic belts including the Riacho Preto, Riacho do Pontal and Riacho Preto belts, which are located along the northern border of the Sao Francisco Craton (Fig. 2.2). The area has been placed within the Brasiliano collisional zone (from ca 750 Ma to 570 Ma), which developed during the convergence of the Neo- to Mesoproterozoic terrains of Borborema Province (Fig. 2.3) with the São Francisco Craton (ALKMIM et al., 1993). The suture is marked by a strong gravity anomaly high flanked by anomaly lows (Fig 2.4b). The positive anomaly corresponds to the lower crustal uplift of the Borborema Province, and the flanking negative anomalies correspond to lower density nappes pushed towards the Craton (OLIVEIRA, 2008). This high gravity domain coincides with the occurrence of basal-ultramafic rocks belonging to Neoproterozoic arch complexes (SÁ, 1994). According to Oliveira (2008), it is possible to observe that the supracrustal bands of the Riacho do Pontal and Sergipana bands were placed allochthon with displacements on the order of 30 to 60 km over the São Francisco Craton (SÁ et al., 1992). This overlapping structure is observed in both magnetic and gravimetric data, with the truncation and displacement of old north-south structures occurring along the border

between the São Francisco Craton and Borborema Terrain. According to Sá et al (1992), the collisional event was overprinted by transcurrent shear zones.

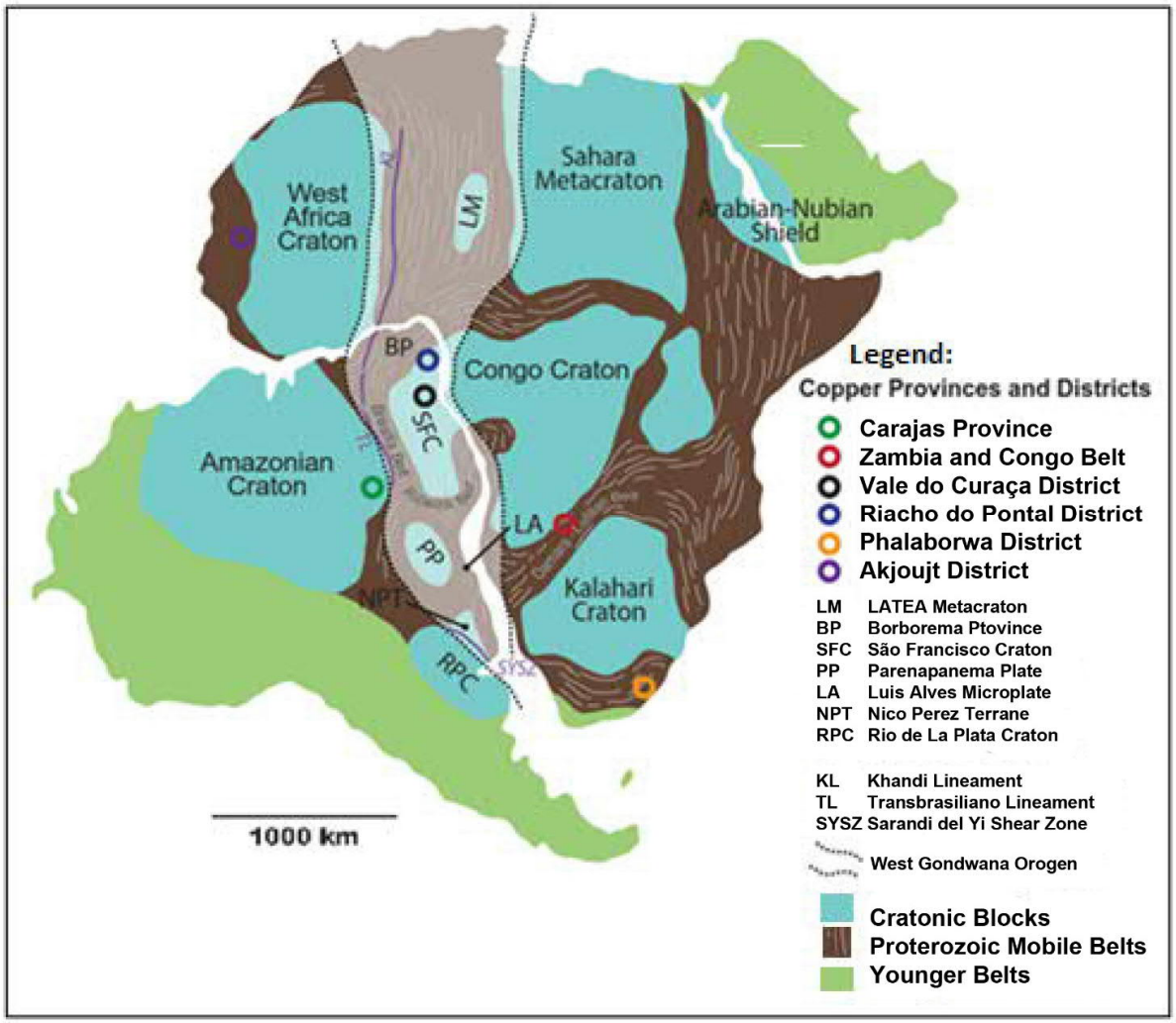

Fig. 2.3 IOCG Provinces and Districts situated in Brazil and Africa: main crustal blocks and Neoproterozoic orogenic belts in South America and Africa, including locations of the West Gondwana Orogen (Modified after GRAY et al., 2008; LIÉGEOIS et al., 2013; BRITO NEVES; FUCK, 2014; GANADE et al., 2016).

Tectonic Setting

IOCG Provinces and Districts in Brazil and Africa are situated mainly along the border of major crustal blocks and in Neoproterozoic orogenic belts (Fig. 2.3). There are at least three IOCG metallogenic provinces with different ages in Brazil that include the Carajás Province (ca 2.72 Ga and ca 2.5 Ga), the Vale do Curaçá District (ca 2 Ga), and the Neoproterozoic (ca 750 Ma – 570 Ma) districts of Riacho do Pontal and Phalaborwa District. The Carajás Mineral Province occurs within sheared felsic intrusive rocks that could represent fragments of a silicic large intrusive province (SLIP) that ranges in age from ca 2.74 to 2.55 Ga (HOLDSWORTH; PINHEIRO, 2000; POLLARD et al., 2018; GRAINGER et al., 2008).

Data

Gravity and Magnetic Data

Gravity and magnetic anomaly data over a x by x area were extracted from public databases available from the Brazilian Geological Survey (CPRM) and reduced to Bouguer gravity using procedures described in Oliveira (2008). A total of 60 stations spaced an average of 5 to 10 km apart, form the gravity database for this study (Fig. 2.4a). Given the coarse spacing of the gravity data, we expect density sources that occur at 5 km depths and beyond will be effectively resolved. The gravity data were gridded using a minimum curvature algorithm onto a 500m grid (Fig. 2.4b).

Airborne magnetic anomaly data were acquired in 2001 as part of the Riacho Seco and Andorinhas Survey that were planned and executed by the Brazilian geological Survey (CBPM, 2001). Data were collected at a nomial height above ground of 100 m along north-south flight lines spaced 500 m and east-west tie lines every 10,000. A total of 48,641 line kilometers of magnetic data were collected. The total magnetic field (TMI) flight line data were gridded onto a 250 m grid (Fig. 2.5). Given the flight-line spacing of the magnetic surveys and height at which the magnetic field measurements were observed, we would expect to resolve magnetic sources that lie at depths of 400 m and deeper (Reid, 1980).

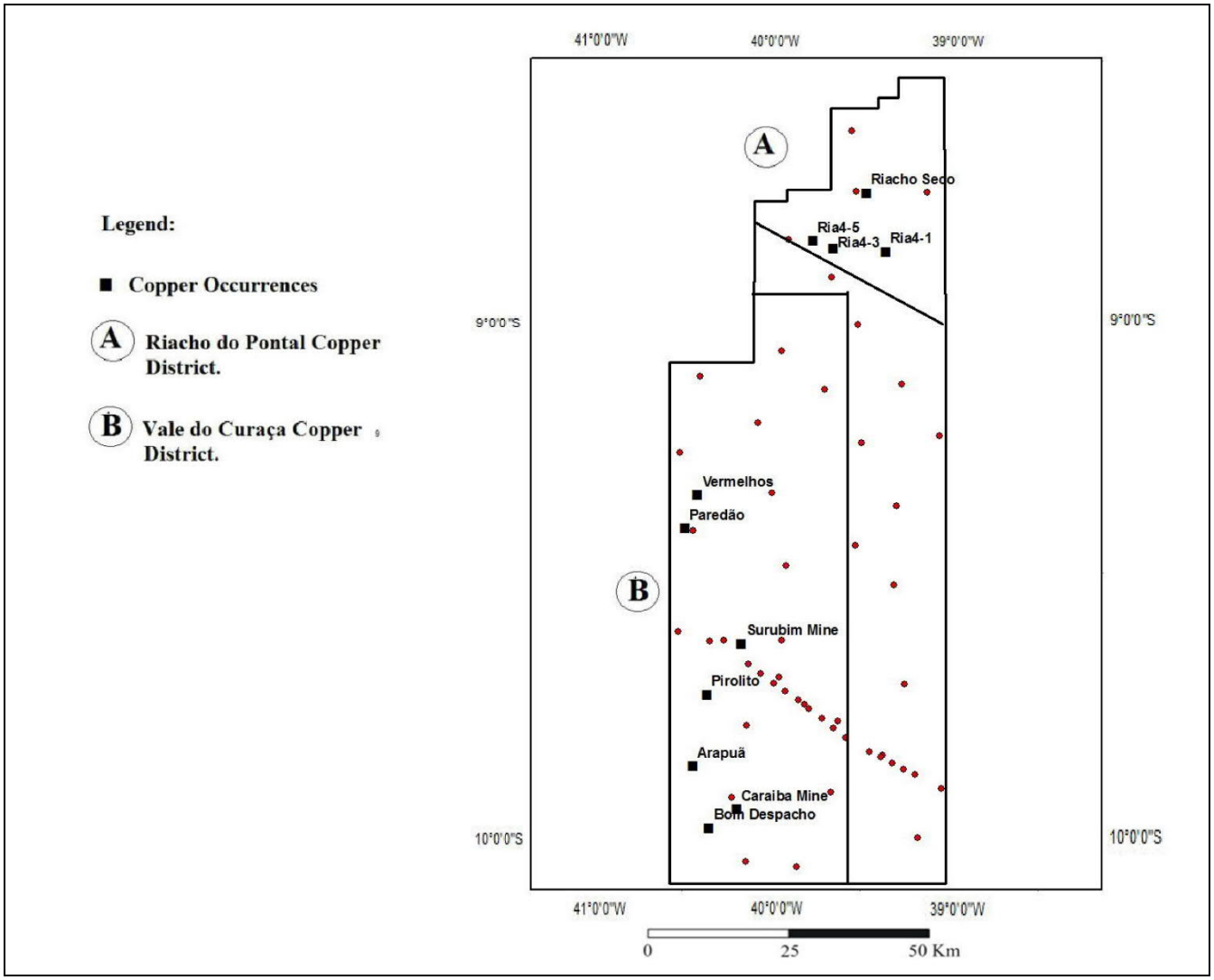
Legend:
Copper Occurrences
A Riacho do Pontal Copper District.
B Vale do Curaça Copper District.
41°0'0"W
40°0'0"W
39°0'0"W
9°0'0"S
10°0'0"S
A
B
Riacho Seco
Ria4-5
Ria4-3
Ria4-1
Vermelhos
Paredão
Surubim Mine
Pirolito
Arapuã
Caraiba Mine
Bom Despacho
0
25
50 Km

(a)

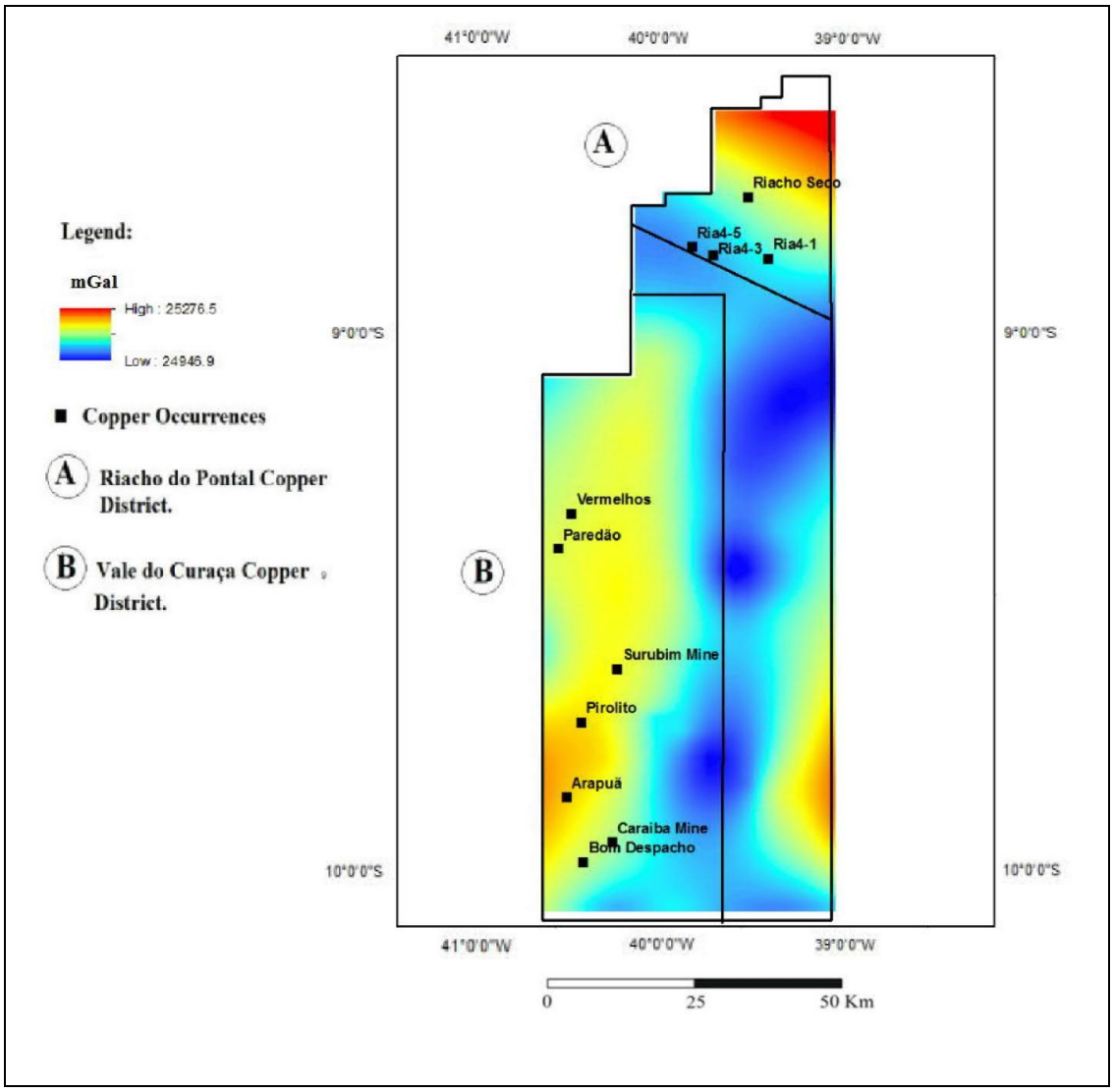

(b)

Fig..2,4. (a) Gravity stations and (b) Bouguer gravity map for the study area. Major Cu occurrences and mines are shown. Block A: the Riacho do Pontal and block B: the Vale do Curaco IOCG District.

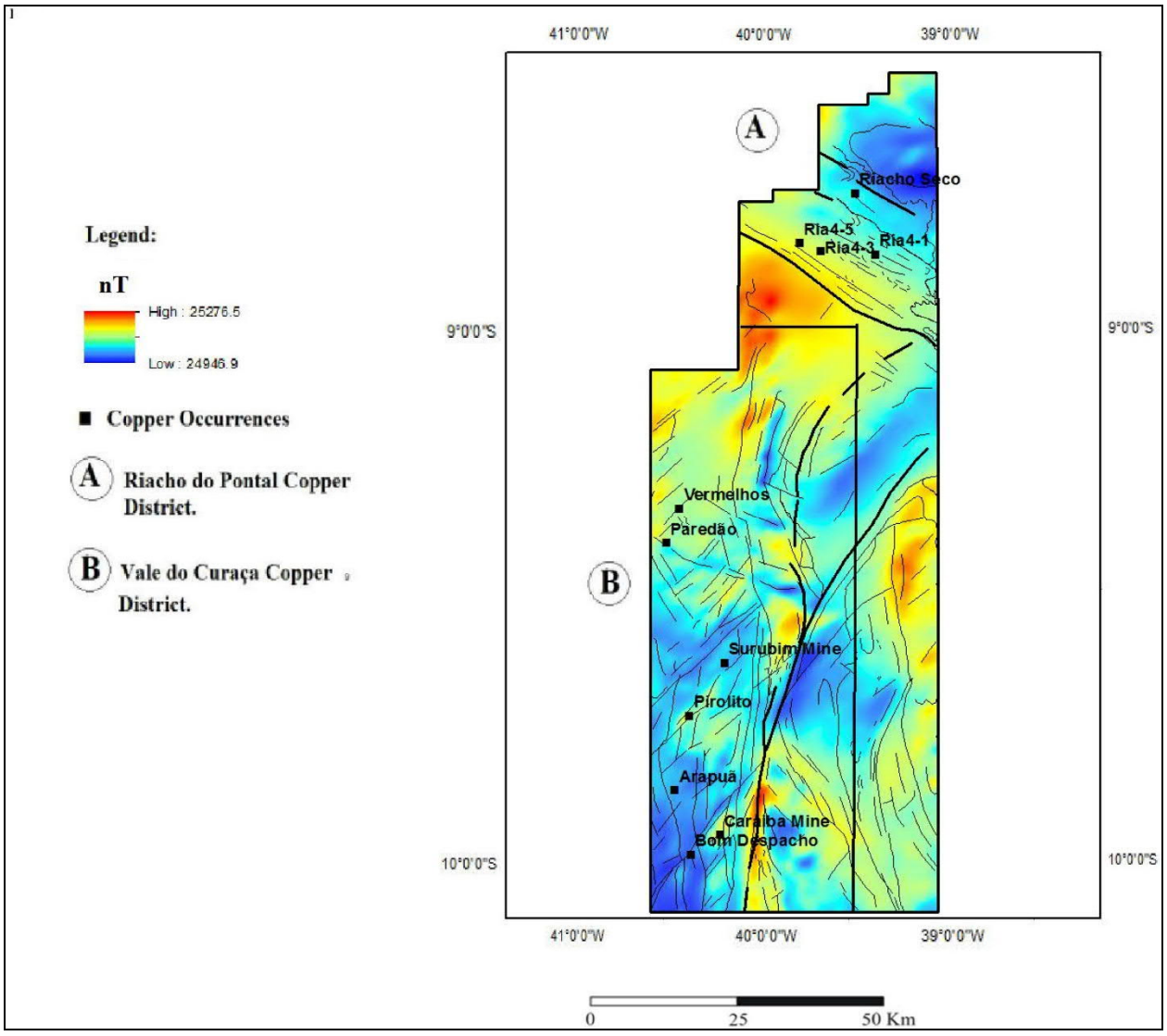

Fig. 2.5 Reduced to pole (RTP) of the total magnetic intensity (TMI) data upward continued to 1000 m above ground. Major Cu mines and occurrences are shown. Block A: the Riacho do Pontal and block B: the Vale do Curaçá IOCG District.

Derivative Products calculated from the Magnetic Data

Several derivative products were calculated from the grid of the TMI in order to enhance magnetic gradients related to deep geologic structures, map magnetic signatures of altered and unaltered rocks, and identify magnetic signatures related to deep magnetic sources. The TMI data were reduced to the magnetic north pole (RTP) using an inclination of -20º and declination of -22.31º. The RTP grid was upward continued to 1000 m above terrain in order to reduce noise caused by the low geomagnetic latitude and enhance magnetic signatures of deeper sources (Fig. 2.5).

The grid of upward continued RTP data was used to calculate the tilt angle of the total horizontal derivative (TAHG) (Ferreira et al. 2013). The TAHG transform clearly identifies tracks of high anomaly gradients that map magnetic contrasts related to geologic structures at a range of depths (Fig. 2.6a). Tracks of the TAHG ridgelines, marking major geologic structures, are shown relative to the gravity anomaly map (Fig. 2.6b).

Euler deconvolution (Thompson, 1982) solutions were calculated from the grid of the magnetic anomaly data and depths to structures (structural index = 0) are shown along major shear zones.

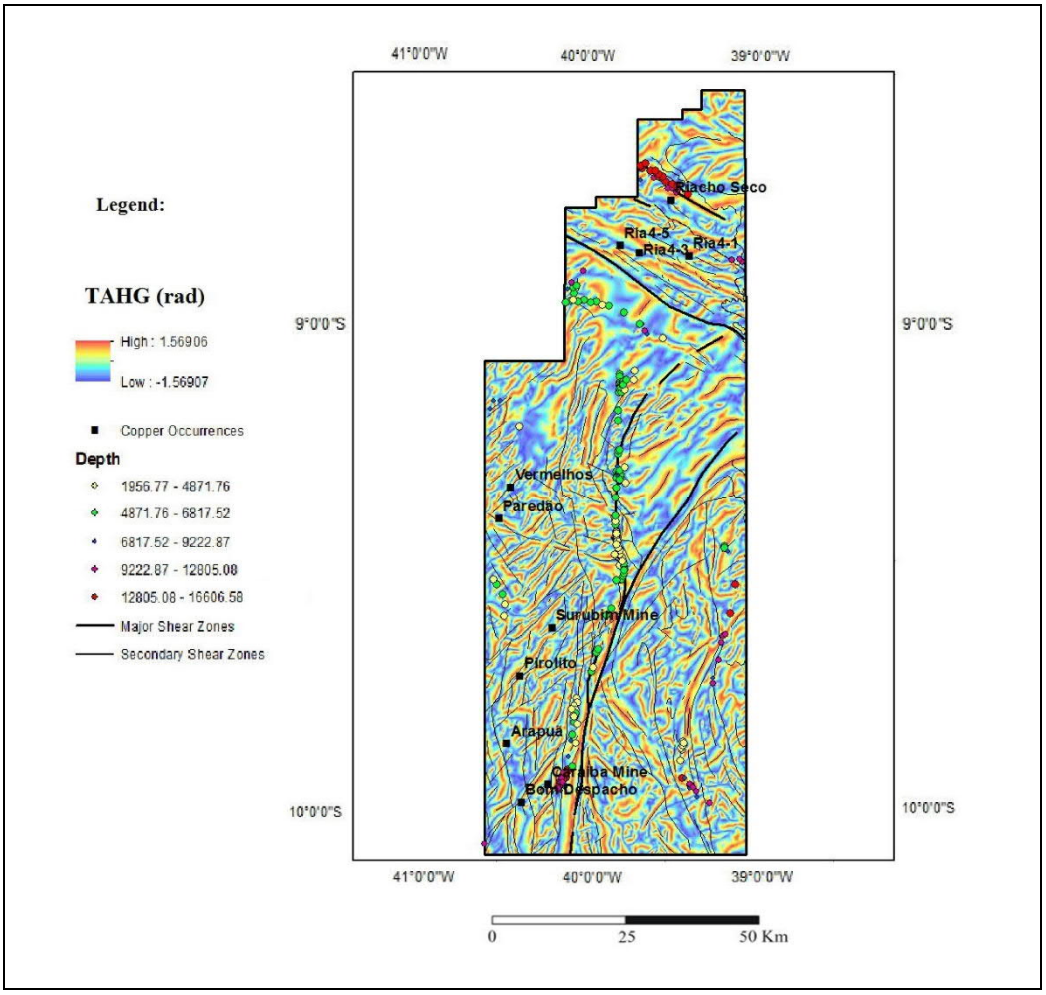

(a)

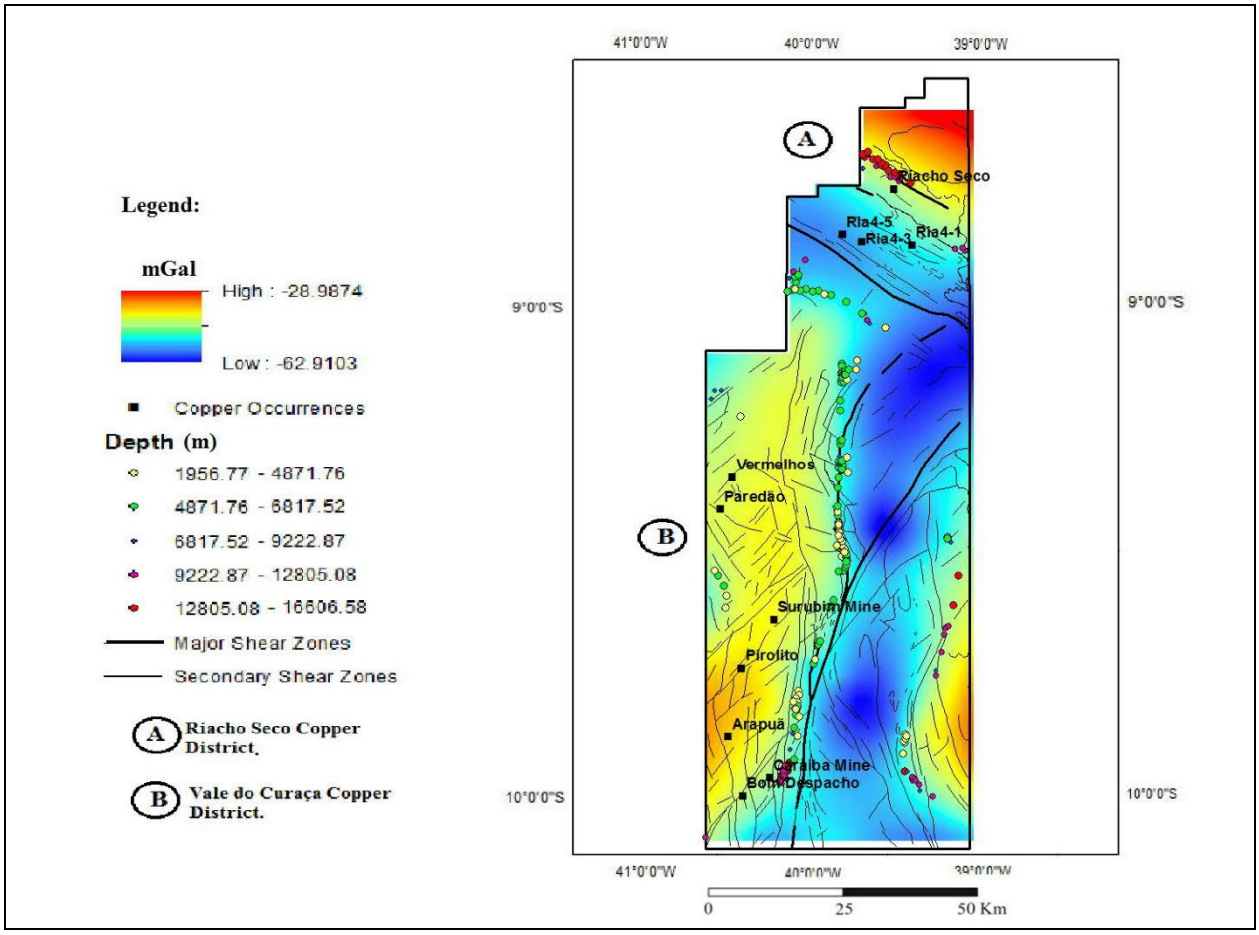

(b)

Fig.2. 6 (a) Map showing the tilt angle of the horizontal gradient (TAHG) of the reduced to pole magnetic anomaly data. (b) Bouguer gravity anomaly map with major and secondary shear structures and TAHG tracks. Both maps include estimates of magnetic structures and their depth to the magnetic structure as colored circles. Depths to the magnetic structures were calculated using the Euler deconvolution method (THOMPSON, 1982). Primary Cu districts and occurrences are shown. Block A: the Riacho do Pontal and block B: the Vale do Curaçá IOCG District.

Petrophysical Data

Magnetic susceptibility, density, and electrical resistivity data were obtained from drill cores and surface rock samples. Measurements are provided as susceptibility in $SIx10^{-3}$, volume rock density in g/cm^3, and electrical resistivity in ohm-m. Magnetic susceptibility was measured using a KT10 PLUS S/C susceptibility meter, rock density was measured by vacuum-saturating the samples, and electrical resistivity was measured with water under vacuum and left to sit for 24 h using a frequency analyzer.

Density and magnetic susceptibility were measured from drill core for 9 samples from Vale do Curaçá District (Fig. 2.7a). Thirty-three drill core samples were measured for density *PCB-RIA4-DH02*), rock types and depth sampled of Riacho do Pontal Copper District.

Table 3: Rock Types and depth of samples of Riacho do Pontal Copper District sampled from two drill holes (*PCB-RIA4-DH01 and PCB-RIA4-DH02*).

PCB-RIA4-DH01	**DEPTH (m)**	**ROCK TYPE**	***PCB-RIA4-DH00002***	**DEPTH (m)**	**ROCK TYPE**
PETRO-01	1,85	Quartz-magnetite-biotite mylonite	**PETRO-01**	2,75	Amphibole-biotite-gneiss
PETRO-02	5,50	Quartz vein	**PETRO-02**	10,60	Quartz vein
PETRO-03	8,70	Biotite mylonite	**PETRO-03**	14,30	Quartz vein
PETRO-04	10,70	Biotite mylonite	**PETRO-04**	26,30	Quartz vein
PETRO-05	13,00	Biotite mylonite	**PETRO-05**	31,80	Quartz vein
PETRO-06	21,00	Biotite mylonite	**PETRO-06**	45,69	Quartz vein
PETRO-07	2	Biotite mylonite	**PETRO-07**	6	Quartz vein

O-07	5,50			0,00	
PETRO-08	32,48	Quartz- biotite - gneiss	**PETRO-08**	73,10	Biotita-quartz vein
PETRO-09	67,70	Quartz- biotite - gneiss	**PETRO-09**	83,60	Quartz vein
PETRO-10	105,30	Quartz- biotite - gneiss	**PETRO-10**	103,50	Quartz vein
PETRO-11	158,00	Quartz- biotite - gneiss	**PETRO-11**	137,00	Biotite-quartz-gneiss
PETRO-12	167,80	Quartz- biotite - gneiss	**PETRO-12**	148,80	Biotite-quartz-gneiss
PETRO-13	173,60	Quartz- biotite - Gneiss	**PETRO-13**	168,10	Biotite-mylonite
PETRO-14	189,00	Quartz- biotite - Gneiss	**PETRO-14**	265,10	Biotite-quartz-gneiss
			PETRO-15	272,00	Biotite-quartz-gneiss
			PETRO-16	318,30	Biotite-quartz-gneiss
			PETRO-17	324,00	Biotite-quartz-gneiss
			PETRO-18	334,30	Biotite-quartz-gneiss
			PETRO-19	392,80	Biotite-quartz-gneiss

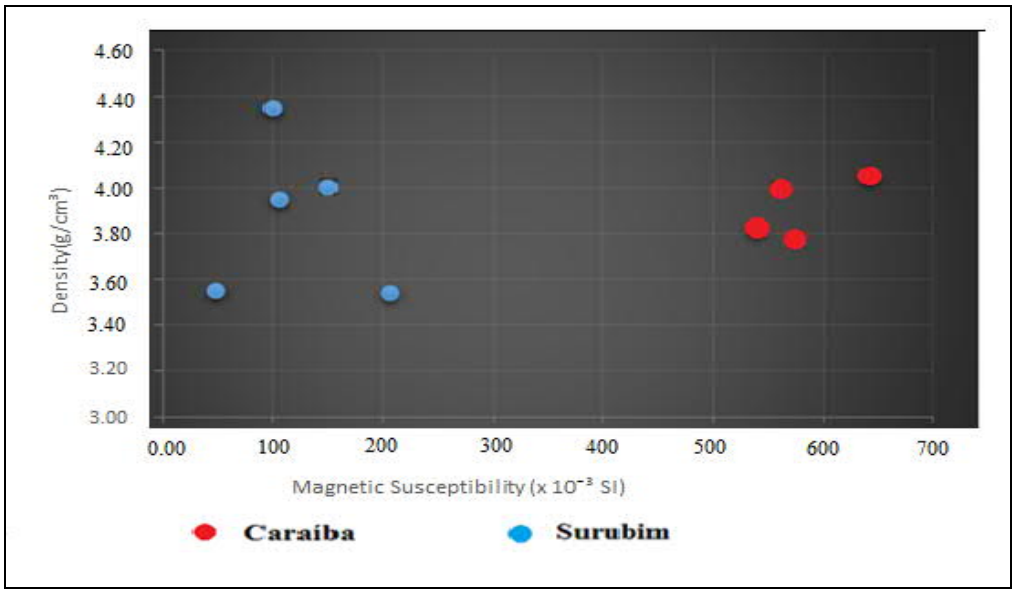

(a)

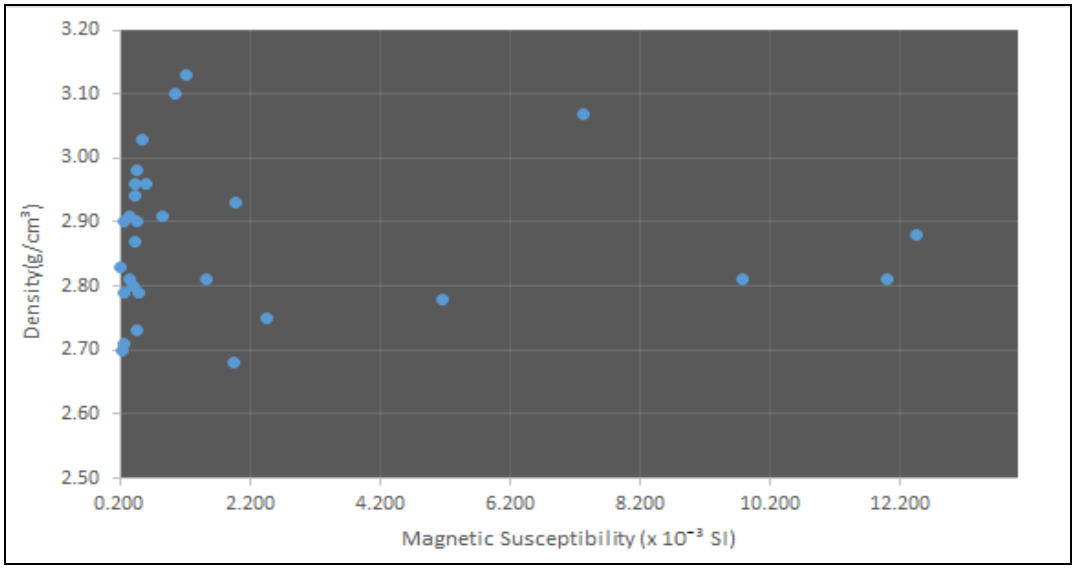

(b)

Fig.2.7 (a**)** Magnetic susceptibility (SI) versus density (g/cm^3) from core samples within the Vale do Curaçá District (Caraíba mine and Surubim mine) and (b**)** the Riacho do Pontal Copper District.

Geologic Data

A geologic map from a compilation of data from Brazil Geological survey (CPRM) was used as a base map Teixeira et al. (2010a). Supplemental geologic information including structural and image interpretation (Landsat 8) were collected for this study along secondary

roads resulting in an additional 300 geological observations (HUHN et. al., 2009). Geologic sections along select profiles were developed with a goal to better understand the structural setting of the area.

Seismic Tomography

Seismic tomography data over an area covering east-central Brazil (Begg, 2010; Minerals Targeting International Pty Ltd) were extracted from a database produced as part of the Global Lithospheric Architecture Mapping (GLAM) Project (GRIFFIN et al., 2013). The data include the Vale do Curaçá, Riacho do Pontal, and the Carajás IOCG province (Fig. 2.8) and are used to determine seismic properties related to the lithosphere underlying the major IOCG provinces in Brazil. Data represent a model of seismic velocities at a depth of 100 km. Development of the model is described in Begg (2009) and Begg (2010).

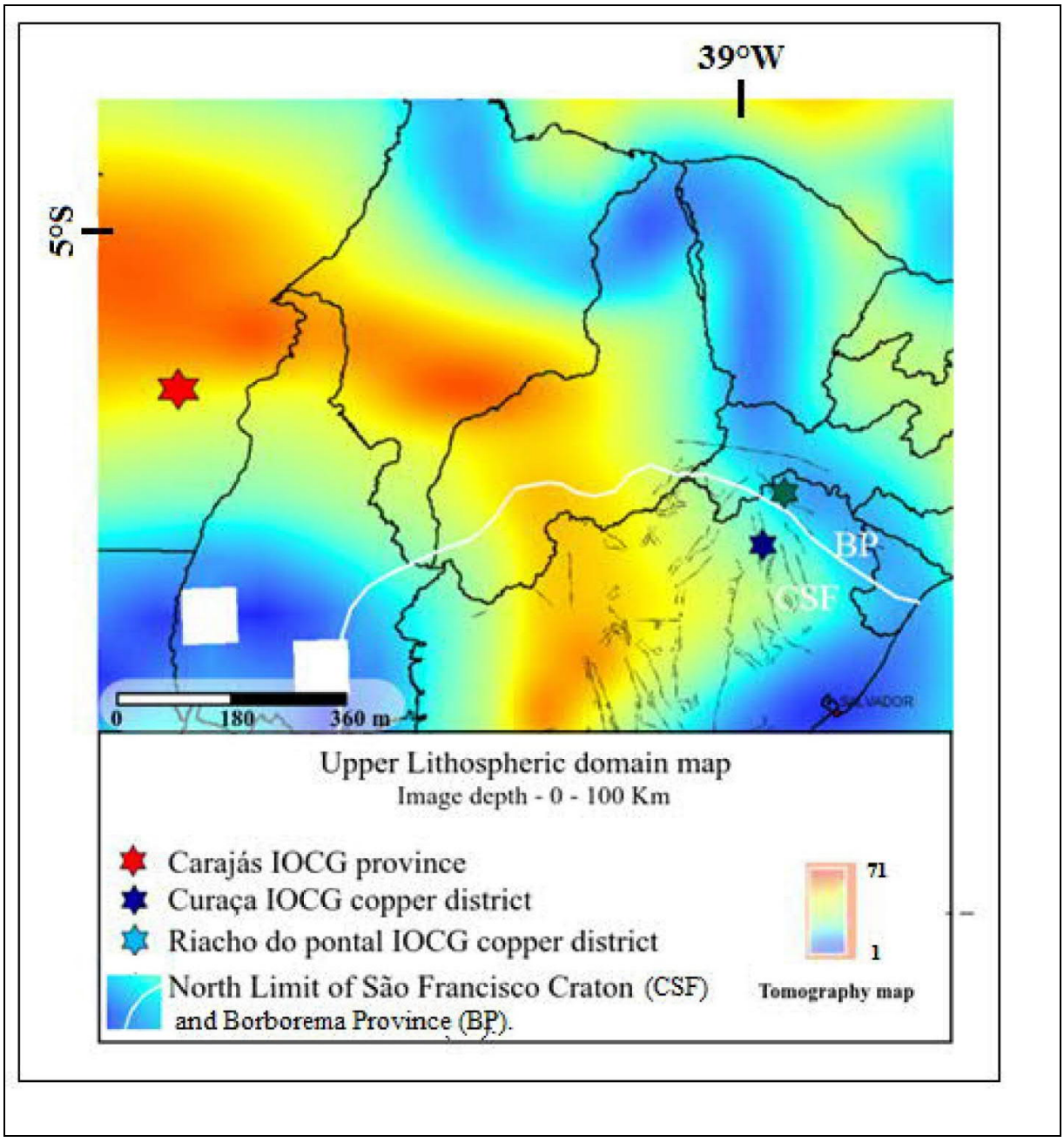

Fig. 2.8. Seismic tomography Image showing the Carajás IOCG Province, Riacho do Pontal and Vale do Curaçá Copper districts at Brazil (BEGG, 2009).

Methods

Magnetic and Gravity Inversion Models

The magnetic potential method is quite sensitive to the magnetic property of the rocks. However, the application of this practice were limited by conventional way of thinking, which assumed rock magnetization is dominated by induced magnetization and that magnetization direction is aligned with the geomagnetic field (MACLEOD and ELLIS, 2013). Modelling

magnetization vector direction and strength using Magnetization Vector Inversion (MVI) have challenged these conventions, and MVI modelling has become an important exploration tool in mining industry (MACLEOD and ELLIS, 2013). VOXI Modelling provides tools for making interpretation of 3D inversion models faster and more accessible to explorers in wideworld.

Magnetic and gravity data were inverted to 3D models using magnetic susceptibility and density, respectively, of select areas over the two copper districts studied to better understand the anatomy of the crust underlying them. 3D models that can be integrated with other project data using a multi-core cloud-based computing platform..

3D Magnetic Inversion

The grid of total field magnetic anomaly data were inverted to a 3D magnetic susceptibility model using the Magnetization Vector Inversion (MVI) method developed by Ellis et al. (2012) and employing software available in the Geosoft Oasis software package (MACLEOD and ELIS, 2013). The MVI method is a particularly effective inversion methodology in areas of low-geomagnetic latitude and in geologic environments where little is known about remnant magnetization of the rocks under study (MACLEOD and ELLIS, 2013). No paleomagnetic studies have been conducted on the rocks within the copper districts. The method assumes that the magnetic signal observed at the surface is associated not only with susceptibility contrasts but also with the direction of the magnetic field magnetization, which allows one to verify the presence of remanence.

Voxels for the magnetic inversion were 250m (x) x 200m (y) x 250 m (z). Input to the models were included petrophysical properties, surface geology, and structural information as qualitative constraint.

3D Density Inversion

VOXI MVI modelling is a Geosoft Oasis Montaj cloud and clustered computing module that it was used tfor the inversion of ground gravity data. The Geosoft package uses a Cartesian Cut Cell (CCC) and an iterative reweighting inversion algorithm developed by Ingam et al. (2003). The algorithm has been simplified by Ellis and MacLeod (2013) that represent geological surfaces with good accuracy. Voxels for the gravity models used voxels

that were sized 250m x 250m x 250m. The model used topography to represent the top of the model and a 5000 m depth to constrain the bottom surface of the model. The Z voxel cell size follows a logarithmic progression with depth. The acceptable absolute error level for all models was set to 0.02 mGal. A linear trend background was removed from the input gravity grid in order to facilitate the modelling process, avoid erroneous results and undesirable edge effects.

Results

2D Gravity and Magnetic Signatures

Vale do Curaçá District

Gravity anomaly signatures over the Vale do Curaçá Copper District (Fig. 5b) show the district is underlain by rocks with high densities in contrast with those surrounding the district. The District is located within an elongate 110 by 22 km-long north-south trending gravity high that occurs over rocks related to the Bom Despacho gneiss, Surubim Gneiss, Banguê gneiss, mafic and ultramafic complex and tonalitic to granodioritic orthogneiss (Fig. 1). Density measurements from these units include gneissic-granite, mylonitic and pyroxenite rocks, which have average densities of 2.78 g/cm³, 3.1 g/cm³ and 3.3 g/cm³, respectively (Fig. 2.7a). The lower gravity anomalies surrounding the gravity high are associated with the following units: Riacho da onça augen gneiss and Acauã Group. Densities measured from these units are generally lower and range from 2,65 g/cm³ to 3,0 g/cm³.

The Caraíba, Surubim and Vermelhos Cu mines and a number of other Cu occurrences are located along the gradient associated with either side of the gravity anomaly high.

Density measurements from core sampled from ore zones within the Caraíba and Surubin mines shows average densities from 3.5 to 4.35 g/cm^3 (Fig. 2.7a). Given the coarse gravity station spacing (Fig. 2.4a), we would not expect anomalies associated with the high density ore to be resolved in the gravity anomaly map. The ore is comprised of high density rocks. The ore comprises chalcopyrite, magnetite and bornite, associated with hornblende, biotite, apatite and zircon. Chalcocite and ilmenite are rare (Lindenmayer, 1981).

The Vale do Curaçá District sits within a long wavelength magnetic anomaly low interrupted by linear NNW trending sets of elongate magnetic highs that record major structural episodes that have juxtaposed rocks with different magnetic susceptibilities.Copper mineralization in the Vale do Curaçá District is associated with linear NNW-trending magnetic anomalies located along the west side of the Itabuna-Salvador-Curaçá Belt (Fig.1). The areas of longer wavelength magnetic low are related with nonmagnetic gneissic rocks, mafic and felsic dykes. The north to northwest--trending magnetic anomalies of the Vale do Curaçá Copper District corresponds with anastomosed structures that have been geologically mapped throughout the district). The NNW-trending structures have been overprinted by at least two cycles of shearing (ROCHA, 1999; SILVA et al., 2007). These later shear faults are recorded in the TAHG map (Fig. 6a) as the NNW-trending set of gradient highs.

The copper occurrences and mines in this district, including areas of strong hydrothermal alteration, are associated low-amplitude magnetic anomalies (TMI). of from ~24,000 to ~25,700 nT (Figure 2.6).

Riacho do Pontal Copper District

The Riacho do Pontal District sits on a gravity gradient that separates a gravity high to the north from a northwest-trending gravity low to the south (Fig. 2.4b). The Bouguer anomaly low is likely related to low density gneiss that partly out crops in the Sobradinho Remanso and South portion of the Riacho Seco Complex (Fig. 1). The Ria4 Cu occurrences within the Riacho do Pontal District are situated along the edge of the gravity gradient. Densities measured from rocks within the Ria4 mine show the less altered rocks have densities that range from 2.7 to 2.78 g/cm³. Rocks that have been more strongly altered have densities that overlap those of the less altered rocks and range from 2.75-3.1g/cm³ (Fig. 2.7b).

The northwest-trending Bouguer gravity low underlying the Riacho do Pontal District geologically corresponds to the collisional suture zone between the higher density cratonic block and the lower density crust forming the Riacho do Pontal mobile belt.

The northeast portion of the Riacho do Pontal Copper District is characterized by a positive gravimetric anomaly with an amplitude up to -40.000 mGals. The gravity high corresponds to foliated orthogneissic rocks of the Riacho Seco Complex. The Riacho Seco Cu occurrences are situated along the gravity gradient, which likely marks a structure that has juxtaposed the denser crust of the craton against the lower density crust underlying the

Riacho do Pontal mobile belt. The area of the gravity gradient includes biotite-garnet rich rocks, which occurs along shear zones, and hosts a series of small number of Cu occurrences.

The magnetic anomaly signature of Cu occurrences in the Riacho do Pontal Copper District are varied and may be located in association with low amplitude magnetic anomalies.

In the Riacho do Pontal Copper District, the copper occurrences (Ria4 and Riacho Seco) are not related to high magnetic anomalies. The Ria4 and Riacho Seco occurrences are hosted, respectively, in nonmagnetic gneiss of the Sobradinho Remanso and Riacho Seco Complexes. The gneissic rocks are pervasively hydrothermally altered and have a range of magnetic susceptibility from 0.2 SI x 10^{-3} in less altered rocks to 12.2 SI x 10^{-3} in more hydrothermally-altered rocks. On a regional scale, the northwest-southeast trending magnetic anomalies overprint longer wavelength northeast-southwest-trending anomalies related to older and deeper parts of the São Francisco Craton.

The copper deposits located in the belt of the Riacho do Pontal Copper District are located in zones without or with very weak magnetic anomalies.

3D Inversion Models

Vale do Curaçá Copper District

The 3D magnetic susceptibility model over the Vale do Curaçá Copper District reveals magnetic features that correspond to numerous geologic structures that reflect episodic tectonic activity. A series of parallel magnetic trends, aligned north-south and that dip 75-85° to the east, are *overprinted* by least two episodes of NS-trending shear faults (D1 and D2). The Caraíba mine is emplaced along a NNW-trending subvertical shear zone, showing an anastomosing shape in both the horizontal and vertical directions. A series of subparallel N-S shear structures have been active and responsible for multiple reactivation events. N-S shearing magnetic zones are related to thrust shear zones (D1) with convergence to the West, and are overprinted by strike slip faults. The D1 and D2 events have controlled the distribution of hydrothermal alteration and mineralization. The NE-SW late shear zones are subvertical.

The Caraíba Mine bodies are strongly related to magnetic and gravimetric NNW trends having SI > 0.005 and with gravimetric anomalies >-10,000 mGal (Figures 2.9 and

2.10). The Caraíba mine and Paredão occurrence have a strong relationship with magnetic anomalies. The other occurrences along the Vale do Curaçá District are not related directly with high gravimetric and magnetic anomalies.

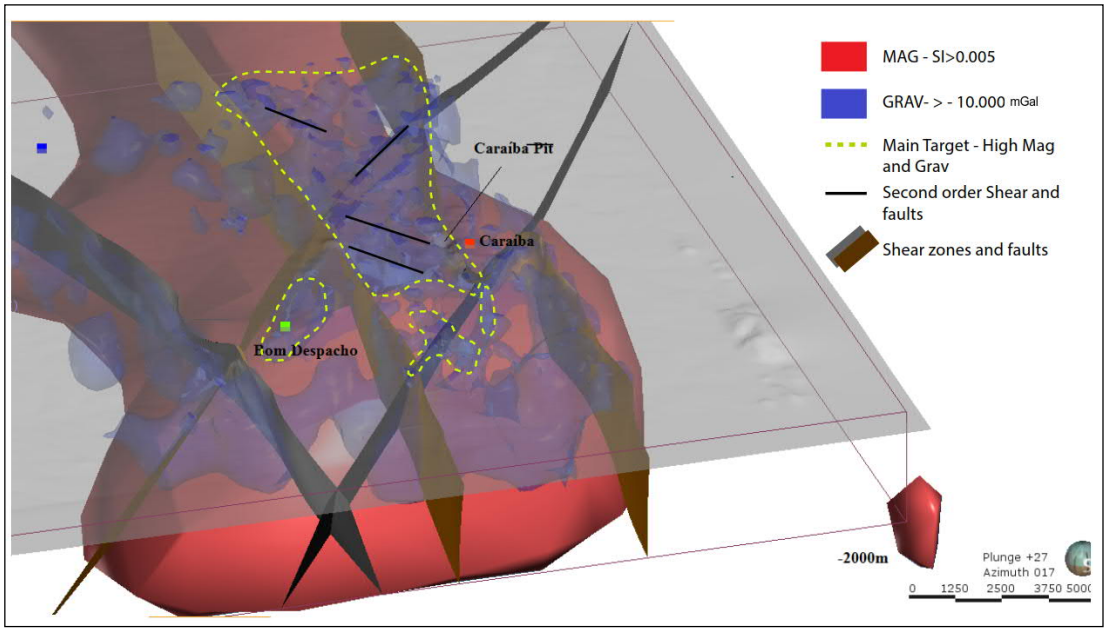

Figure 2.9 - Draping structure and MVI magnetic and gravimetric inversion onto the terrain surface surrounding the Caraíba mine (Curaçá Copper District). In the Vale do Curaçá District, it is possible to observe a series of subparallel N-S magnetic trends. Most anomalies are related to geological units represented by the mafic granulites and granulitic orthogneiss. Some magnetic anomalies are related to the N-S and NE-SW structural trends. The Caraíba Mine bodies are strongly related to a magnetic and gravimetric N-NS trend, SI > 0,005, with gravimetric anomalies >-10,000 mGal. Dashed red area represents main target with more potential to host new IOCG orebodies at the Caraíba Mine.

The Caraíba mine is related to magnetic and gravity anomalies along N-S trending shear zones. The host rocks are granulitic orthogneiss and ultramafic bodies. The mine is situated about 1 km from the N-S shear zone that was displaced by NW-SE shear zones. Sodic and potassic hydrothermal alterations are mapped along the N-S and secondary NE shear zones. In 3D tectonic settings, the mine is intrinsically related to high magnetics associated with a gravimetric anomaly (Figure 2.10). The orebodies are oriented in a subvertical direction and are controlled by a stretching lineation.

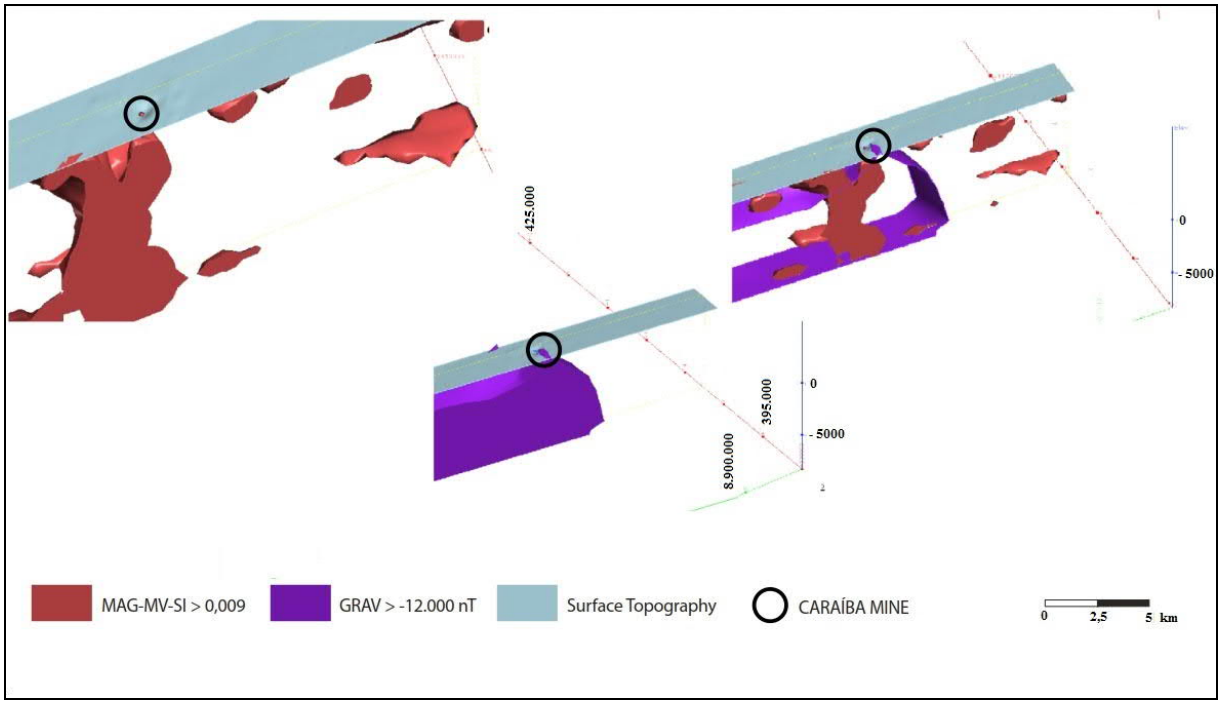

Figure 2.10 – 3D gravity and magnetic inversion integrated at the Caraíba mine. The Caraíba mine is strongly related to magnetic and gravity anomalies. The potential continuity in depth of ore zones related with magnetic and gravity anomalies is quite promising and should be investigated in further work.

The magnetic trends (SI>0.005) are juxtaposed with shear structures and faults with different magnetism intensities (Figure 2.6). The Caraíba mine situated in the central-west portion of the Itabuna-Salvador-Curaçá Belt and recognized as the most fertile trend is more magnetic (SI>0.009) than are mines located in the eastern portion. Geologically, the regional magnetic trends are related to more intense metamorphic granulitic processes overprinting geological units: the Bom Despacho Gneiss, the Surubim, Banguê and tonalitic to granodioritic orthogneiss. Late NE-SW shear zones are quite common crosscutting N-S early magnetic trends. The ore zones from Caraíba and Surubim mines have a range of magnetic susceptibility from 30 SI X 10^{-3} SI to 700 SI x 10^{-3}.

3D magnetic and gravity inversions shows two main NNW prospective trends, both with a sigmoidal shear shape. These trends are positioned in the zone of contact between domains with high magnetic (SI>0.005) and gravimetric anomalies (>-10,000nT) and show a contrast in density and magnetite content. Trend I is 60km in length and 7km in width, hosts the Caraíba, Surubim and Vermelho mines and other deposits and is the most important trend for host IOCG deposits in the Vale do Curaçá Copper District .Trend II is 35 km in length and 5 km in width. Geologically, these trends are hosted mainly along the contact between

Surubim gneiss, tonalitic to granodioritic orthogneiss, and gebbronorite and/or norite bodies (Figure 2.11).

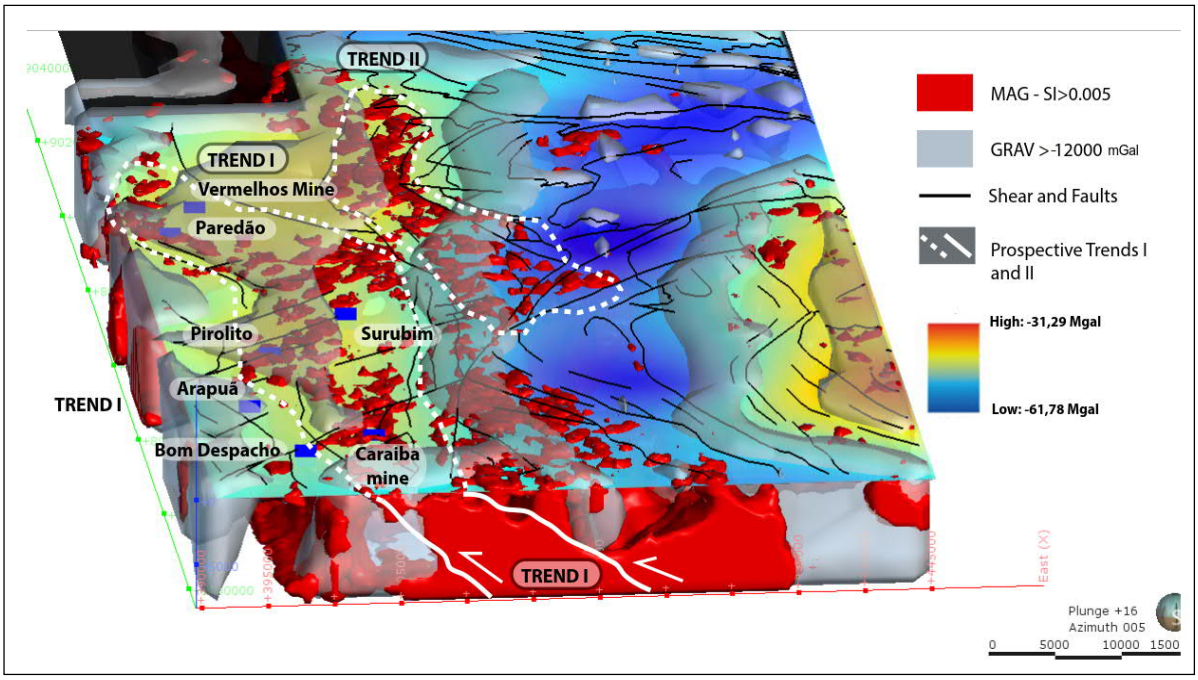

Figure 2.11: The IOCG mineral system in the region of the Vale do Curaçá Copper District, in regional terms, shows two main porospective trends. The trends are positioned in the contact zone between domains with high magnetic (SI>0.005) and gravimetric anomalies (>-10,000 mGal) and show a contrast in density and magnetite content.

Riacho do Pontal District

The 3D magnetic inversion over the Riacho do Pontal Copper District shows that the Ria4 prospect and Riacho Seco deposit do not show correlation with magnetic anomalies. The occurrences of copper in the region are positioned at magnetic lows. This observation is explained by the fact that the mineralized zone is related to hematite zones and the content of iron oxide is low (<2%). The exploration drilling program (Ria4-DH01) crosscut 32 m @ 1% copper (HUHN et. al 2014; HUHN and SILVA, 2018). The results obtained in the magnetic inversions conducted in the region of the Riacho do Pontal Copper District show weak magnetic anomalies along a NW-SE trend. The discrete linear magnetic features are related to

shear zones. These NW-SE features overlap over older and deeper NE-SW features. However, analysis of the Riacho do Pontal District magnetic anomalies in 3D at the Riacho Seco deposit shows a low magnetic anomaly close to the surface and change in depth (>400 m) to an area with high magnetic signature, reaching up to 24,500 nT (Figure 2.12). The results allow for the possibility of a continuous model for follow up of the deposits as related to deeper magnetic anomalies.

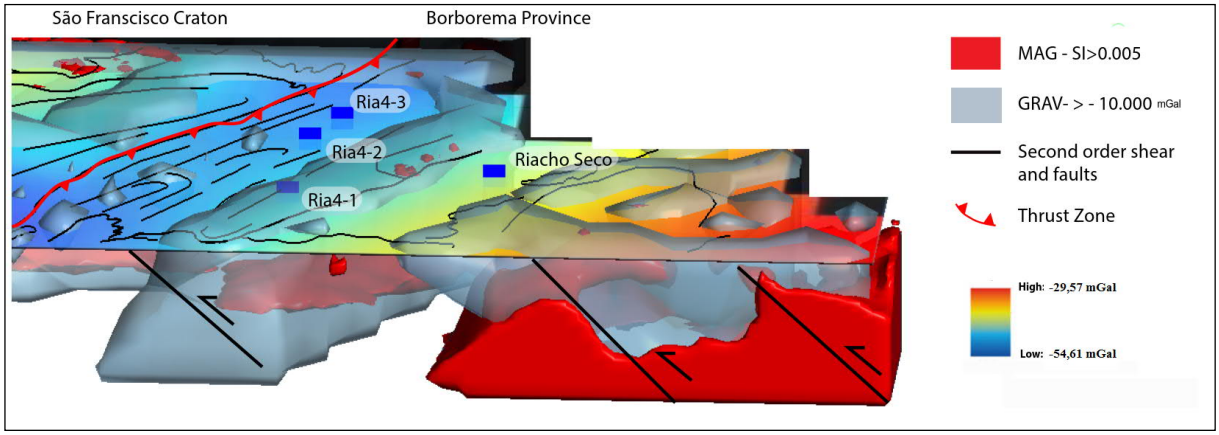

Figure 2.12: The MVI magnetic gravimetric inversions in the region of the Riacho do Pontal Copper District. In the region of the Riacho Seco Deposit and the Riacho do Pontal prospects the magnetic and gravity anomalies are weaker (SI<0.002; Grav <-10,000 mGal) and deeper (>1,5 km)

Discussion

Vale do Curaçá and Riacho do Pontal District IOCG Mineral Systems

Understanding the IOCG systems at different scales allows tracing some parameters leading to the formation of districts or fertile provinces (GRAINGER et al., 2008; POLLARD et al., 2018; GROVES et al., 2016).

More recently, a new generation of ore system exploration models has been developed to take advantage of the massive volume of data available to the exploration industry (LESHER et al., 2017; BARNETT; WILLIAMS, 2012). Improving exploration competitiveness is necessary with more sophisticated integration of different data sets. The challenge remains in decreasing the size of exploration areas and increasing the success rate of drilling programs (LESHER et al., 2017; COOKE et al., 2017). Thus, for the Vale do Curaçá and Riacho do Pontal copper districts, the main footprint that shows the ore system signature was recognized (Figure 2.13). The more important geological, structural, geochemical, mineralogical and petrophysical parameters of these copper districts are summarized below and illustrated on figure 2.13.

At a regional scale lithospheric major structures control the traps of IOCG mineralizing systems or heat-magmas, or the fluid flow is frequently evident in gravity and magnetic databases (CLARK, 2014).

Lithospheric Setting Expressed in the Seismic Tomography

The high zones (in red) in tomographic map represents high velocity domains that represents microcontinental blocks (mantle lithosphere domain). They are flanked by low velocity domains that represents lower velocities that reflect refertilisation of the SCLM and/or a higher temperature along fault zones. Frequently, deposits concentrate along prominent trans-lithospheric structures, particularly in lower-velocity regions (blue) or on the flanks of velocity highs (Courtesy of BEGG et. al., 2010).

A world map of the lithosphere produced from an integration of geophysical, geological, and geochemical data, shows approximately 70% of the existing subcontinental lithospheric mantle (SCLM) may be of Archean origin (BEGG et. al. 2010). Implications for

an Archean SCLM is that most preserved Proterozoic crust overlies older Archean SCLM that has been variably re-fertilized and metasomatised by mantle melts associated with convergent margin and mantle plume processes (BEGG et al., 2009; GRIFFIN et al., 2008).

In general, seismic tomography images can show boundaries of cratons and discontinuities related to the subcontinental lithospheric mantle (SCLM). These discontinuities are favorable for the repeated ascension of magmas (GRIFFIN et al., 2008; GRIFFIN et al., 2013). Preserved cratonic regions (SCLM) can be mapped as areas presenting a high seismic velocity. At a global scale, it has been shown that smaller volumes of magmas directly originating from the mantle are positioned at the craton edge along the flanks of a prominent northwest-trending velocity high (Fig. 2.8).

Domains of high seismic velocity can represent ancient blocks of metasomatized subcontinental lithospheric mantle (SLCM) within a discrete mantle lithosphere domain flanked by major faults (BEGG et al., 2010; GRIFFIN et al., 2013). The IOCG Carajás Province, Vale do Curaçá and Riacho do Pontal Copper districts are located in the transition zone between domains of high and low velocities (Fig. 4), and may reflect re-fertilization of the subcontinental lithospheric mantle (SCLM) and or zones of higher lithospheric and mantle temperatures. Ore deposits that originate from mantle magmas such as diamond, platinum-group elements (PGE), Ni-Cu-(PGE) and copper porphyry and IOCG deposits are situated along cratonic edges and can be related to the tectonic evolution of the SCLM (GRIFFIN et al., 2013; BEGG et al., 2010; CZARNOTA et al., 2013). In this context, the extensive gradients flanking either side of the high speed velocity high through east central Brazil should be evaluated in more detail (Fig. 2.8).

Craton edges are characterized by a thin lithosphere and are strongly tectonized zones creating trans-tensional or trans-pressional sites along trans-lithospheric faults (BEGG et al., 2009). These major shear zones or fault zones are frequently used for melt introduction into the crust. For example, IOCG districts in Australia including the world class Olympic Dam in the Gawler Craton and within Eastern rocks of Mount Isa inlier of Australia are related to the presence of large intrusive provinces (LIPs) that contain a considerable presence of intrusive felsic rocks (PIRAJNO; BAGAS, 2008; McPhie et al., 2011; PIRAJNO; HOATSON, 2012; HITZMAN, 2000; GROVES et al., 2016).

Fertile provinces that lead to the formation of world class deposits require melting of subcontinental lithospheric mantle (SCLM) on the margins of cratons, which is responsible for magmatic ascension; associated high heat; and volatile flow (GRIFFIN et al., 2013;

HOLDSWORTH; PINHEIRO, 2000**).** The deposits occur in long lived subparallel regional structures that have been focus of multiple reactivation events (SILVA et al., 1993; ROCHA, 1999; SILVA et al., 1996; TEIXEIRA et al., 2010a; HUHN et. al. 2014; HUHN and SILVA, 2018). In the Riacho do Pontal and Vale do Curaçá Copper Districts structural interpretantion shows that early thrust zones are reused several times and are overprinted by strike-slip shear zones (SILVA et al., 1993, SILVA et al., 1996).

Structural Control

Sigmoidal or "SC-shape" structures are indicative of major shear systems (references). Fractal patterns that mimick SC structures are systematically repeated from macro-scales to micro-scales. These structures are critical pathways for upward flux of fluids promoting the interaction between fluid-rock. Duplex, shear bands, and asymmetrical structures are quite common along the shear system. The structural controls and traps used for orogenic gold in shear zones are the same for IOCG deposits. The more important traps for host orebodies are: a) interconnection zones between "SC" structures; b) fractal second- or thrid- order "C" structures; c) bends along shear zones in both horizontal and vertical planes where high grade breccia are typically hosted; d) fault intersections that are highly favorable for host breccia ores, and e) ductile shear zones reactivated by late brittle faults that enrich older zones and can generate new mineralized bodies.

Frequently, lithological boundaries between units with different competence are crucial for the hosting high deformation corridors. In this manner, zones of contact with competent rocks such as paragneiss, mafic granulite, granulitic orthogneiss and BIFs are usually traps for percolation of hydrothermal fluids related with shear zones. At Vale do Curaçá Copper District, only considering the epigenetic IOCG mineralization process, the host rocks are pedominantly mafic and felsic granutitic rocks.

The ore bodies often assume a sigmoidal shape as they are often hosted in shear zones. However, pipe breccia zones along hydrothermal corridors can be found. Among the explanations for the evolution of IOCG systems is that they develop by direct melting of the SLCM and are positioned in hear zones initially as a pipe breccia reworked by shear deformation. Variation in the direction and dipping along the shear zones, both horizontally and vertically, acts as a structural trap for both hydrothermal breccias and pipe breccias.

Typically, rich breccia zones are situated in a central hydrothermal system zone in transtensional structures.

Geophysical Implications for Alteration

Hydrothermal alteration is characterized by early high temperature Na (albite) alteration (500-400 ºC; POLLARD, 2006) to lower temperature k-Fe (<350 ºC) alteration (TEIXEIRA et al., 2010b; HUHN et al., 2014; JULIANI at al., 2016; Garcia et al., 2018; HUHN and SILVA, 2018). High temperature albite alteration can be linked to a magmatic-hydrothermal systems (OLIVER, 2004; POLLARD, 2006; POLLARD et al., 2018). Iron is strongly soluble at high temperature and saline fluids and is caused by increasing of H+ in the fluid system resulting in a more intense Fe fluxes (WILLIAMS, 1994). Thus, magnetite (hematite) bodies and/or disseminated magnetite (hematite) infill along shear zones.

Hydrothermal alteration is related to intermediate- to high-temperature fluids in the Riacho do Pontal and Vale do Curaçá Districts. The alteration halo extends from 1 km to 5 km in width, following the major shear zones. Sodic alteration is more distal and potassic, and calcic and ferric alterations are more proximal in both districts.. The southern deposits and Sussuarana, Caraíba and Surubim mines are related to deeper and high temperature sodic/potassic hydrothermal alteration, in contrast with the Vermelho deposit, in which hydrolytic alteration occurred in shallower zones in the IOCG hydrothermal system as initially described by Hitzman et al. (1992, 2000). Typically, a series of magnetic dipoles are linked to shear zones and hydrothermal halos.

The general hydrothermal zoning pattern for IOCG deposits is usually vertical, from magnetite-dominant at depth to hematite-dominant at shallower levels (HITZMAN et al., 1992; HITZMAN, 2000). Using this model, it is possible to interpret the Riacho do Pontal District as positioned in the shallowest portion of the IOCG system (Figure 2.12). In this way, additional work must be performed identifying deeper (or more eroded) areas of the IOCG system related to more magnetic and density areas (such as the Riacho Seco target).

In 2D and 3D mapping, it is possible to verify the variation in these parameters with distance in the direction of the mines, deposits or occurrences. The increase and decrease in the intensity of these processes represent the vectorization of the IOCG systems studied.

Exploration Potential

Riacho do Pontal District

- Structural - increase in intensity of shearing and in density of structures in direction of secondary structures. The foliation tends to be vertical;
- Stream sediment and soil – Anomalies of Cu, Ni, Fe and La in stream sediment and Cu (Ni, Ce and La) in soil;
- Low magnetic anomalies related with Kd- (kd-anomalous potassium)related to shear zones (HUHN and SILVA, 2018);
- Low magnetic anomalies (rich hematite related to ore zones).

Vale do Curaçá District

- The District of Vale do Curaçá is associated, regionally, with high gravimetric and magnetic associated with the portion west of the Itabuna-Salvador-Curaçá orogen;
- The IOCG mineral system in the Vale do Curaçá Copper District, in the regional context, shows two main magnetic trends.
- The Caraíba Mine bodies are strongly related to magnetic and gravimetric NNW trends having SI > 0.09 and with gravimetric anomalies <-10,000 mGal;
- Hydrothermal Alteration – An increase in the anomalies related to hydrothermal processes i) an distal sodic alteration; (ii) the mineralized zone is intensely related calcic-ferric alteration;
- Increase in Fe acinolite FeOt/Mg/MgO+FeOt) and Fe-Biotite (Fet/Mg) towards more hydrothermalized altered zones (Figure 13);
- The regional gravity signatures over the Vale do Curaçá and Riacho do Pontal Districts (Fig. 5) suggest the bulk density of the crust underlying the districts are related to geologic units with different densities

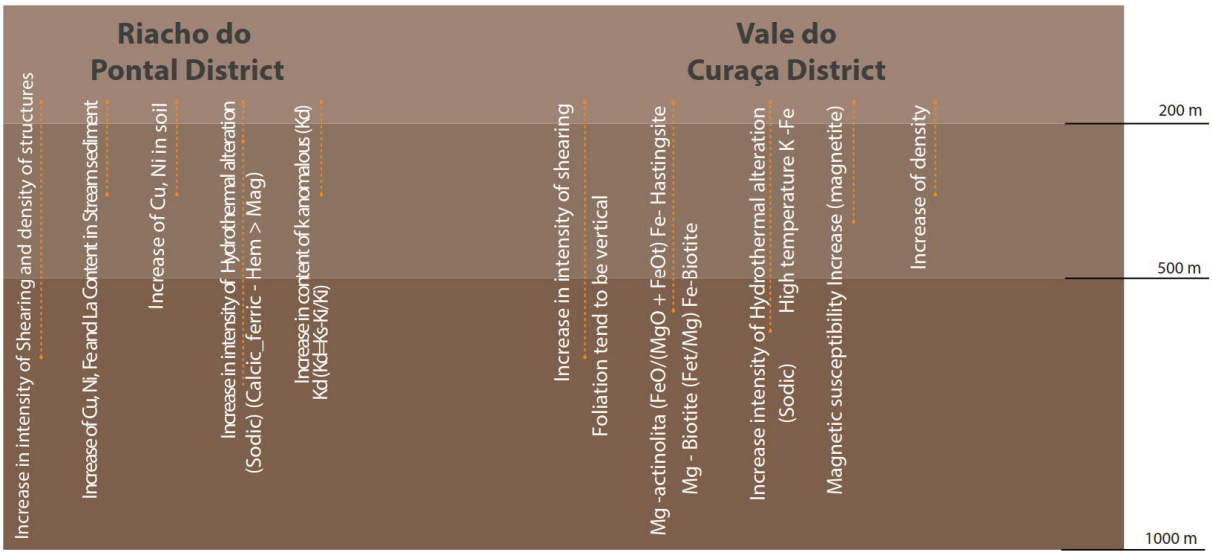

Figure 2.13: The main geological geochemical, structural and geophysical vectoring illustrating the footprint of the Vale do Curaçá and Riacho do Pontal Copper Districts.

However, a paradigm remains at the Vale do Curaçá District that is not typical; selection of new targets that are not necessarily hosted in ultramafic rocks. The IOCG system can develop in any host rock at varying depths. A full understanding of the IOCG model for mining companies can greatly expand exploration in the district.

Conclusions

Knowledge of the signature of IOCG deposits in Brazil shows that these deposits can be hosted in any type of rock, with different styles of hydrothermal alteration and at different depths. The main conclusions obtained in the present study of the Riacho do Pontal and Vale do Curaçá copper districts are as follows:

1 - The Vale do Curaçá District is part of Paleoproterozoic Itabuna-Salvador-Curaçá orogen. It represents a collision event involving the Gavião, Jequié and Serrinha blocks in the

Rhyacian to Orosirian transition (BARBOSA; SABATÉ, 2004). The Riacho do Pontal District is situated over a Neoproterozoic collisional zone;

2 - The Vale do Curaçá and Riacho do Pontal Copper Districts are hosted in different gravimetric domains. The vale do Curaçá copper district is in a high gravimetric domain. It is 110 km in length and 22 km in width and shows a strong anomaly with a wavelength of up to -40 mGal. The Caraíba, Surubim and Vermelhos mines and a number of copper occurrences are positioned in this site;

3 - The gravimetric signature of the Riacho do Pontal District is mainly by a negative Bouguer NW-SE anomaly (below -45 mGal). This negative Bouguer anomaly represents the collisional suture between the cratonic block and the mobile belt Riacho do Pontal.The IOCG occurrences of the Ria4 prospects are located in these low gravimetric signature domains. The rocks, slightly altered, have a density of the order of 2.7-2.78 g / cm^3 and the rocks most strongly altered show density of 2.75-3.1 g / cm^3;

4- The magnetic signature of the districts of the Vale of the Curaçá and the Riacho do Pontal are quite distinct. Copper corridors in the Vale do Curaçá Copper District are associated with sigmoidal magnetic anomalies located in the western portion of the Itabuna-Salvador-Curaçá Orogen. On the other hand, the copper deposits located in the belt of the Riacho do Pontal District are situated in zones without or with the presence of very weak magnetic anomalies;

5 - MVI magnetic and gravity inversion shows two main NNW prospective trends. Trends I and II have a sigmoidal shear shape. These trends are positioned in the contact zone between domains with high magnetic (SI>0.005) and gravimetric anomalies (>-10,000 nT) and show a contrast in density and magnetite content. Trend I is 60 km in length and 7 km in width, hosts the Caraíba, Surubim and Vermelho mines and other deposits and is the most important trend for hosting IOCG deposits in the Vale do Curaçá District;

6 - The general hydrothermal zoning pattern for IOCG deposits is usually vertical, from magnetite-dominant to depth to hematite-dominant at upper levels. It is possible to interpret the neo-proterozoic Riacho do Pontal District as positioned in the shallowest portion of the IOCG system. In this way, additional work must be performed by searching for deeper (or more eroded) areas of the IOCG system related to more magnetic and dense areas (targets on north portion of the Riacho Seco target);

7 - The large areas flanking high speed sismic tomomography image that already control in a broad scale Carajás IOCG Province and Riacho do Pontal and Vale do Curaçá

Copper Districts in Brazil should be evaluated in more detailed in further exploratory program;

8 – Regional results od this work enlarge the geological, structural and geophysical understanding of Riacho do Pontal and Vale do Curaça IOCG districts. The use of a broader database of petrophysical data may improve the geophysical models elaborated in this work.

Acknowledgments

The authors gratefully acknowledge Vale S. A. for support of this study. We would like to thank Annne MCCafferty from USGS and the Vale exploration team for extensive discussions. A.M. Silva gratefully acknowledges the National Council for Scientific and Technological Development (CNPq) for the research grant (307177/2014-9). We would also like to thank Victoria Basileu for special support in developing the figures.

References

ALKMIN, F.F; BRITO, Neves B.; CASTRO, J. Alves. Arcabouço tectônico do Cráton São Francisco: uma revisão. In: DOMINGUES, J.M.L.; MISI A. (eds.). **O Cráton do São Francisco**. Salvador, SBG/ SGM/CNPq, 1993. p. 45-62.

ALKMIN, FF; MARSHAK, S; FONSECA, MA. Assembling West Gondwana in the Neoproterozoic: clues from the Sao Francisco craton region, Brazil. **Geology**, n.29, p.319–322, 2001.

AUSTIN, J. et al. Remanence, self-demagnetization and their ramifications for magnetic modelling of iron oxide copper-gold deposits: An example from Candelaria, Chile: **Journal of Applied Geophysics**, v. 109, p. 242–255, 2014.

AUSTIN, J.; FOSS, C. Rich, attractive and extremely dense: a geophysical review of Australian IOCGs [ext. abs.]: International Geophysical Conference and Exhibition, 22nd, Brisbane, Australia, Extended Abstracts, 2012. 4 p.

BARBOSA, J. S. F.; SABATÉ, P. Archean and Paleoproterozoic crust of the São Francisco Craton, Bahia, Brazil: geodynamic features. **Precambrian Research**, v. 133, p. 1-27, 2004.

BARBOSA, J.S.F. The granulites of the Jequié complex and Atlantic mobile belt,southern Bahia, Brazil: an expression of archean-proterozoic plate convergence. In: VIELZEUF, D.; VIDAL, P. (Eds.). **Granulites and crustal evolution**. Springer Verlag, 1990. p.195-221

BARBOSA, J.S.F.; DOMINGUEZ, J.M.L (eds.). **Geologia da Bahia**: texto explicativo. Salvador: SGM, 1996. 400 p.

BARNETT, C.T.; WILLIAMS, P.M. A radical approach to exploration: Let the data speak for themselves. **Society of Economic Geologists Newsletter,** n.90, v.1, p.12-17, 2012.

BARRIE, C.T.; HANNINGTON, M.D. Introduction: classification of VMS deposits based on host rock composition. In: _____. Volcanic-associated massive sulfide deposits: processes and examples in modern and ancient settings. **Reviews in Economic Geology**, n.8, Denver, Society of Economic Geologists, 1999. p. 2-10.

BARTON, M.D. Iron oxide (-Cu-Au-REE-P-Ag-U-Co) **systems**: Treatise on Geochemistry, 2nd ed., v. 13, p. 515–541, 2014.

BEGG, G.C. et al. Lithospheric, cratonic and geodynamic setting of Ni-Cu-PGE sulphide deposits. **Econ. Geol**. n.105, p.1057–1070, 2010.

BEGG, G.C. et al. The lithospheric architecture of Africa: Seismic tomography, mantle petrology and tectonic evolution. **Geosphere**, n.5, p. 23-50, 2009.

BELPERIO, A.; FLINT, R.; FREEMAN, H. Prominent Hill: A hematite-dominated, iron oxide copper-gold system. **Economic Geology**, v. 102, p. 1499–1510, 2007.

BLEWETT, R.S. et al. Scale-integrated architecture of a world-class gold mineral system: The Archaean eastern Yilgarn Craton, Western Australia. **Precambrian Research**, n.183, p.230–250, 2010.

BRITO, Neves BB; FUCK, R.A. The basement of the South American platform: half Laurentian (N-NW) half Gondwanan (E-SE) domains. **Precambrian Research**, n.244, p.75-86, 2014.

CLARK, D.A. Magnetic effects of hydrothermal alteration in porphyry copper and iron-oxide copper-gold systems. **A review: Tectonophysics**, v. 624–625, p. 46–65, 2014.

CLARK, D.A.; GEUNA, S.; SCHMIDT, P.W. Predictive magnetic exploration models for porphyry, epithermal and iron oxide copper-gold deposits: Implications for exploration, exploration and mining: Commonwealth Scientific and Industrial Research Organization (CSIRO) Exploration and Mining Report,2013. 1073R.

CLARK, J.M. **Defining the style of mineralization at the Cairn Hill magnetite-sulphide deposit, Mount Woods Inlier, Gawler Craton, South Australia**. The University of Adalaide. 2014. 69p.

COMPANHIA BAIANA DE PESQUISA MINERAIS – CBPM. **Informações Geológicas e de Recursos Minerais do Estado da Bahia**. 2011. Disponível em: < http://www.cbpm.com.br/igba/>. Acesso em: 22 mar. 2014.

COMPANHIA BAIANA DE PESQUISA MINERAIS – CBPM. **Levantamento aerogeofísico Projeto Riacho Seco Andorinhas**. 2001. Relatório Técnico. 2001. 80p.

COOKE, D.R. et al. New advances in detecting the distal geochemical footprints of porphyry systems – Epidote mineral Chemistry as a tool for vectoring and fertility assessments. **Society of Economic Geologists,** Special Publication, n.18, p.127–152, 2014.

CORRIVEAU, L., MUMIN, A.H., and SETTERFIELD, T., 2010a, IOCG environments in Canada: Characteristics, geological vectors to ore and challenges, in Porter, T.M., ed., Hydrothermal iron oxide copper-gold & related deposits: A global perspective: Adelaide, Australia, Porter Geoscience Consultancy Publishing, v. 4, p. 311–344.

CORRIEAU, L., MUMIN, H., and MONTREUIL, J. F., 2011, The Great Bear magmatic zone (Canada): The IOCG spectrum and related deposit types: Society for Geology Applied to Mineral Deposits, Biennial Meeting, 11th, 26-29 September 2011, Antofagasta, Chile, Proceedings, Universidad Católica del Norte, v. 1, p. 524–526.

COSTA, I. A Aerogeofísica em Carajás pelo Serviço Geológico do Brasil. CPRM. Serviço Gologico do Brasil. 2017. ppt. 65p. www.cprm.gov.br.

CZARNOTA, M. et al. Spatial and temporal patterns of Cenozoic dynamic topography around Australia. **Geochem. Geophys**., n.14, p.634–658, 2013.

DELGADO, L.M.; SOUSA, J.D. **Projeto Cobre Curaçá**. Geologia Econômica do Distrito Cuprífero do Rio Curaçá, Bahia, 1975. Relatório Final. DNPM/CPRM.

DELGADO, L.M.; SOUZA, J.D. **Projeto Cobre Curaçá**. Cobre no Vale do Rio Curaçá, Estado da Bahia, Departamento Nacional de Produção Mineral, Seção Geologia Econômica, 1981. p. 7-149 (in Portuguese).

DREHER, A.M. et al. New geologic, fluid inclusion and stable isotope studies on the controversial Igarapé Bahia Cu-Au deposit, Carajás Province, Brazil. **Mineral Deposita** n.43,p.161–184, 2008.

ELLIS, R.G.; WET B. de, MacLeod. Inversion of magnetic data for remanent and induced sources. **ASEG Extended Abstracts,** p.1-4, 2012.

ESDALE, D. et al. The Olympic Dam copper-uranium-gold-silver-rare earth element deposit, South Australia: A geophysical case history. **Australian Society of Exploration Geophysicists Special Publication**, n.22, p.147–16, 2003.
FLECK, R.J.; SUTTER, J.F.; ELLIOT, D.H. Interpretation of discordant $^{40}Ar/^{39}Ar$ age-spectra of Mesozoic tholeiites from Antarctica.In: SKINNER, B.J. (ed.). **Economic Geology**, 75th Anniversary Volume, Denver, Society of Economic Geologists, p. 485-627, 1981.

FREITAS, J.P.S. **Elaboração do modelo geomecânico tridimensional para avaliação e setorização geotécnica dos realces da mineração Caraíba**. 2016. 2019f. Mestrado (Engenharia Geotécnica) – UFOP, 2016.

GANADE, C.E. et al. Tightening-up NE Brazil and NW Africa connections: New U–Pb/Lu–Hf zircon data of a complete plate tectonic cycle in the Dahomey belt of the West Gondwana Orogen in Togo and Benin. **Precambrian Research**, n.276, p.24–42, 2016.

GANADE, C.E.; WEINBERG, R.F.; CORDANI, U.G. Extruding the Borborema Province (NE-Brazil): a two-stage Neoproterozoic collision process. **Terra Nova**, n.26, p.157–168, 2014.

GARCIA, P.M.P. et al. Tectonic and metallogenic evolution of the Curaçá Valley Copper Province,Bahia, Brazil: A review based on new SHRIMP zircon U-Pb dating and sulfur isotope geochemistry. **Ore Geology Reviews**, n.93, p.361–381, 2018.

GARCIA, P.M.P. **Metalogênese dos depósitos cupríferos de Caraíba, Surubim, Vermelhos e Sussuarana, Vale do Curaçá, Bahia, Brasil**. 2013. 225 f. Dissertação (Mestrado) - Instituto de Geociências, Universidade Federal da Bahia, Salvador, 2013.

GRAINGER, C.J. et al. Metallogenesis of the Carajás Mineral Province, Southern Amazon Craton, Brazil: varying styles of Archean through Paleoproterozoic to Neoproterozoic base- and precious-metal mineralisation. **Ore Geol Rev.,** n.33, p.451–489, 2008.

GRAY, D.R. et al. A Damara orogen perspective on the assembly of southwestern Gondwana. In: PANKHURST, R.J. et al. (Eds.). **West Gondwana**: Pre-cenozoic Correlations across the South Atlantic Region, Geological Society Special Publications. London, 2008, 294p.

GRIFFIN, W.L. et al. The composition and evolution of lithospheric mantle: A reevaluation and its tectonic implications. **Journal of Petrology**, v. 50, p. 1185-1204, 2008.

GRIFFIN, W.L.; BEGG, G.C.; O'REILLY, S.Y. Continental-root control on the genesis of magmatic ore deposits. **Nature Geoscience**, v. 6, 2013.

GROVES, D.; GOLDFARD, R.J.; SANTOSH, M. The conjunction of factors that lead to formation of giant gold provinces and deposits in non-arc settings. **Geoscience Frontiers**, n.7, p.303-314, 2016.

GROVES, D.I. et al. Iron oxide copper gold (IOCG) deposits through Earth history: Implications for origin, lithospheric setting, and distinction from other epigenetic iron oxide deposits. **Economic Geology**, v. 105, p. 641–654, 2010.

HART, J.; FREEMAN, H. Geophysics of Prominent Hill deposit, South Australia**. Australian Society of Exploration Geophysicists**, v. 110, p. 27–30, 2004.

HAYWARD, N. et al. Geophysical signature of the NICO Au-Co-Bi-Cu deposit and its iron oxide-alkali alteration system, Northwest Territories, Canada. **Economic Geology**, v. 111, p. 2087–2109, 2016.

HAYWARD, N. et al. The application of rapid potential field methods for the targeting of IOCG mineralisation based on physical property data, Great Bear magmatic zone, Canada. **Journal of Applied Geophysics**, v. 94, p. 42–58, 2013.

HITZMAN, M.W. Iron oxide-Cu-Au deposits: what, where, when, and why. In: PORTER, T.M. (ed.). **Hydrothermal iron oxidecopper-gold and related deposits**: a global perspective, Adelaide, Australian Mineral Foundation, 2000. p. 9-25

HITZMAN, M.W.; ORESKES, N.; EINAUDI, M.T. Geological characteristics and tectonic setting of Proterozoic iron oxide (Cu-U-Au-REE) deposits. **Precambrian Research**, n.58, p.241-287, 1992.

HOLDSWORTH, R.E.; PINHEIRO, R.V.L. The anatomy of shallow-crustal transpressional structures: insights from the Archean Carajás fault zone, Amazon, Brazil. **J Struct Geol.,** n.22, p.1105–1123, 2000.

HUHN, S.R.B.; NASCIMENTO, J.A.S. São os depósitos cupríferos de Carajás do tipo Cu-Au-U-ETR? In: COSTA M.L., ANGÉLICA R.S. (coords.). **Contribuições à Geologia da Amazônia**. Belém: FINEP.SBG-NO, 1997. p. 143-160.

HUHN, S.R.B.; SILVA, A.M. Favourability Potential for IOCG type of Deposits in the Riacho do Pontal Belt: New insights for identifying prospects of IOCG type deposits in NE Brazil. **Brazilian Journal of Geology**, 2018. No prelo.

HÜHN, S.R.B.et al. Geology of the Riacho do Pontal iron oxide copper-gold (IOCG) prospect, Bahia, Brazil: hydrothermal alteration approached via hierarchical cluster analysis. **Brazilian Journal of Geology**, n.44, v.2, p.309-324, June 2014.

JULIANI, C.; MONTEIRO, L.V.; FERNANDES, C.M.D. Potencial mineral: cobre. In: _____. **Recursos Mineral do Brasil**: problemas e desafios, 2016. 134-153p.

LEÃO-SANTOS, M.; LI, Y.; MORAES, R. Application of 3D magnetic amplitude inversion to iron oxide-copper-gold deposits at low magnetic latitudes: A case study from Carajás Mineral Province, Brazil: **Geophysics**, n.80, v. 2, B13–B22, 2015. doi: 10.1190/geo2014-0082.1.

LESHER, M. et al. Integrated Multi-Parameter Exploration Footprints of the Canadian Malartic Disseminated Au, McArthur River-Millennium Unconformity U, and Highland Valley Porphyry Cu Deposits: Preliminary Results from the NSERC-CMIC Mineral Exploration Footprints Research Network. In: PROCEEDINGS of Exploration 17: Sixth Decennial International Conference on Mineral Exploration" edited by V. Tschirhart and M.D. Thomas, 2017, p. 325–347, 2018.

LI, Y.; OLDENBURG, D.W. 3-D inversion of magnetic data. **Geophysics**, v. 61, p.394–408, 1996.

LIÉGEOIS, J.P.; STERN, R.J. Sr-Nd isotopes and geochemistry of granite-gneisses complexes from the Meatiq and Hafafit domes, Eastern Desert, Egypt: no evidencefor pre-Neoproterozoic crust. **Journal of African Earth Sciences**, n.57, p.31-40, 2010.

LIMA, H. M. et al. Geochemical and detrital zircon geochronological investigation of the metavolcanosedimentary Araticum complex, sergipano fold belt: Implications for the evolution of the Borborema Province, NE Brazil. **Journal of South American Earth Sciences,** n.86,p.176-192, 2018a.

LINDENMAYER, Z.G. Evolução geológica do Vale do Rio Curaçá e dos corpos máfico-ultramáficos mineralizados a cobre (Orgs.). In: INDA, H.A.V.; MARINHO, M.M.; DUARTE, F.B. (Eds.). **Geologia e Recursos Minerais do Estado da Bahia**: textos básicos. Salvador: SME, p. 72-110, 1981. V.4

LINDENMAYER, Z.G. **Evolução geológica do vale do rio Curaçá e dos corpos máfico-ultramáficos mineralizados a cobre.** 1982. 140f. Dissertação (Mestrado) - Instituto de Geociências, Universidade Federal da Bahia, Bahia, 1982.140 p.

LINDENMAYER, Z.G.; TEIXEIRA, J.B.G. Ore genesis at the Salobo copper deposit, Serra dos Carajás. In: SILVA, S.G.; MISI, A. (eds). **Base metal deposits of Brazil**. Belo Horizonte, MME/CPRM/DNPM, 1999. p 33–43.

MAIER, W.D.; BARNES, S.J. The origin of Cu sulfide deposits at Curaçá Valley, Bahia, Brazil: evidence form Cu, Ni, Se and platinum – Group Element Concentrations. **Economic Geology,** n.49, v.2, p.165, 1999.

MCCAFFERTY, A.E.; PHILLIPS, J.D.; DRISCOLL, R.L. Magnetic and Gravity Gradiometry Framework For Mesoproterozoic Iron-Oxide-Apatite and Iron-Copper-Gold Deposits, Southesat Missouri. **Economic Geology**, v.111, p 1859-1882, 2016.

MCPHIE, J. et al. The fluorine link between a supergiant ore deposit and silicic large igneous province. **Geology**, v. 39, p. 1003–1006, 2011.
MELO, G.H.C. et al. Temporal evolution of the giant Salobo IOCG deposit, Carajás Province (Brazil): constraints from paragenesis of hydrothermal alteration and U-Pb geochronology. **Mineralium Deposita**, n.52, p.709-732, 2016.

MENDONCA, R. J. et. al. 2018 Updated Mineral Resources and Mineral Reserves Statements of Mineração Caraíba's Vale do Curaçá Mineral Assets, Curaçá Valley. 2018. Bahia. Brazil. 284p.

MISI, A.; TEIXEIRA, J.B. **Mapa metalogenético digital do estado da Bahia**. 2. ed. Salvador: CBPM/SICM., 2008. 1 CD-ROM.

MONTEIRO, L.V.S. et al. Mineral chemistry of ore and hydrothermal alteration at the Sossego iron oxide-copper-gold deposit, CarajásMineral Province, Brazil. **Ore Geol Rev**., n.34, p.317–336, 2008b.

MONTEIRO, L.V.S. et al. Spatial and temporal zoning of hydrothermal alteration and mineralization in the Sossego iron oxide-copper-gold deposit, Carajás Mineral province, Brazil: paragenesis and stable isotope constraints. **Mineral Deposita,** n.43, p.129–159, 2008a.

NISBET, B.; COOKE, J.; WILLIAMS, C. Exploration for iron oxide copper gold deposits in Zambia and Sweden; comparison with the Australian experience Hydrothermal Iron Oxide-Gold and Related Deposits. A Global Prspective (ed). T. M. Porter. **PGC Publishing, Adelaide**, v.1, p.297-308, 2000.

O'DRISCOLL, Est. The application of lineament tectonics to the discovery of the Olympic Dam Cu-Au-U deposit at Roxby Downs, South Australia. **Global Tectonics andMetallogeny**, n.1,v.3, p. 43-57, 1985.

OLIVEIRA, E.P. et al. Age, composition, and source of continental arc- and syn-collisiongranites of the neoproterozoic Sergipano belt, southern Borborema province, Brazil. **J. S. Am. Earth Sci**., n.58, p.257–280, 2014.

OLIVEIRA, E.P. et al. Contrasting copper and chromium metallogenic evolution of terranes in thePaleoproterozoic Itabuna-Salvador-Curaçá orogen, São Francisco Craton, Brazil:new zircon (SHRIMP) and SmeNd (model) ages and their significance fororogen-parallel escape tectonics. **Precambrian Research**, n.128, p.143-165, 2004.

OLIVEIRA, E.P.; TARNEY, J. Genesis of the Precambrian copper-rich Caraíba hypersthenite-norite complex, Brazil. **Mineralium Deposita,** n.30, v.5, p.351-373,1995.

OLIVEIRA, R.G. **Arcabouço geofísico, isostasia e causas do magmatismo cenozóico da Província Borborema e de sua margem Continental (Nordeste do Brasil).** 2008. 411f. PhD (Thesis) - Universidade Federal do Rio Grande do Norte, Natal, 2008.

OLIVEIRA, R.G.; MEDEIROS, V.C. Contrastes geofísicos e heterogeneidade crustal do terreno Pernambuco-Alagoas, Província Borborema, NE Brasil. In*:* SBG-Núcleo Nordeste. SIMPÓSIO DE GEOLOGIA DO NORDESTE. 17., Recife, **Resumos…** Boletim 16, 2000. p. 176.

OLIVER, N.H.S. Modelling the role of sodic alteration in the genesis of iron-oxidecopper-gold deposits, Eastern Mt Isa Block, Australia, **Econ. Geol**., n.99, p.1145-1176, 2004.

ORIOLO, S.et al. Timing of deformation in the Sarandí del YíShear Zone, Uruguay: implications for the amalgamation of Western Gondwanaduring the Neoproterozoic

Brasiliano e Pan-African Orogeny. **Tectonics**, n.35, p.54e771, 2016. Disponivel em: < http://dx.doi.org/10.1002/2015TC004052>; Acesso em: 05.07.2017

PADILHA, A. V; Melo, R.C. 8th Chapter. Evolução Geológica. In: MELO, R. C. (Eds.),PLGB. **Pintadas**. Folha SC-24-Y-D-V. Texto Explicativo. 1991. Escala 1:100.000. DNPM, Brasília p. 129-157.

PIRAJNO, F.; BAGAS, L. A review of Australia's Proterozoic mineral systems and genetic models. **Precambrian Research**, v. 166, p. 54–80, 2008.

PIRAJNO, F.; HOATSON, D.M. A review of Australia's large igneous provinces and associated mineral systems: Implications for mantle dynamics through geological time. **Ore Geology Reviews**, v. 48, p. 2–54, 2012.

POLLARD, P.J. An intrusion-related origin for Cu-Au mineralization in iron oxide copper gold (IOCG) provinces. **Mineral Deposita**, n.41, p.179–187,2006.

POLLARD, P.J. et al. 40Ar-39Ar dating of Archean iron oxide Cu-Au and Paleoproterozoic granite-related Cu-Au deposits in the Carajás Mineral Province, Brazil: implications for genetic models. 2018. **Mineralium Deposita**. Disponivel em: <https://doi.org/10.1007/s00126-018-0809-1>. Acesso em: 05.03.208

POTTER, E.G.; CORRIVEAU, L.; KERSWILL, J.K. Potential for iron oxide-copper–gold and affiliated deposits in the proposed national park area of the East Arm, Northwest Territories: Insights from the Great Bear magmatic zone and global analogs. In: WRIGHT, D.F. et al. (eds.). **Mineral and energy resource assessment for the proposed Thaidene Nene National Park reserve, East Arm of Great Slave Lake, Northwest Territories, Geological Survey of Canada, Open File 7196**. 2013. Chapter 19.

REQUIA, K. et al. Re-Os and Pb-Pb geochronology of the Archean Salobo iron oxide copper-gold deposit, Carajás Mineral Province, northern Brazil. **Mineralium Deposita**, n.38, v.6, p.727-738, 2003.
Reviews, v. 30, p. 56–73, 2007.

ROCHA, A. M. R. **Metassomatismo hidrotermal e controle da mineralização aurífera na área da Mina Futura, depósito de Caraíba, Bahia**. 1999. 118f. Thesis - UniversidadeFederal do Rio Grande do Norte, Natal, 1999.

SÁ, E. F de Jardim; MACEDO, M.H.F.; FUCK, R.A. Terrenos proterozóicos na Província Borborema e a margem norte do Cráton São Francisco. **Revista Brasileira de Geociências**, n.22, v.4,p.472-480, 1992.

SÁ, de Jardim. **A Faixa Seridó (Província Borborema, NE do Brasil) e o seu significado geodinâmico na Cadeia Brasiliana/Pan-Africana**. 1994. 803f. PhD (Thesis) -Instituto de Geociências, Universidade de Brasília, Brasília, 1994. 803 p.

SANDRIN, A.; ELMING, S.Å. Physical properties of rocks from borehole TJ71305 and geophysical outline of the Tjårrojåkka Cu-prospect, northern Sweden. **Ore Geology**

SILVA FILHO, A.F. et al. SHRIMP U–Pb zircon geochronology and Nd signatures of supracrustal sequences and orthogneisses constrain the Neoproterozoicevolution of the Pernambuco–Alagoas domain, southern part of Borborema Province, NE Brazil. **Int. J. Earth Sci**., n.103, p.2155–2190, 2014.

SILVA, FC Alves da; CHAUVET, A; FAURE, M. Thrusting, Wrench-Type Tectonics and granite emplacement during an early Proterozoic Basin closure: The example of the Itapecuru greenstone belt NE-Brasil. In: SIMPOSIO DO CSF. 2., **Anais …** 1993. p.67-69, 1993.

SILVA, L.J.H.D. et al. U-Pb and Sm-Nd geochronology of amphibolites from the Curaçá belt, São Francisco craton, Brazil: Tectonic implications. **Gondwana Res**., n.12, p.454-467, 2007. Approximation of terrestrial lead isotope.

SILVA, L.J.H.D. Geologia e controle estrutural do depósito cuprífero Caraíba, Vale do Curaçá, Bahia. Geologia e Recursos Naturais do Estado da Bahia, SME, 1985. Série Textos Básicos, 6. p.51–123

SILVA, L.J.H.D.; OLIVEIRA, J.G.; GAAL, E.G. Implication of the Caraíba deposit's structural controls on the emplacement Brazilian. **Journal of Geology**, n.44, v.2, p.309-324, 1996.

SKIRROW R. The Olympic IOCG province (Gawler craton): Lithospheric to district-scale controls on ore formation, and targeting of IOCG mineral systems: Geoconferences IOCG Workshop, Perth, Australia, 29 May 2014, 40 p. 2014. Disponível em: <http://geoconferences.org.au/wp-content/uploads/PR_TeamWA_R_Skirrow.pdf>

SMITH, R.J. Geophysics of iron oxide copper-gold deposits. In: PORTER, T.M. (ed.). Hydrothermal iron oxide copper-gold and related deposits. **A global perspective**: Adelaide, PGC Publishing, v. 2, p. 357–367, 2002.

TALLARICO, F.H.B. et al. Geology and SHRIMP U–Pb geochronology of the Igarapé Bahia Deposit, Carajás Copper–Gold Belt, Brazil: an Archean (2.57 Ga) example of iron–oxide Cu–Au–(U–REE) mineralization. **Econ Geol**, n.100,p.7–28, 2005.

TEIXEIRA, J.B.G. et al. Depósitos de cobre do Vale do Rio Curaçá, Bahia. In: BRITO, R.S.C.; SILVA, M.G.; KUYUMJIAN, R.M. (eds.). **Modelos de depósitos de cobre do Brasil e sua resposta ao intemperismo**. Brasília, CPRM, 2010a, 190 p

TEIXEIRA, J.B.G. et al. Geotectonic setting and metallogeny of the northern São Francisco craton, Bahia, Brazil. **Journal of South American Earth Sciences**, n.30, p. 71-83, 2010b.

VALE S.A. **Projeto Furnas, 2012:** Relatório Final de Geologia: Internal report: Technical report, 2012.

VASCONCELOS, P.M. et al. $^{40}Ar/^{39}$Argeochronology at the Instituto de Geociências, USP: instrumentation, analytical procedures, and calibration. **Annals of the Brazilian Academy of Sciences**, v. 74, p. 297-342, 2002.

WILLIAMS, P. J. Iron mobility during synmetamorphic in the Selwyn Range area, NW Queensland: Implications for the origin of iron-stone-hosted Au-Cu **deposits: Minerallium Deposita**. v.29, p.250-260, 1994.

XAVIER, R.P. et al. Composition and source of salinity of ore-bearing fluids in Cu-Au systems of the Carajás Mineral Province, Brazil. In: **Proceedings of the 10th bienial meeting of the SGA**, n. 1, p 272–274, 2009.

XAVIER, R.P. et al. The iron oxide copper-gold deposits of the Carajás Mineral Province, Brazil: an updated and critical review. In: PORTER, T.M (ed). **Hydrothermal iron oxide copper-gold and related deposits**: a global perspective, v3 – advances in understanding of IOCG deposits. PGCPublishing, Adelaide, 2010. p 285–306.

CAPÍTULO 03 - CONCLUSÕES FINAIS

As principais conclusões obtidas no presente estudo sobre os Distritos cupríferos Riacho do Pontal e Vale do Curaçá são apresentadas a seguir:

1-As mineralizações de cobre nos Distritos Riacho do Pontal e Vale do Curaçá estão intrinsicamente associadas à zonas de cisalhamento mapeadas nos dados multifonte, que foram . reativadas e superpostas por eventos deformacioanais tardios;

2- A evolução estrutural nos Distritos Riacho do Pontal e Vale do Curaçá é marcada por zonas de cavalgamento superpostas por zonas de cisalhamento transcorrente;

3 - Padrões fractais representando estruturas SC são sistematicamente repetidos em macro, meso e micro-escalas. Essas estruturas são caminhos críticos para o fluxo ascendente de fluidos promovendo a interação entre a rocha fluida. Duplex, bandas de cisalhamento e estruturas assimétricas são bastante comuns ao longo do sistema de cisalhamento. Os “traps” mais importantes para os corpos de minério são representados por zonas de interconexão entre estruturas “SC”, estruturas fractais “C” de “segunda” ou terceira ordem e mudanças na inclinação do mergulho ao longo das zonas de cisalhamento nos planos horizontal e vertical. Normalmente brechas de minério estão hospedadas nestes traps. Ressalta-se que a interseção de falhas é favorável para os minérios do tipo “brecha-pipe”;

4-Os distritos Vale do Curaçá e Riacho do Pontal estão posicionados em domínios gravimétricos distintos. O Distrito cuprífero do Vale do Curaçá está localizado em um domínio com alto gravimétrico com 110 km de comprimento e 22 km de largura e mostra uma forte anomalia com comprimento de onda de até -40 mGal. As minas Caraíba, Surubim e Vermelhos e uma série de ocorrências de cobre estão posicionadas neste domínio;

5 - A assinatura gravimétrica do Distrito Riacho do Pontal é caracterizada principalmente por uma anomalia Bouguer NW-SE negativa (abaixo de -45 mGal). Esta anomalia Bouguer negativa representa a sutura colisional entre o bloco cratônico e o cinturão móvel de Riacho do Pontal. Geologicamente, essas áreas estão relacionadas a rochas do Complexo Sobradinho Remanso e a porção sul do Complexo Riacho Seco. As ocorrências IOCG dos prospectos Ria4 estão localizadas nesses domínios de baixa assinatura gravimétrica. As rochas, pouco alteradas, apresentam uma densidade da ordem de de 2,7-2,78 g / cm^3 e as rochas mais fortemente alteradas mostram densidade de 2,75-3,1 g / cm^3;

6 -A assinatura magnética dos distritos do Vale do Curaçá e do Riacho do Pontal são bastante distintas. As ocorrências de cobre situadas no Distrito do Vale do Curaçá estão

associadas a anomalias magnéticas, sigmóidais, situadas na porção oeste da Faixa Itabuna-Salvador-Curaçá . Por outro lado, os depósitos de cobre localizados no cinturão do Distrito do Riacho do Pontal localizam-se em zonas sem ou com a presença de anomalias magnéticas muito fracas;

7 – Os modelos gerados a partir da inversão de dados magnéticos e gravimétricos mostram dois principais “trends” prospectivos. Os “trends” I e II têm um gemetria sigmoidal e estão posicionadas na zona de contato entre domínios com anomalias magnéticas (SI> 0,005) e gravimétricas (> -10.000 mGal) e possuem um contraste na densidade e no teor de magnetita. O trend I apresenta 60 km de comprimento por 7 km de largura e hospeda as minas da Caraíba, Surubim e Vermelho e outros depósitos. Representa a direção mais importante para hospedar depósitos de IOCG no Distrito Vale do Curaçá. O “trend” II apresenta 35 km de comprimento por 5 km de largura. Geologicamente, estes trends representar oo o contato tectônico entre o gnaisse Surubim e ortognaisse tonalítico a granodiorítico e que hospedam os prospectos conhecidos;

8- Os corpos da Mina da Caraíba estão fortemente são marcados por anomalias magnéticas e gravimétricas do NNW, com susceptibilidade (SI) > 0,09 e com anomalias gravimétricas <-10.000 mGal. As rochas hospedeiras são ortognaisses granulíticos e corpos ultramáficos. A mina está situada a cerca de 1 km da zona de cisalhamento N-S que é truncada por zonas de cisalhamento do NW-SE. A zona mineralizada de Caraiba está relacionada é marcada por alta frequencia nos produtos derivados de dados magnéticos e gravimétricos;

9 - Os Prospectos Ria4 (1, 3 e 5) e o depósito do Riacho Seco não apresentam correlação com anomalias magnéticas. As ocorrências de cobre na região são posicionadas em baixos magnéticos. Essa observação é explicada pelo fato de que a zona mineralizada está relacionada às zonas de hematita (> minério de magnetita). No entanto, a análise das anomalias magnéticas do Riacho do Pontal em 3D no depósito de Riacho Seco mostra uma baixa anomalia magnética próxima à superfície e mudança de profundidade (> 500 m) para uma área com alta assinatura magnética, atingindo anomalias de até 24.500 nT (Figura 2.11). Os resultados abrem a possibilidade de um modelo contínuo para a busca de depósitos relacionados a anomalias magnéticas em maior profundidade.

10- The fuzzy analysis were used to assess the Riacho do Pontal Belt at the regional scale indicated that moderately and highly favorable areas have the potential to host IOCG

deposits. The modeling was validated with a drilling exploration program for the target RIA4. Drill hole RIA4-DH001 intersected a 32-m thick mineralized zone @ 1.15% Cu;

11- As grandes áreas que flanqueiam imagens de tomografia sismica de alta velocidade que já controlam em larga escala a Província de IOCG de Carajás e os distritos de cobre do Riacho do Pontal e do Vale do Curaçá no Brasil devem ser avaliadas em mais detalhes em programas exploratórios futuros.

References

ALKMIN, F.F; BRITO, Neves B.; CASTRO, J. Alves. Arcabouço tectônico do Cráton São Francisco: uma revisão. In: DOMINGUES, J.M.L.; MISI A. (eds.). **O Cráton do São Francisco**. Salvador: SBG/ SGM/CNPq, 1993. p. 45-62.

ALKMIN, FF; MARSHAK, S; FONSECA, MA. Assembling West Gondwana in the Neoproterozoic: clues from the Sao Francisco craton region, Brazil. **Geology**, n.29, p.319–322, 2001.

AUSTIN, J. et al. Remanence, self-demagnetization and their ramifications for magnetic modelling of iron oxide copper-gold deposits: An example from Candelaria, Chile: **Journal of Applied Geophysics**, v. 109, p. 242–255, 2014.

AUSTIN, J.; FOSS, C. Rich. **Attractive and extremely dense: a geophysical review of Australian IOCGs [ext. abs.]:** International Geophysical Conference and Exhibition. 22nd. Brisbane, Australia: Extended Abstracts, 2012. 4 p.

BARBOSA, J. S. F.; SABATÉ, P. Archean and Paleoproterozoic crust of the São Francisco Craton, Bahia, Brazil: geodynamic features. **Precambrian Research**, v. 133, p. 1-27, 2004.

BARBOSA, J.S.F. The granulites of the Jequié complex and Atlantic mobile belt,southern Bahia, Brazil: an expression of archean-proterozoic plate convergence. In: VIELZEUF, D.; VIDAL, P. (Eds.). **Granulites and crustal evolution**. Springer Verlag, 1990. p.195-221

BARBOSA, J.S.F.; DOMINGUEZ, J.M.L (eds.). **Geologia da Bahia**: texto explicativo. Salvador: SGM, 1996. 400 p.

BARNETT, C.T.; WILLIAMS, P.M. A radical approach to exploration: Let the data speak for themselves. **Society of Economic Geologists Newsletter,** n.90, v.1, p.12-17, 2012.

BARRIE, C.T.; HANNINGTON, M.D. Introduction: classification of VMS deposits based on host rock composition. In: _____. Volcanic-associated massive sulfide deposits: processes and examples in modern and ancient settings. **Reviews in Economic Geology**, n.8, Denver, Society of Economic Geologists, 1999. p. 2-10.

BARTON, M.D. Iron oxide (-Cu-Au-REE-P-Ag-U-Co) **systems**: Treatise on Geochemistry, 2nd ed., v. 13, p. 515–541, 2014.

BEGG, G.C. et al. Lithospheric, cratonic and geodynamic setting of Ni-Cu-PGE sulphide deposits. **Econ. Geol**., n.105, p.1057–1070, 2010.

BEGG, G.C. et al. The lithospheric architecture of Africa: Seismic tomography, mantle petrology and tectonic evolution. **Geosphere**, n.5, p. 23-50, 2009.

BELPERIO, A.; FLINT, R.; FREEMAN, H. Prominent Hill: A hematite-dominated, iron oxide copper-gold system. **Economic Geology**, v. 102, p. 1499–1510, 2007.

BLEWETT, R.S. et al. Scale-integrated architecture of a world-class gold mineral system: The Archaean eastern Yilgarn Craton, Western Australia. **Precambrian Research**, n.183, p.230–250, 2010.

BRITO, Neves BB; FUCK, R.A. The basement of the South American platform: half Laurentian (N-NW) half Gondwanan (E-SE) domains. **Precambrian Research**, n.244, p.75-86, 2014.

CLARK, D.A. Magnetic effects of hydrothermal alteration in porphyry copper and iron-oxide copper-gold systems. **A review: Tectonophysics**, v. 624–625, p. 46–65, 2014.

CLARK, D.A.; GEUNA, S.; SCHMIDT, P.W. **Predictive magnetic exploration models for porphyry, epithermal and iron oxide copper-gold deposits**: Implications for exploration, exploration and mining: Commonwealth Scientific and Industrial Research Organization (CSIRO) Exploration and Mining Report,2013. 1073R.

CLARK, J.M. **Defining the style of mineralization at the Cairn Hill magnetite-sulphide deposit, Mount Woods Inlier, Gawler Craton, South Australia**. The University of Adalaide. 2014. 69p.

COMPANHIA BAIANA DE PESQUISA MINERAIS – CBPM. **Informações Geológicas e de Recursos Minerais do Estado da Bahia**. 2011. Disponível em: < http://www.cbpm.com.br/igba/>. Acesso em: 22 mar. 2014.

COMPANHIA BAIANA DE PESQUISA MINERAIS – CBPM. **Levantamento aerogeofísico Projeto Riacho Seco Andorinhas**. 2001. Relatório Técnico. 2001. 80p.

COOKE, D.R. et al. New advances in detecting the distal geochemical footprints of porphyry systems – Epidote mineral Chemistry as a tool for vectoring and fertility assessments. **Society of Economic Geologists,** Special Publication, n.18, p.127–152, 2014.

CORRIVEAU, L., MUMIN, A.H., and SETTERFIELD, T. IOCG environments in Canada: Characteristics, geological vectors to ore and challenges, in Porter, T.M., ed., Hydrothermal iron oxide copper-gold & related deposits: A global perspective: Adelaide, Australia, **Porter Geoscience Consultancy Publishing**, v. 4, p. 311–344, 2010a.

CORRIEAU, L.; MUMIN, H.; MONTREUIL, J. F. The Great Bear magmatic zone (Canada): The IOCG spectrum and related deposit types: Society for Geology Applied to Mineral Deposits, **Biennial Meeting**, 11th, 26-29 September 2011, Antofagasta, Chile, Proceedings, Universidad Católica del Norte, v. 1, p. 524–526, 2011.

COSTA, I. **A Aerogeofísica em Carajás pelo Serviço Geológico do Brasil**. CPRM. Serviço Gologico do Brasil. 2017. p. 65p. Disponível em: <www.cprm.gov.br.>

CZARNOTA, M. et al. Spatial and temporal patterns of Cenozoic dynamic topography around Australia. **Geochem. Geophys**., n.14, p.634–658, 2013.

DELGADO, L.M.; SOUSA, J.D. **Projeto Cobre Curaçá**. Geologia Econômica do Distrito Cuprífero do Rio Curaçá, Bahia, 1975. Relatório Final. DNPM/CPRM.

DELGADO, L.M.; SOUZA, J.D. **Projeto Cobre Curaçá**. Cobre no Vale do Rio Curaçá, Estado da Bahia, Departamento Nacional de Produção Mineral, Seção Geologia Econômica, 1981. p. 7-149 (in Portuguese).

DREHER, A.M. et al. New geologic, fluid inclusion and stable isotope studies on the controversial Igarapé Bahia Cu-Au deposit, Carajás Province, Brazil. **Mineral Deposita** n.43,p.161–184, 2008.

ELLIS, R.G.; WET B. de, MacLeod. Inversion of magnetic data for remanent and induced sources. **ASEG Extended Abstracts,** p.1-4, 2012.

ESDALE, D. et al. The Olympic Dam copper-uranium-gold-silver-rare earth element deposit, South Australia: A geophysical case history. **Australian Society of Exploration Geophysicists Special Publication**, n.22, p.147–16, 2003.

FLECK, R.J.; SUTTER, J.F.; ELLIOT, D.H. Interpretation of discordant $^{40}Ar/^{39}Ar$ age-spectra of Mesozoic tholeiites from Antarctica. **Geochimica et Cosmochimica Acta**, v. 41, p. 15-32, 1977.

FRANKLIN, J.M.; LYDON, J.W.; SANGSTER, D. Volcanic-associated massive sulfide deposits. In: SKINNER, B.J. (ed.). **Economic Geology**, 75th Anniversary Volume, Denver, Society of Economic Geologists, p. 485-627, 1981.

FREITAS, J.P.S. **Elaboração do modelo geomecânico tridimensional para avaliação e setorização geotécnica dos realces da mineração Caraíba**. 2016. 2019f. Mestrado (Engenharia Geotécnica) – UFOP, 2016.

GANADE, C.E. et al. Tightening-up NE Brazil and NW Africa connections: New U–Pb/Lu–Hf zircon data of a complete plate tectonic cycle in the Dahomey belt of the West Gondwana Orogen in Togo and Benin. **Precambrian Research**, n.276, p.24–42, 2016.

GANADE, C.E.; WEINBERG, R.F.; CORDANI, U.G. Extruding the Borborema Province (NE-Brazil): a two-stage Neoproterozoic collision process. **Terra Nova**, n.26, p.157–168, 2014.

GARCIA, P.M.P. et al. Tectonic and metallogenic evolution of the Curaçá Valley Copper Province,Bahia, Brazil: A review based on new SHRIMP zircon U-Pb dating and sulfur isotope geochemistry. **Ore Geology Reviews**, n.93, p.361–381, 2018.

GARCIA, P.M.P. **Metalogênese dos depósitos cupríferos de Caraíba, Surubim, Vermelhos e Sussuarana, Vale do Curaçá, Bahia, Brasil**. 2013. 225 f. Dissertação (Mestrado) - Instituto de Geociências, Universidade Federal da Bahia, Salvador, 2013.

GRAINGER, C.J. et al. Metallogenesis of the Carajás Mineral Province, Southern Amazon Craton, Brazil: varying styles of Archean through Paleoproterozoic to Neoproterozoic base- and precious-metal mineralisation. **Ore Geol Rev.,** n.33, p.451–489, 2008.

GRAY, D.R. et al. A Damara orogen perspective on the assembly of southwestern Gondwana. In: PANKHURST, R.J. et al. (Eds.). **West Gondwana**: Pre-cenozoic Correlations across the South Atlantic Region, Geological Society Special Publications. London, 2008, 294p.

GRIFFIN, W.L. et al. The composition and evolution of lithospheric mantle: A reevaluation and its tectonic implications. **Journal of Petrology**, v. 50, p. 1185-1204, 2008.

GRIFFIN, W.L.; BEGG, G.C.; O'REILLY, S.Y. Continental-root control on the genesis of magmatic ore deposits. **Nature Geoscience**, v. 6, 2013.

GROVES, D.; GOLDFARD, R.J.; SANTOSH, M. The conjunction of factors that lead to formation of giant gold provinces and deposits in non-arc settings. **Geoscience Frontiers**, n.7, p.303-314, 2016.

GROVES, D.I. et al. Iron oxide copper gold (IOCG) deposits through Earth history: Implications for origin, lithospheric setting, and distinction from other epigenetic iron oxide deposits. **Economic Geology**, v. 105, p. 641–654, 2010.

HART, J.; FREEMAN, H. Geophysics of Prominent Hill deposit, South Australia**. Australian Society of Exploration Geophysicists**, v. 110, p. 27–30, 2004.

HAYWARD, N. et al. Geophysical signature of the NICO Au-Co-Bi-Cu deposit and its iron oxide-alkali alteration system, Northwest Territories, Canada. **Economic Geology**, v. 111, p. 2087–2109, 2016.

HAYWARD, N. et al. The application of rapid potential field methods for the targeting of IOCG mineralisation based on physical property data, Great Bear magmatic zone, Canada. **Journal of Applied Geophysics**, v. 94, p. 42–58, 2013.

HITZMAN, M.W. Iron oxide-Cu-Au deposits: what, where, when, and why. In: PORTER, T.M. (ed.). **Hydrothermal iron oxidecopper-gold and related deposits**: a global perspective, Adelaide, Australian Mineral Foundation, 2000. p. 9-25

HITZMAN, M.W.; ORESKES, N.; EINAUDI, M.T. Geological characteristics and tectonic setting of Proterozoic iron oxide (Cu-U-Au-REE) deposits. **Precambrian Research**, n.58, p.241-287, 1992.

HOLDSWORTH, R.E.; PINHEIRO, R.V.L. The anatomy of shallow-crustal transpressional structures: insights from the Archean Carajás fault zone, Amazon, Brazil. **J Struct Geol.,** n.22, p.1105–1123, 2000.

HUHN, S.R.B.; NASCIMENTO, J.A.S. São os depósitos cupríferos de Carajás do tipo Cu-Au-U-ETR? In: COSTA M.L., ANGÉLICA R.S. (coords.). **Contribuições à Geologia da Amazônia**. Belém: FINEP.SBG-NO, 1997. p. 143-160.

HUHN, S.R.B.; SILVA, A.M. Favourability Potential for IOCG type of Deposits in the Riacho do Pontal Belt: New insights for identifying prospects of IOCG type deposits in NE Brazil. **Brazilian Journal of Geology**, 2018. No prelo.

HÜHN, S.R.B.et al. Geology of the Riacho do Pontal iron oxide copper-gold (IOCG) prospect, Bahia, Brazil: hydrothermal alteration approached via hierarchical cluster analysis. **Brazilian Journal of Geology**, n.44, v.2, p.309-324, June 2014.

JULIANI, C.; MONTEIRO, L.V.; FERNANDES, C.M.D. Potencial mineral: cobre. In: _____. **Recursos Mineral do Brasil**: problemas e desafios, 2016. 134-153p.

LEÃO-SANTOS, M.; LI, Y.; MORAES, R. Application of 3D magnetic amplitude inversion to iron oxide-copper-gold deposits at low magnetic latitudes: A case study from Carajás Mineral Province, Brazil: **Geophysics**, n.80, v. 2, B13–B22, 2015. doi: 10.1190/geo2014-0082.1.

LESHER, M. et al. Integrated Multi-Parameter Exploration Footprints of the Canadian Malartic Disseminated Au, McArthur River-Millennium Unconformity U, and Highland Valley Porphyry Cu Deposits: Preliminary Results from the NSERC-CMIC Mineral Exploration Footprints Research Network. In: PROCEEDINGS of Exploration 17: Sixth Decennial International Conference on Mineral Exploration" edited by V. Tschirhart and M.D. Thomas, 2017, p. 325–347, 2018.

LI, Y.; OLDENBURG, D.W. 3-D inversion of magnetic data. **Geophysics**, v. 61, p.394–408, 1996.

LIÉGEOIS, J.P.; STERN, R.J. Sr-Nd isotopes and geochemistry of granite-gneisses complexes from the Meatiq and Hafafit domes, Eastern Desert, Egypt: no evidencefor pre-Neoproterozoic crust. **Journal of African Earth Sciences**, n.57, p.31-40, 2010.

LIMA, H. M. et al. Geochemical and detrital zircon geochronological investigation of the metavolcanosedimentary Araticum complex, sergipano fold belt: Implications for the evolution of the Borborema Province, NE Brazil. **Journal of South American Earth Sciences,** n.86,p.176-192, 2018a.

LINDENMAYER, Z.G. Evolução geológica do Vale do Rio Curaçá e dos corpos máfico-ultramáficos mineralizados a cobre (Orgs.). In: INDA, H.A.V.; MARINHO, M.M.; DUARTE, F.B. (Eds.). **Geologia e Recursos Minerais do Estado da Bahia**:textos básicos. Salvador: SME, p. 72-110, 1981. V.4

LINDENMAYER, Z.G. **Evolução geológica do vale do rio Curaçá e dos corpos máfico-ultramáficos mineralizados a cobre.** 1982. 140f. Dissertação (Mestrado) - Instituto de Geociências, Universidade Federal da Bahia, Bahia, 1982.140 p.

LINDENMAYER, Z.G.; TEIXEIRA, J.B.G. Ore genesis at the Salobo copper deposit, Serra dos Carajás. In: SILVA, S.G.; MISI, A. (eds). **Base metal deposits of Brazil**. Belo Horizonte, MME/CPRM/DNPM, 1999. p 33–43.

MAIER, W.D.; BARNES, S.J. The origin of Cu sulfide deposits at Curaçá Valley, Bahia, Brazil: evidence form Cu, Ni, Se and platinum – Group Element Concentrations. **Economic Geology,** n.49, v.2, p.165, 1999.

MCCAFFERTY, A.E.; PHILLIPS, J.D.; DRISCOLL, R.L. Magnetic and Gravity Gradiometry Framework For Mesoproterozoic Iron-Oxide-Apatite and Iron-Copper-Gold Deposits, Southesat Missouri. **Economic Geology**, v.111, p 1859-1882, 2016.

MCPHIE, J. et al. The fluorine link between a supergiant ore deposit and silicic large igneous province. **Geology**, v. 39, p. 1003–1006, 2011.

MELO, G.H.C. et al. Temporal evolution of the giant Salobo IOCG deposit, Carajás Province (Brazil): constraints from paragenesis of hydrothermal alteration and U-Pb geochronology. **Mineralium Deposita**, n.52, p.709-732, 2016.

MISI, A.; TEIXEIRA, J.B. **Mapa metalogenético digital do estado da Bahia**. 2. ed. Salvador: CBPM/SICM., 2008. 1 CD-ROM.

MONTEIRO, L.V.S. et al. Mineral chemistry of ore and hydrothermal alteration at the Sossego iron oxide-copper-gold deposit, CarajásMineral Province, Brazil. **Ore Geol Rev**., n.34, p.317–336, 2008b.

MONTEIRO, L.V.S. et al. Spatial and temporal zoning of hydrothermal alteration and mineralization in the Sossego iron oxide-copper-gold deposit, Carajás Mineral province, Brazil: paragenesis and stable isotope constraints. **Mineral Deposita,** n.43, p.129–159, 2008a.

NISBET, B.; COOKE, J.; WILLIAMS, C. Exploration for iron oxide copper gold deposits in Zambia and Sweden; comparison with the Australian experience Hydrothermal Iron Oxide-Gold and Related Deposits. A Global Prspective (ed). T. M. Porter. **PGC Publishing, Adelaide**, v.1, p.297-308, 2000.

O'DRISCOLL, Est. The application of lineament tectonics to the discovery of the Olympic Dam Cu-Au-U deposit at Roxby Downs, South Australia. **Global Tectonics andMetallogeny**, n.1,v.3, p. 43-57, 1985.

OLIVEIRA, E.P. et al. Age, composition, and source of continental arc- and syn-collisiongranites of the neoproterozoic Sergipano belt, southern Borborema province, Brazil. **J. S. Am. Earth Sci**., n.58, p.257–280, 2014.

OLIVEIRA, E.P. et al. Contrasting copper and chromium metallogenic evolution of terranes in thePaleoproterozoic Itabuna-Salvador-Curaçá orogen, São Francisco Craton, Brazil:new zircon (SHRIMP) and SmeNd (model) ages and their significance fororogen-parallel escape tectonics. **Precambrian Research**, n.128, p.143-165, 2004.

OLIVEIRA, E.P.; TARNEY, J. Genesis of the Precambrian copper-rich Caraíba hypersthenite-norite complex, Brazil. **Mineralium Deposita,** n.30, v.5, p.351-373,1995.

OLIVEIRA, R.G. **Arcabouço geofísico, isostasia e causas do magmatismo cenozóico da Província Borborema e de sua margem Continental (Nordeste do Brasil).** 2008. 411f. PhD (Thesis) - Universidade Federal do Rio Grande do Norte, Natal, 2008.

OLIVEIRA, R.G.; MEDEIROS, V.C. Contrastes geofísicos e heterogeneidade crustal do terreno Pernambuco-Alagoas, Província Borborema, NE Brasil. In*:* SBG-Núcleo Nordeste. SIMPÓSIO DE GEOLOGIA DO NORDESTE. 17., Recife, **Resumos…** Boletim 16, 2000. p. 176.

OLIVER, N.H.S. Modelling the role of sodic alteration in the genesis of iron-oxidecopper-gold deposits, Eastern Mt Isa Block, Australia, **Econ. Geol**., n.99, p.1145-1176, 2004.

ORIOLO, S.et al. Timing of deformation in the Sarandí del YíShear Zone, Uruguay: implications for the amalgamation of Western Gondwanaduring the Neoproterozoic

Brasiliano e Pan-African Orogeny. **Tectonics**, n.35, p.54e771, 2016. Disponivel em: < http://dx.doi.org/10.1002/2015TC004052>. Acesso em: 05.07.2017.

PADILHA, A. V; Melo, R.C. 8th Chapter. Evolução Geológica. In: Melo, R. C. (Eds.),PLGB. Pintadas. Folha SC-24-Y-D-V. Texto Explicativo. 1991. Escala 1:100.000. DNPM, Brasília p. 129-157.

PIRAJNO, F.; BAGAS, L. A review of Australia's Proterozoic mineral systems and genetic models. **Precambrian Research**, v. 166, p. 54–80, 2008.

PIRAJNO, F.; HOATSON, D.M. A review of Australia's large igneous provinces and associated mineral systems: Implications for mantle dynamics through geological time. **Ore Geology Reviews**, v. 48, p. 2–54, 2012.

POLLARD, P.J. An intrusion-related origin for Cu-Au mineralization in iron oxide copper gold (IOCG) provinces. **Mineral Deposita**, n.41, p.179–187,2006.

POLLARD, P.J. et al. 40Ar-39Ar dating of Archean iron oxide Cu-Au and Paleoproterozoic granite-related Cu-Au deposits in the Carajás Mineral Province, Brazil: implications for genetic models. 2018. **Mineralium Deposita**. Disponivel em: <https://doi.org/10.1007/s00126-018-0809-1>. Acesso em: 05.03.208

POTTER, E.G.; CORRIVEAU, L.; KERSWILL, J.K. Potential for iron oxide-copper–gold and affiliated deposits in the proposed national park area of the East Arm, Northwest Territories: Insights from the Great Bear magmatic zone and global analogs. In: WRIGHT, D.F. et al. (eds.). **Mineral and energy resource assessment for the proposed Thaidene Nene National Park reserve, East Arm of Great Slave Lake, Northwest Territories, Geological Survey of Canada, Open File 7196**. 2013. Chapter 19.

REQUIA, K. et al. Re-Os and Pb-Pb geochronology of the Archean Salobo iron oxide copper-gold deposit, Carajás Mineral Province, northern Brazil. **Mineralium Deposita**, n.38, v.6, p.727-738, 2003.
Reviews, v. 30, p. 56–73, 2007.

ROCHA, A. M. R. **Metassomatismo hidrotermal e controle da mineralização aurífera na área da Mina Futura, depósito de Caraíba, Bahia**. 1999. 118f. Thesis - UniversidadeFederal do Rio Grande do Norte, Natal, 1999.

SÁ, E. F de Jardim; MACEDO, M.H.F.; FUCK, R.A. Terrenos proterozóicos na Província Borborema e a margem norte do Cráton São Francisco. **Revista Brasileira de Geociências**, n.22, v.4,p.472-480, 1992.

SÁ, de Jardim. **A Faixa Seridó (Província Borborema, NE do Brasil) e o seu significado geodinâmico na Cadeia Brasiliana/Pan-Africana**. 1994. 803f. PhD (Thesis) -Instituto de Geociências, Universidade de Brasília, Brasília, 1994. 803 p.

SANDRIN, A.; ELMING, S.Å. Physical properties of rocks from borehole TJ71305 and geophysical outline of the Tjårrojåkka Cu-prospect, northern Sweden. **Ore Geology**

SILVA FILHO, A.F. et al. SHRIMP U–Pb zircon geochronology and Nd signatures of supracrustal sequences and orthogneisses constrain the Neoproterozoicevolution of the Pernambuco–Alagoas domain, southern part of Borborema Province, NE Brazil. **Int. J. Earth Sci**., n.103, p.2155–2190, 2014.

SILVA, FC Alves da; CHAUVET, A; FAURE, M. Thrusting, Wrench-Type Tectonics and granite emplacement during an early Proterozoic Basin closure: The example of the Itapecuru greenstone belt NE-Brasil. In: SIMPOSIO DO CSF. 2., **Anais …** 1993. p.67-69, 1993.

SILVA, L.J.H.D. et al. U-Pb and Sm-Nd geochronology of amphibolites from the Curaçá belt, São Francisco craton, Brazil: Tectonic implications. **Gondwana Res**., n.12, p.454-467, 2007. Approximation of terrestrial lead isotope.

SILVA, L.J.H.D. Geologia e controle estrutural do depósito cuprífero Caraíba, Vale do Curaçá, Bahia. Geologia e Recursos Naturais do Estado da Bahia, SME, 1985. Série Textos Básicos, 6. p.51–123

SILVA, L.J.H.D.; OLIVEIRA, J.G.; GAAL, E.G. Implication of the Caraíba deposit's structural controls on the emplacement Brazilian. **Journal of Geology**, n.44, v.2, p.309-324, 1996.

SKIRROW R. **The Olympic IOCG province (Gawler craton):** Lithospheric to district-scale controls on ore formation, and targeting of IOCG mineral systems: Geoconferences IOCG Workshop, Perth, Australia, 29 May 2014, 40 p. 2014. Disponível em: <http://geoconferences.org.au/wp-content/uploads/PR_TeamWA_R_Skirrow.pdf>

SMITH, R.J. Geophysics of iron oxide copper-gold deposits, *in* Porter, T.M., ed., Hydrothermal iron oxide copper-gold and related deposits. **A global perspective**: Adelaide, PGC Publishing, v. 2, p. 357–367, 2002.

TALLARICO, F.H.B. et al. Geology and SHRIMP U–Pb geochronology of the Igarapé Bahia Deposit, Carajás Copper–Gold Belt, Brazil: an Archean (2.57 Ga) example of iron–oxide Cu–Au–(U–REE) mineralization. **Econ Geol**, n.100,p.7–28, 2005.

TEIXEIRA, J.B.G. et al. Depósitos de cobre do Vale do Rio Curaçá, Bahia. In: BRITO, R.S.C.; SILVA, M.G.; KUYUMJIAN, R.M. (eds.). **Modelos de depósitos de cobre do Brasil e sua resposta ao intemperismo**. Brasília, CPRM, 2010a, 190 p

TEIXEIRA, J.B.G. et al. Geotectonic setting and metallogeny of the northern São Francisco craton, Bahia, Brazil. **Journal of South American Earth Sciences**, n.30, p. 71-83, 2010b.

VALE S.A**. Projeto Furnas, 2012.** Relatório Final de Geologia: Internal report: Technical report, 2012.

VASCONCELOS, P.M. et al. $^{40}Ar/^{39}Ar$geochronology at the Instituto de Geociências, USP: instrumentation, analytical procedures, and calibration. **Annals of the Brazilian Academy of Sciences**, v. 74, p. 297-342, 2002.

WILLIAMS, P. J. Iron mobility during synmetamorphic in the Selwyn Range area, NW Queensland: Implications for the origin of iron-stone-hosted Au-Cu **deposits: Minerallium Deposita**. v.29, p.250-260, 1994.

XAVIER, R.P. et al. Composition and source of salinity of ore-bearing fluids in Cu-Au systems of the Carajás Mineral Province, Brazil. In: PROCEEDINGS of the 10th bienial meeting of the SGA, n. 1, p 272–274, 2009.

XAVIER, R.P. et al. The iron oxide copper-gold deposits of the Carajás Mineral Province, Brazil: an updated and critical review. In: PORTER, T.M (ed). **Hydrothermal iron oxide copper-gold and related deposits**: a global perspective, v3 – advances in understanding of IOCG deposits. PGCPublishing, Adelaide, 2010. p 285–306.

APÊNDICE I

Geocronological Data

APPENDIX IA: Detrital zircon U-PB

Three samples were selected for detrital zircon U-Pb analyses: garnet-biotite paragneiss (sample DH001-003) and biotite paragneiss (sample DH002-009). The results are in Table 4. Sixty-three (63) spots from sample DH-001-003 were measured. All spots show concordant analysis.

Spot Name	(ppm)	h (ppm)	h/U	ommon ^{206}Pb%	06Pb* (ppm)	^{06}Pb*/^{238}U	%	rr. Corr.	^{07}Pb*/^{06}Pb*	%	^{206}Pb/^{238}U Age		^{207}Pb/^{206}Pb Age		Di scordancy (%)
DH001-003															
DH001-003-1.1	40	6	.19	.00	5	.373	.0	.81	.1254	.73	**044**	**18**	**035**	**13**	**0**
DH001-003-2.1	74	2	.25	.02	6	.372	.9	.81	.1253	.66	**038**	**16**	**034**	**12**	**0**
DH001-003-3.1	54	3	.22	.00	9	.373	.0	.81	.1265	.68	**044**	**17**	**050**	**12**	**0**
DH001-003-4.1	30	6	.34	-	4	.375	.8	.81	.1261	.61	**053**	**15**	**044**	**11**	**-1**
DH001-003-5.1	33	7	.30	-	06	.369	.8	.87	.1271	.49	**027**	**15**	**058**	**9**	**2**
DH001-003-6.1	37	4	.18	.09	3	.368	.1	.82	.1246	.79	**021**	**20**	**023**	**14**	**0**
DH001-003-7.1	88	8	.21	-	1	.379	.9	.80	.1263	.67	**070**	**16**	**047**	**12**	**-1**
DH001-003-8.1	01	6	.24	-	5	.376	.4	.77	.1267	.17	**059**	**25**	**052**	**21**	**0**
DH001-003-9.1	57	0	.20	-	0	.370	.9	.81	.1257	.67	**030**	**16**	**038**	**12**	**0**
DH001-003-10.1	88	2	.23	.00	1	.377	.0	.98	.1269	.62	**062**	**52**	**055**	**11**	**0**
DH001-003-11.1	72	3	.20	-	6	.380	.9	.81	.1265	.67	**078**	**17**	**050**	**12**	**-2**
DH001-003-12.1	15	7	.16	.10	4	.347	.1	.76	.1236	.89	**922**	**18**	**009**	**16**	**5**
DH001-003-13.1	74	6	.21	.02	3	.354	.0	.85	.1253	.65	**953**	**17**	**033**	**11**	**5**
DH001-003-14.1	57	1	.20	.00	1	.374	.7	.93	.1250	.67	**050**	**30**	**028**	**12**	**-1**

DH001-003-15.1	39	7	.20	-	4	.368	.0	.80	.1256	.75	**022**	**17**	**037**	**13**	**1**
DH001-003-16.1	99	6	.24	.02	5	.381	.0	.85	.1261	.62	**083**	**18**	**044**	**11**	**-2**
DH001-003-17.1	73	7	.22	-	5	.370	.9	.81	.1266	.66	**030**	**16**	**051**	**12**	**1**
DH001-003-18.1	78	7	.25	-	8	.369	.9	.86	.1256	.52	**026**	**15**	**038**	**9**	**1**
DH001-003-19.1	67	6	.22	-	4	.375	.6	.92	.1270	.69	**055**	**28**	**057**	**12**	**0**
DH001-003-20.1	03	6	.16	.04	3	.375	.1	.78	.1252	.88	**052**	**19**	**032**	**16**	**-1**
DH001-003-21.1	58	4	.22	-	8	.357	.0	.81	.1258	.68	**969**	**16**	**041**	**12**	**4**
DH001-003-22.1	64	8	.24	.05	2	.369	.9	.94	.1246	.69	**023**	**32**	**023**	**12**	**0**
DH001-003-23.1	59	6	.24	.02	1	.372	.4	.96	.1271	.66	**038**	**42**	**058**	**12**	**1**
DH001-003-24.1	93	5	.24	.02	2	.372	.9	.81	.1257	.62	**039**	**15**	**038**	**11**	**0**
DH001-003-25.1	45	1	.22	.04	1	.384	.9	.85	.1252	.55	**094**	**16**	**031**	**10**	**-4**
DH001-003-26.1	47	8	.20	.08	8	.377	.0	.79	.1251	.74	**064**	**17**	**030**	**13**	**-2**
DH001-003-27.1	30	0	.27	.02	4	.372	.8	.82	.1245	.56	**041**	**14**	**022**	**10**	**-1**
DH001-003-28.1	78	1	.24	.04	5	.359	.0	.83	.1229	.68	**979**	**17**	**999**	**12**	**1**
DH001-003-29.1	52	7	.19	.00	9	.373	.0	.92	.1252	.83	**042**	**34**	**032**	**15**	**-1**
DH001-003-30.1	78	0	.12	.13	6	.364	.0	.82	.1246	.72	**002**	**18**	**023**	**13**	**1**
DH001-003-31.1	37	4	.18	.11	3	.366	.1	.97	.1251	.78	**010**	**54**	**030**	**14**	**1**
DH001-003-32.1	70	1	.25	-	3	.365	.1	.98	.1271	.67	**008**	**53**	**058**	**12**	**3**
DH001-003-33.1	24	0	.16	.00	9	.368	.4	.93	.1248	.92	**019**	**42**	**026**	**16**	**0**
DH001-003-34.1	57	5	.23	.02	0	.374	.9	.81	.1259	.68	**046**	**16**	**041**	**12**	**0**
DH001-003-35.1	30	4	.19	.03	2	.374	.1	.94	.1259	.75	**048**	**36**	**041**	**13**	**0**
DH001-003-36.1	84	5	.26	.00	8	.364	.2	.96	.1270	.62	**003**	**37**	**056**	**11**	**3**
DH001-003-37.1	40	5	.18	.03	5	.378	.0	.81	.1258	.71	**066**	**17**	**040**	**13**	**-2**
DH001-003-38.1	59	8	.11	.55	9	.363	.9	.66	.1211	.06	**995**	**16**	**973**	**19**	**-1**

DH001-003-39.1	95	3	.23	.06	1	.365	.0	.84	.1255	.62	**006**	**17**	**036**	**11**	**2**
DH001-003-40.1	65	1	.19	.00	3	.376	.0	.84	.1248	.66	**059**	**18**	**025**	**12**	**-2**
DH001-003-41.1	60	4	.15	-	1	.370	.4	.96	.1255	.68	**030**	**42**	**036**	**12**	**0**
DH001-003-42.1	02	7	.24	.05	3	.365	.6	.94	.1257	.61	**007**	**28**	**038**	**11**	**2**
DH001-003-43.1	31	2	.18	.03	2	.375	.1	.84	.1266	.74	**052**	**20**	**052**	**13**	**0**
DH001-003-44.1	39	9	.21	.05	5	.375	.6	.92	.1245	.72	**051**	**29**	**021**	**13**	**-2**
DH001-003-45.1	48		.01	.04	06	.356	.3	.94	.1234	.48	**964**	**22**	**006**	**8**	**2**
DH001-003-46.1	02	5	.23	-	4	.368	.2	.97	.1259	.59	**022**	**38**	**042**	**10**	**1**
DH001-003-47.1	77	0	.24	.04	7	.371	.9	.81	.1259	.65	**034**	**15**	**042**	**11**	**0**
DH001-003-48.1	44	9	.21	.03	5	.364	.9	.93	.1248	.72	**000**	**32**	**025**	**13**	**1**
DH001-003-49.1	31	2	.18	.08	0	.359	.1	.82	.1263	.78	**977**	**19**	**047**	**14**	**4**
DH001-003-50.1	49	0	.21	.00	0	.389	.1	.85	.1266	.66	**119**	**20**	**051**	**12**	**-4**
DH001-003-51.1	50	2	.22	-	7	.363	.7	.92	.1259	.69	**995**	**29**	**041**	**12**	**3**
DH001-003-52.1	59	3	.21	.02	1	.373	.9	.81	.1278	.65	**043**	**16**	**068**	**12**	**1**
DH001-003-53.1	21		.02	.00	8	.356	.7	.84	.1240	.48	**962**	**13**	**015**	**8**	**3**
DH001-003-54.1	75	5	.21	-	5	.367	.9	.80	.1272	.67	**017**	**16**	**060**	**12**	**2**
DH001-003-55.1	06	8	.18	.00	3	.368	.1	.79	.1260	.82	**019**	**19**	**042**	**15**	**1**
DH001-003-56.1	37	7	.20	.00	3	.370	.6	.96	.1266	.71	**031**	**45**	**052**	**12**	**1**
DH001-003-57.1	27	1	.17	.00	0	.367	.9	.97	.1262	.74	**014**	**51**	**045**	**13**	**2**
DH001-003-58.1	28	0	.16	.08	1	.368	.8	.96	.1251	.77	**020**	**49**	**030**	**14**	**1**
DH001-003-59.1	07	5	.22	.07	5	.365	.0	.84	.1238	.62	**006**	**17**	**012**	**11**	**0**
DH001-003-60.1	80	2	.24	-	7	.367	.8	.94	.1266	.64	**015**	**31**	**051**	**11**	**2**
DH001-003-61.1	52	9	.20	.09	7	.360	.1	.83	.1239	.71	**982**	**18**	**014**	**13**	**2**
DH001-003-62.1	31	5	.20	.05	2	.373	.1	.83	.1257	.75	**044**	**20**	**039**	**13**	**0**

DH001-003-63.1	36	1	.22	.09	4	.367	.2	.97	.1244	.58	**016**	**37**	**021**	**10**	**0**
DH002-009															
DH002-009-1.1	49		.01	.32	09	.169	.8	.98	.1312	.57	009	26	114	10	56
DH002-009-2.1	26	35	.49	.09	39	.174	.3	.91	.1400	.05	036	22	227	18	58
DH002-009-3.1_core	23	66	.53	.06	49	.536	.9	.90	.2124	.42	**766**	**19**	**924**	**7**	**7**
DH002-009-3.2	13	4	.05	.13	03	.384	.8	.85	.1790	.49	093	14	644	8	24
DH002-009-4.1	51	49	.44	.03	50	.496	.4	.91	.2043	.66	596	31	861	11	11
DH002-009-5.1	47	2	.26	.00	03	.485	.8	.90	.1990	.42	549	18	818	7	12
DH002-009-7.1	80	72	.47	-	68	.516	.8	.92	.2106	.32	683	16	910	5	10
DH002-009-8.1_core	21	18	.55	-	08	.568	.9	.87	.2153	.50	**898**	**21**	**946**	**8**	**2**
DH002-009-9.1	60	0	.10	.20	01	.155	.3	.88	.0990	.68	31	11	606	13	45
DH002-009-10.1	00	0	.52	-	5	.641	.2	.88	.2976	.64	192	30	458	10	10
DH002-009-11.1	78	7	.10	.23	39	.208	.6	.95	.1123	.52	216	17	837	9	37
DH002-009-12.1	68	36	.96	.46	3	.206	.1	.96	.1594	.63	206	23	450	11	56
DH002-009-13.1	16	5	.31	.01	18	.434	.8	.89	.2030	.41	325	15	851	7	22
DH002-009-14.1	29	5	.16	-	7	.239	.2	.97	.1607	.86	379	40	463	15	49
DH002-009-14.2	057	5	.01	.19	8	.108	.9	.85	.0875	.22	59	12	372	24	55
DH002-009-16.1	183	2	.05	.32	18	.116	.5	.94	.0819	.89	06	17	243	17	46
DH002-009-17.1	69	38	.61	.16	20	.246	.5	.96	.1796	.42	417	19	650	7	52
DH002-009-18.1	79	4	.07	.18	7	.116	.6	.96	.0810	.74	07	17	222	15	44
DH002-009-19.1	31	04	.34	.09	6	.178	.3	.92	.1474	.59	055	13	316	10	59
DH002-009-20.1	49	16	.48	.02	22	.568	.8	.91	.2164	.38	**899**	**20**	**954**	**6**	**2**
DH002-009-23.1	052	8	.07	.38	0	.099	.1	.90	.0721	.02	09	12	88	21	40
DH002-009-24.1	16	8	.10	.04	35	.220	.5	.97	.1506	.41	280	18	353	7	50

DH002-009-25.1	52	0	.09	.16	14	.156	.6	.96	.1337	.48	35	14	147	8	60
DH002-009-26.1	31		.01	.09	07	.134	.8	.98	.0894	.60	09	21	414	12	45
DH002-009-27.1	98	17	.24	.08	2	.214	.8	.96	.1558	.50	250	20	411	9	53
DH002-009-28.1	02	5	.03	.17	03	.199	.1	.91	.1414	.52	170	12	245	9	52
DH002-009-29.1	75		.01	.71	1	.095	.9	.77	.0698	.61	85	11	23	33	38
DH002-009-30.1_core	99	0	.26	.00	6	.560	.0	.80	.2172	.76	**866**	**24**	**960**	**12**	**4**
DH002-009-30.2	01	08	.14	.22	5	.124	.7	.95	.0860	.86	52	19	338	17	46
DH002-009-32.1	38	4	.12	.19	9	.138	.7	.97	.1062	.61	35	21	734	11	55
DH002-009-33.1	54		.01	.75	7	.091	.8	.66	.0679	.03	64	10	65	42	36
DH002-009-35.1_core	8	4	.57	-	0	.599	.2	.90	.2204	.59	**024**	**29**	**983**	**10**	**-2**
DH002-009-36.1	34	65	.51	.01	49	.519	.1	.99	.2136	.33	693	46	933	5	10
DH002-009-37.1	76	00	.37	.03	34	.565	.4	.97	.2156	.35	**888**	**33**	**948**	**6**	**3**
DH002-009-39.1	59	5	.09	.13	2	.144	.4	.88	.1143	.26	70	19	869	23	57

Table 4: U-PB detrital ages from garnet-biotite paragneiss and biotite paragneiss.

Ar-Ar Ages

The samples were loaded into a 21-pit Aluminium disk along with the neutron fluence monitor Fish Canyon Sanidine (age 28.201 ± 0.046 Ma), following the geometry illustrated in Vasconcelos et al. (2002). The irradiation disks were closed with aluminium covers, wrapped in aluminium foil and vacuum heat sealed into quartz vials. All samples were irradiated for 14 hours over the period from 8 June 2016 to 10 June 2016 in the Cadmium-lined B-1 CLICIT facility, a TRIGA-type reactor, Oregon State University, USA.

The mass spectrometer sensitivity was calculated based on the analysis of an air pipette (1.634 x 10^{-13} moles ^{40}Ar) on the Faraday detector (4.257 mV) equipped with a 1 x 10^{11} Ohms resistor, yielding a Faraday sensitivity of 3.84 x 10^{-9} moles/nA. The current multiplier sensitivity measured on a Balzers 217 Electron Multiplier, operated with a gain of ~145,000 is ~4.5 x 10^{-14} moles/nA.

Incremental heating plateau ages are according to the definition of Fleck (1977): “a sequence of two or more steps corresponding to a least 50% of the total ^{39}Ar released, the age values of which are within 2σ from the mean value calculated by weighting with inverse variance”. Plateau age errors are reported at the 95% confidence level (2σ), and include the errors in the irradiation correction factors and the error in J, but do not include the uncertainty in the potassium decay constants.

Results of Geochonological Data

Detrital Zircon U-PB

There is one dominant U-Pb zircon population (one main age peak) with an age of 2039 Ma (Figure B). Most of the grains appear round to subrounded.

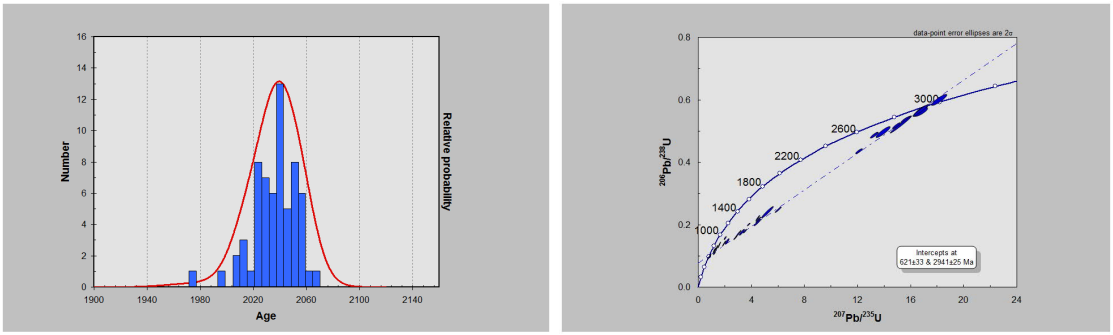

(i) (ii)

Figure B – Histogram and concordia diagram for Pb206/U238 ages of detrital zircon grains extracted from garnet-biotite paragneiss (DH1-003) and garnet-biotite paragneiss (DH1-009) from the Riacho do Pontal Belt.

Several grains from sample DH002-009 have metamictic zones. Overall, 35 spots were measured. Only 6 spots show concordancy <10%, and usually, those spots are related to zircon core measurements. The concordant analyses show an age group of ca. 2940 Ma. All the other spot measurements suggest that the grains had undergone either significant post- or predepositional modification. In the Tera-Wasserburg diagram, the upper intercept age is 2941 +/- 25 Ma. The lower intercept, which could represent metamorphic overgrowth or Pb-loss, is set at 621 +/- 25 Ma.

Detrital zircon data from the garnet-biotite paragneiss and biotite paragneiss of the Riacho do Pontal Belt indicated an age spectrum between 2945 Ma, 2039 Ma and 634 Ma

with maximum age of protolith deposition of approximately 621 Ma (Figure C). This age can be interpreted as a portion of the Pernambuco-Alagoas block, which has Ediacaran-Cryogenian ages of approximately 630-570 Ma (OLIVEIRA et al., 2014; SILVA FILHO et al., 2014; LIMA et al., 2018).

APPENDIX I B : ^{A40}Ar-^{39}Ar Ages

Plateau age errors are reported at the 95% confidence level (2σ) and include the errors in the irradiation correction factors and the error in J, but they do not include the uncertainty in the potassium decay constants. Most of the mineralizations were dated in biotite and amphibole. The PCB-R002 sample represents biotite amphibole mylonite, associated with RIA4 copper mineralization.

Ar dates in biotite held at the University of Queensland, Australia provided one plateau set in the range of 609 Ma (Figure C). The results show that the main hydrothermal event related to IOCG deposits and occurrences at the Riacho do Pontal belt has a Neoproterozoic age.

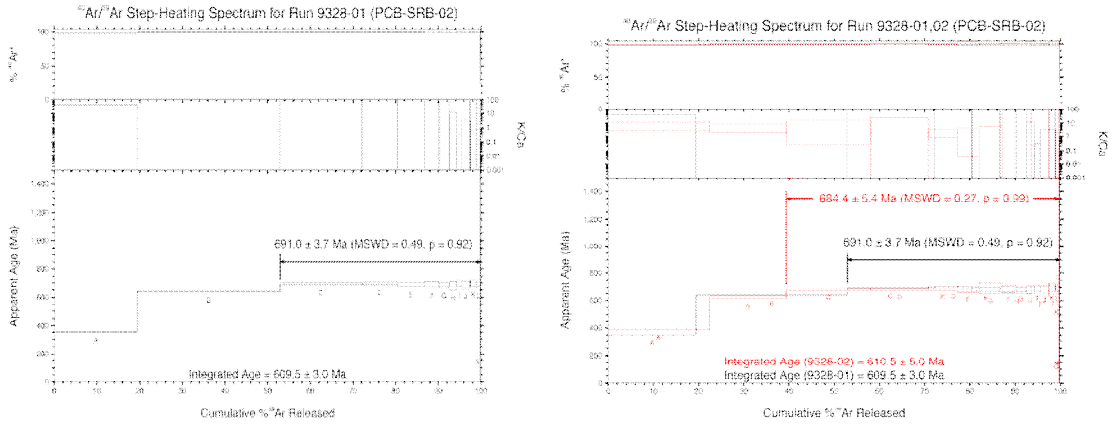

Figure C: Spectrum of apparent ^{40}Ar-^{39}Ar ages for sample PCB-SBH-02.

Tabulated Data ^{40}Ar-^{39}Ar

^{0}Ar-^{39}Ar numerical data. Isotope ratios are corrected for electron multiplier baseline, background, discrimination, interfering isotopes generated during neutron irradiation, and post-irradiation decay of ^{39}Ar and ^{37}Ar. Errors in this table are 1σ. The heating time for all analyses was ~45 seconds, not including the laser ramp-up time. Abbreviations used are: % Rad., % radiogenic argon; Discr. discrimination. The error in the J factor is not included in the tabulated error in the age in Appendix A, but is included in all plateau, age probability, and isochron ages throughout the text. The mass spectrometer gain was calculated based on the analysis of an air pipette (1.634 x 10^{-13} moles ^{40}Ar) on the Faraday detector (4.257 mV) equipped with a 1 x 10^{11} Ohms resistor, yielding a Faraday sensitivity of 3.84 x 10^{-9} moles/nA. The current multiplier sensitivity measured on a Balzers 217 Electron Multiplier, operated with a gain of ~145,000 is ~4.5 x 10^{-14} moles/nA. The historical irradiation correction factors for the CLICIT facility, TRIGA reactor, Oregon State University, USA are: (2.64 ± 0.02) x 10^{-4} for (^{36}Ar/^{37}Ar)Ca, (7.04 ±0.06) x 10^{-4} for (^{39}Ar/^{37}Ar)Ca, and (8 ± 3) x 10^{-4} for (^{40}Ar/^{39}Ar)K (values determined at the Berkeley Geochronology Center).

Tabulated Data

^{40}Ar-^{39}Ar numerical data. Isotope ratios are corrected for electron multiplier baseline, background, discrimination, interfering isotopes generated during neutron irradiation, and post-irradiation decay of ^{39}Ar and ^{37}Ar. Errors in this table are 1σ. The heating time for all analyses was ~45 seconds, not including the laser ramp-up time. Abbreviations used are: % Rad., % radiogenic argon; Discr., discrimination. The error in the J factor is not included in the tabulated error in the age in Appendix A, but is included in all plateau, age probability, and isochron ages throughout the text. The mass spectrometer gain was calculated based on the analysis of an air pipette (1.634×10^{-13} moles ^{40}Ar) on the Faraday detector (4.257 mV) equipped with a 1×10^{11} Ohms resistor, yielding a Faraday sensitivity of 3.84×10^{-9} moles/nA. The current multiplier sensitivity measured on a Balzers 217 Electron Multiplier, operated with a gain of ~145,000 is $\sim 4.5 \times 10^{-14}$ moles/nA. The historical irradiation correction factors for the CLICIT facility, TRIGA reactor, Oregon State University, USA are: $(2.64 \pm 0.02) \times 10^{-4}$ for $(^{36}Ar/^{37}Ar)Ca$, $(7.04 \pm 0.06) \times 10^{-4}$ for $(^{39}Ar/^{37}Ar)Ca$, and $(8 \pm 3) \times 10^{-4}$ for $(^{40}Ar/^{39}Ar)K$ (values determined at the Berkeley Geochronology Center).

		36Ar/	36/39	37Ar/	37/39	38Ar/	38/39	40Ar/	40/39	40Ar*/	40*/39		%Ar40*	Age	Age Ma	Ar39	Ar40		J	Run	Run	Ar40
Run ID	Sample	39Ar	Error 1s	39Ar	Error 1s	39Ar	Error 1s	39Ar	Error 1s	39Ar	Error 1s	%Ar40*	Error 1s	Ma	Error 1s	Moles	Moles	J	Error 1s	Date	Hour	Disc
9327-01A	PCB-SRB-01	0.2105251	0.412125	-22.74762	41.37804	0.0141903	0.1746761	-16.10228	29.17716	-79.45747	147.5363	501.1858	411.5399	-622.3765	1380.007	-1.34E-17	2.16E-16	0.003672	7.00E-06	11/7/2016	19.31	1.0022
9327-01B	PCB-SRB-01	0.1608713	0.0616852	7.468675	3.134157	0.0669914	0.0434866	5.633932	2.795376	-42.03822	17.25409	-742.4156	354.2566	-302.4837	135.1657	5.29E-17	2.98E-16	0.003672	7.00E-06	11/7/2016	21.60	1.0022
9327-01C	PCB-SRB-01	0.1048241	0.0283938	3.498598	1.410659	0.0275231	0.0216437	10.52926	2.501729	-20.54946	7.411521	-194.7082	66.23236	-141.5414	53.10536	9.44E-17	9.94E-16	0.003672	7.00E-06	11/7/2016	22.69	1.0022
9327-01D	PCB-SRB-01	0.074524	0.0250179	4.488755	1.396665	0.0464047	0.0246068	15.3983	3.360426	-6.52634	6.592981	-42.25423	42.21832	-43.76068	44.74805	1.05E-16	1.62E-15	0.003672	7.00E-06	11/7/2016	23.71	1.0022
9327-01E	PCB-SRB-01	0.0623262	0.0157793	2.158524	0.7517007	0.0595251	0.0163249	13.9523	2.373263	-4.494419	4.278762	-32.16655	30.48304	-30.02202	28.8206	1.59E-16	2.21E-15	0.003672	7.00E-06	11/8/2016	0.77	1.0022
9327-01F	PCB-SRB-01	0.0944117	0.0174658	0.9341482	0.7573959	0.0534915	0.0141231	13.88325	2.28387	-14.24048	4.408606	-102.5128	30.66943	-96.89304	30.81656	1.83E-16	2.54E-15	0.003672	7.00E-06	11/8/2016	1.84	1.0022
9327-01G	PCB-SRB-01	0.089788	0.014956	2.037618	0.6097232	0.0589976	0.0143094	9.729901	1.896471	-16.94277	3.926545	-173.9001	42.66913	-115.8819	27.73732	2.09E-16	2.03E-15	0.003672	7.00E-06	11/8/2016	3.04	1.0022
9327-01H	PCB-SRB-01	0.0687603	0.0121497	1.800142	0.5521781	0.0619263	0.0129666	5.989545	1.597031	-14.41677	3.518169	-240.4316	77.02047	-98.1258	24.60913	2.41E-16	1.45E-15	0.003672	7.00E-06	11/8/2016	4.13	1.0022
9327-01I	PCB-SRB-01	0.0678328	0.0130046	0.797486	0.5020184	0.0381985	0.0126568	-50.00168	6.81142	-70.23095	9.850831	140.3776	7.833531	-538.0753	87.93489	-2.42E-16	1.21E-14	0.003672	7.00E-06	11/8/2016	5.21	1.0022
9327-01J	PCB-SRB-01	0.0841395	0.0311133	2.371778	1.226218	0.0642958	0.0303178	-726.1737	208.2333	-752.3428	216.1688	103.4338	1.098144	NaN	-812.4493	-1.16E-16	8.43E-14	0.003672	7.00E-06	11/8/2016	6.31	1.0022
9327-01K	PCB-SRB-01	-0.0574346	0.0072565	-1.00706	0.2856278	-0.002818	0.0068745	902.6309	76.70767	919.0604	78.06553	101.8911	0.2610204	2662.563	118.2116	4.33E-16	3.91E-13	0.003672	7.00E-06	11/8/2016	7.33	1.0022
9327-01L	PCB-SRB-01	-0.0300996	0.003127	-0.1366041	0.1473722	0.0005188	0.0039704	761.6096	35.30033	770.5114	35.71871	101.1785	0.1879567	2422.31	61.79199	8.55E-16	6.51E-13	0.003672	7.00E-06	11/8/2016	8.41	1.0022
9327-01M	PCB-SRB-01	-0.002374	0.0006524	-0.0709366	0.0297671	0.0115206	0.0008855	573.8304	11.36722	574.5046	11.3816	100.1226	0.080195	2046.704	24.24708	4.68E-15	2.68E-12	0.003672	7.00E-06	11/8/2016	9.47	1.0022
9327-01N	PCB-SRB-01	0.0008078	0.0002849	0.0093263	0.0069628	0.0134874	0.0003297	562.9315	2.862629	562.6938	2.862873	99.9573	0.0565288	2021.365	6.185258	1.62E-14	9.11E-12	0.003672	7.00E-06	11/8/2016	10.56	1.0022
9327-01O	PCB-SRB-01	0.0025537	0.0002441	0.0062909	0.0030283	0.014107	0.0003269	566.4507	2.414479	565.6904	2.412996	99.86551	0.0842595	2027.828	5.194653	4.41E-14	2.50E-11	0.003672	7.00E-06	11/8/2016	11.91	1.0022
9327-01P	PCB-SRB-01	0.0023494	0.0003262	0.0115687	0.0059518	0.0145672	0.0004594	568.1769	3.293659	567.4801	3.291719	99.87673	0.196347	2031.677	7.07125	2.09E-14	1.19E-11	0.003672	7.00E-06	11/8/2016	14.03	1.0022
9327-01Q	PCB-SRB-01	0.0037084	0.0004116	0.0349968	0.0094354	0.0149677	0.0005786	558.1629	3.619737	557.0712	3.615407	99.80215	0.0494446	2009.177	7.864065	1.32E-14	7.39E-12	0.003672	7.00E-06	11/8/2016	15.02	1.0022

		36Ar/	36/39	37Ar/	37/39	38Ar/	38/39	40Ar/	40/39	40Ar*/	40*/39		%Ar40*	Age	Age Ma	Ar39	Ar40		J	Run	Run	Ar40
Run ID	Sample	39Ar	Error 1s	39Ar	Error 1s	39Ar	Error 1s	39Ar	Error 1s	39Ar	Error 1s	%Ar40*	Error 1s	Ma	Error 1s	Moles	Moles	J	Error 1s	Date	Hour	Disc
9327-01R	PCB-SRB-01	-0.0002479	0.0004967	0.0174488	0.0156703	0.013757	0.0007508	562.8777	5.037334	562.9591	5.040283	100.0134	0.1911275	2021.938	10.88611	7.71E-15	4.34E-12	0.003672	7.00E-06	11/8/2016	16.09	1.0024
9327-01S	PCB-SRB-01	-0.0049452	0.0012583	0.038955	0.0483555	0.0115694	0.0018856	610.5634	24.63952	612.0585	24.70323	100.2423	0.1781607	2124.984	50.39241	2.33E-15	1.43E-12	0.003672	7.00E-06	11/8/2016	17.07	1.0024
9327-01U	PCB-SRB-01	-0.0092259	0.0016233	-0.257718	0.0685683	0.0061739	0.002114	555.6752	18.73864	558.3092	18.82991	100.4921	0.1521998	2011.867	40.89689	1.78E-15	9.92E-13	0.003672	7.00E-06	11/8/2016	18.15	1.0024
9327-01V	PCB-SRB-01	-0.0191209	0.0029669	-0.3037036	0.1287886	0.0082771	0.0035248	583.4454	29.57094	589.0063	29.85787	100.9744	0.2411094	2077.336	62.53752	9.85E-16	5.75E-13	0.003672	7.00E-06	11/8/2016	19.18	1.0024
9327-01W	PCB-SRB-01	-0.0247335	0.0034913	-0.192276	0.1788914	0.0010957	0.0044004	580.8051	37.58533	588.0951	38.06286	101.2688	0.2894975	2075.427	79.80734	7.58E-16	4.40E-13	0.003672	7.00E-06	11/8/2016	20.15	1.0024
9327-01X	PCB-SRB-01	-0.0175063	0.0032009	-0.3987346	0.1169667	0.0059619	0.0037159	598.2899	31.42441	603.3186	31.69269	100.8684	0.2528901	2107.067	65.29559	9.57E-16	5.72E-13	0.003672	7.00E-06	11/8/2016	21.16	1.0024
9327-01Z	PCB-SRB-01	0.0006728	0.0011345	-0.0608292	0.0539978	0.0109853	0.0012545	551.3199	9.734274	551.0902	9.73582	99.96269	0.1300893	1996.12	21.33072	2.16E-15	1.19E-12	0.003672	7.00E-06	11/9/2016	7.32	1.0024
9327-01AA	PCB-SRB-01	0.0030419	0.0004462	0.0364923	0.0141645	0.0151169	0.0005713	563.3773	3.485077	562.4855	3.482699	99.83933	0.0571036	2020.915	7.526274	7.74E-15	4.36E-12	0.003672	7.00E-06	11/9/2016	8.36	1.0024
9327-01AB	PCB-SRB-01	0.0003069	0.0011144	-0.0187217	0.0282076	0.0138726	0.0007539	552.7478	5.74058	552.6468	5.749162	99.98319	0.0996819	1999.527	12.57238	4.30E-15	2.38E-12	0.003672	7.00E-06	11/9/2016	9.35	1.0024
9327-01AC	PCB-SRB-01	0.0099923	0.0042632	0.3366604	0.1909855	0.0172211	0.0047207	551.2732	27.10949	548.4427	27.00703	99.46357	0.4337324	1990.31	59.36199	6.19E-16	3.41E-13	0.003672	7.00E-06	11/9/2016	10.33	1.0024
9327-01AD	PCB-SRB-01	0.0641514	0.0208598	1.613089	0.8823215	0.0316582	0.0172334	573.2742	111.5303	554.8632	108.1905	96.68071	1.302211	2004.368	235.9592	1.43E-16	8.20E-14	0.003672	7.00E-06	11/9/2016	11.37	1.0024
9327-02B	PCB-SRB-01	-0.0003693	0.0020643	0.1160319	0.1231478	0.0094669	0.0022244	548.2029	12.51679	548.3649	12.53681	100.0217	0.1423055	1990.139	27.55876	9.63E-16	5.28E-13	0.003672	7.00E-06	11/9/2016	18.33	1.0024
9327-02C	PCB-SRB-01	-0.0005989	0.0032534	-0.3935285	0.1805664	0.0165253	0.0032194	549.3553	30.70333	549.354	30.7105	100.0271	0.2174949	1992.312	67.42742	6.62E-16	3.64E-13	0.003672	7.00E-06	11/9/2016	19.33	1.0024
9327-02D	PCB-SRB-01	0.0047616	0.0035398	0.2247652	0.2018408	0.0112779	0.0033389	548.8505	17.52879	547.5301	17.52167	99.74409	0.2315611	1988.303	38.55585	5.88E-16	3.23E-13	0.003672	7.00E-06	11/9/2016	20.32	1.0024
9327-02E	PCB-SRB-01	0.0052137	0.0041661	0.3306437	0.2049276	0.0219502	0.0035196	548.0327	20.6229	546.6263	20.61263	99.72074	0.2555368	1986.313	45.40745	5.58E-16	3.06E-13	0.003672	7.00E-06	11/9/2016	21.32	1.0024
9327-02F	PCB-SRB-01	-0.0011451	0.003582	-0.2326804	0.2002347	0.0101669	0.0036776	556.0726	18.8561	556.3061	18.89154	100.0582	0.2175413	2007.512	41.12994	5.28E-16	2.93E-13	0.003672	7.00E-06	11/9/2016	22.44	1.0024
9327-02G	PCB-SRB-01	0.0017788	0.0043067	0.0336422	0.2036459	0.0115783	0.004089	541.3082	24.29227	540.7913	24.30398	99.90235	0.2649743	1973.413	53.92331	4.99E-16	2.70E-13	0.003672	7.00E-06	11/9/2016	23.45	1.0024
9327-02H	PCB-SRB-01	0.0071997	0.0040992	0.034305	0.2640054	0.0089347	0.0044452	541.5842	21.93779	539.4488	21.88652	99.60351	0.2715358	1970.432	48.64001	4.67E-16	2.53E-13	0.003672	7.00E-06	11/10/2016	0.49	1.0024
9327-02I	PCB-SRB-01	0.0129706	0.0053721	0.4720563	0.2522209	0.0134996	0.0050783	542.0842	25.2416	538.4225	25.13062	99.29228	0.3343159	1968.15	55.92029	4.20E-16	2.28E-13	0.003672	7.00E-06	11/10/2016	1.65	1.0024
9327-02J	PCB-SRB-01	-0.0017824	0.0053863	-0.240216	0.3005719	0.0114532	0.0051814	562.8217	25.77107	563.241	25.8365	100.0913	0.3168458	2022.547	55.78338	3.80E-16	2.14E-13	0.003672	7.00E-06	11/10/2016	2.74	1.0024
9327-02K	PCB-SRB-01	-0.0042226	0.0051808	0.5339919	0.2788282	0.014378	0.0058182	524.4462	23.08003	525.9414	23.20623	100.2483	0.3401332	1940.161	52.44554	3.95E-16	2.07E-13	0.003672	7.00E-06	11/10/2016	3.76	1.0024
9327-02L	PCB-SRB-01	0.0133378	0.0058443	0.4170134	0.331663	0.0130254	0.0057238	540.5805	26.6986	536.784	26.57628	99.26925	0.3637474	1964.5	59.2569	3.72E-16	2.01E-13	0.003672	7.00E-06	11/10/2016	4.76	1.0024
9327-02M	PCB-SRB-01	0.0049495	0.0057735	0.1936727	0.3152104	0.0174954	0.0061658	541.597	24.73588	540.2059	24.73635	99.72997	0.3509937	1972.114	54.92215	3.62E-16	1.96E-13	0.003672	7.00E-06	11/10/2016	5.90	1.0024
9327-02N	PCB-SRB-01	-0.009694	0.006151	0.8030815	0.3086125	0.0019519	0.0060269	548.0871	26.60173	551.3472	26.83763	100.5392	0.3745297	1996.683	58.78163	3.44E-16	1.89E-13	0.003672	7.00E-06	11/10/2016	6.94	1.0024
9327-02O	PCB-SRB-01	0.005169	0.005321	1.131468	0.2768986	0.0118803	0.0061098	579.1049	27.38132	578.0994	27.40182	99.74848	0.3241756	2054.346	58.12939	3.88E-16	2.25E-13	0.003672	7.00E-06	11/10/2016	7.97	1.0024
9327-02P	PCB-SRB-01	0.0026022	0.0055494	0.3827512	0.3513877	0.0177708	0.006665	552.9221	29.01514	552.3202	29.03914	99.86488	0.3392768	1998.813	63.52849	3.25E-16	1.80E-13	0.003672	7.00E-06	11/10/2016	9.02	1.0024
9327-02Q	PCB-SRB-01	-0.0032564	0.0058714	0.5451961	0.3581273	0.0170997	0.0055351	574.2315	27.26392	575.4619	27.38933	100.1767	0.3427947	2048.742	58.28365	3.59E-16	2.06E-13	0.003672	7.00E-06	11/10/2016	10.12	1.0024
9327-02R	PCB-SRB-01	0.0046151	0.0056111	0.1062398	0.3249447	0.0034162	0.0048406	525.8508	22.47762	524.5177	22.48539	99.73934	0.3466563	1936.941	50.90725	3.80E-16	2.00E-13	0.003672	7.00E-06	11/10/2016	11.18	1.0024
9327-02S	PCB-SRB-01	-0.0058327	0.0080167	1.028063	0.447318	-0.0002245	0.0075927	556.6614	35.57939	558.8767	35.82696	100.3268	0.4709662	2013.1	77.75984	2.48E-16	1.38E-13	0.003672	7.00E-06	11/10/2016	12.20	1.0024
9327-02T	PCB-SRB-01	0.0036191	0.0093918	-0.4593369	0.4998698	-0.0053184	0.0089224	558.4999	42.31444	557.2047	42.29671	99.79991	0.5410064	2009.467	91.98702	2.11E-16	1.18E-13	0.003672	7.00E-06	11/10/2016	13.24	1.0024
9327-02U	PCB-SRB-01	-0.003056	0.0105133	0.2603661	0.5903992	0.0197258	0.0093987	492.7596	47.66427	493.7807	47.87537	100.1894	0.6897294	1865.974	112.7392	2.09E-16	1.03E-13	0.003672	7.00E-06	11/10/2016	14.28	1.0024
9327-02V	PCB-SRB-01	0.027281	0.0120878	-0.0024033	0.6295092	-0.0138544	0.010144	542.4953	48.81351	534.3453	48.21142	98.49802	0.7014153	1959.055	107.8216	1.67E-16	9.06E-14	0.003672	7.00E-06	11/10/2016	15.38	1.0024
9327-02W	PCB-SRB-01	0.0116891	0.0112908	1.459402	0.6542124	0.0047748	0.0112088	479.1279	43.65463	476.2285	43.56845	99.2948	1.596278	1824.16	105.0028	1.78E-16	8.52E-14	0.003672	7.00E-06	11/10/2016	16.44	1.0024
9327-02X	PCB-SRB-01	0.0042201	0.0182388	2.376444	1.075956	-0.0018142	0.0162847	552.3613	77.35128	552.1882	77.64768	99.80465	1.058631	1998.524	169.8958	1.07E-16	5.91E-14	0.003672	7.00E-06	11/10/2016	17.58	1.0024
9327-02Y	PCB-SRB-01	-0.0410925	0.030503	2.930374	1.804599	-0.0347345	0.0255227	695.1622	156.8138	709.0868	160.5181	101.7967	1.283255	2312.79	295.07	6.79E-17	4.72E-14	0.003672	7.00E-06	11/10/2016	18.63	1.0024
9327-02Z	PCB-SRB-01	-0.0274756	0.0235795	3.981207	1.399424	-0.0270042	0.0202919	548.0062	99.1437	558.0459	101.4752	101.5521	1.292559	2011.295	220.465	8.76E-17	4.80E-14	0.003672	7.00E-06	11/10/2016	19.71	1.0024
9327-02AA	PCB-SRB-01	-0.0098015	0.0217938	3.244197	1.494397	-0.0214814	0.0222109	540.4203	90.33409	544.813	91.50681	100.587	1.247784	1982.314	202.0272	8.52E-17	4.60E-14	0.003672	7.00E-06	11/10/2016	20.78	1.0024
9327-02AB	PCB-SRB-01	0.0064245	0.024639	0.9892105	1.62571	-0.0352701	0.0285774	609.0192	142.191	607.5869	142.1465	99.69676	1.272998	2115.84	291.44	6.53E-17	3.98E-14	0.003672	7.00E-06	11/10/2016	21.83	1.0024
9327-02AC	PCB-SRB-01	0.0094188	0.0048762	0.7082153	0.2492273	0.0075589	0.0047517	563.3359	20.31363	560.8511	20.28676	99.51035	0.2860597	2017.38	43.92662	4.60E-16	2.59E-13	0.003672	7.00E-06	11/10/2016	22.90	1.0024
9327-02AD	PCB-SRB-01	0.0054581	0.0052409	0.1829344	0.2852805	0.0043255	0.0060034	581.6634	28.0873	580.1195	28.06042	99.72211	0.3007856	2058.626	59.38545	3.22E-16	1.87E-13	0.003672	7.00E-06	11/10/2016	23.99	1.0024
9327-02AE	PCB-SRB-01	2.717267	48.82171	-615.767	11050.12	3.510723	63.03421	-16316.27	292776.9	-12048.1	151663.1	105.26	4.63673	NaN	-23235.15	-7.79E-19	1.27E-14	0.003672	7.00E-06	11/11/2016	1.09	1.0024
9327-02AF	PCB-SRB-01	-0.0911012	0.209148	16.23204	22.32316	-0.5545581	0.6883993	662.8392	801.6741	699.0725	856.7926	104.2836	8.120768	2294.287	1591.223	1.12E-17	7.40E-15	0.003672	7.00E-06	11/11/2016	2.14	1.0024
9327-02AG	PCB-SRB-01	0.2474792	0.2938659	43.11938	45.70848	-0.1952659	0.2469588	475.4363	495.1747	417.2655	450.0601	85.14992	8.958276	1676.147	1177.418	1.34E-17	6.36E-15	0.003672	7.00E-06	11/11/2016	3.16	1.0024
9327-02AH	PCB-SRB-01	0.2878979	1.177733	59.04496	221.4369	-0.85262	3.209107	1412.906	5245.189	1388.026	5374.336	94.23101	10.64663	3261.355	5839.537	3.62E-18	5.12E-15	0.003672	7.00E-06	11/11/2016	4.22	1.0024
9327-02AI	PCB-SRB-01	-0.0777085	0.0409159	3.133145	2.178282	-0.0420644	0.035665	532.2872	135.4366	556.9294	142.42	104.4031	2.08398	2008.868	309.8384	5.39E-17	2.87E-14	0.003672	7.00E-06	11/11/2016	5.36	1.0024
9327-02AJ	PCB-SRB-01	0.5711003	8.257371	455.6555	6401.972	1.11221	15.76116	3902.774	54825.35	5498.601	112746	96.52938	15.17742	5508.876	35246.04	9.15E-19	3.57E-15	0.003672	7.00E-06	11/11/2016	6.58	1.0024
9328-01A	PCB-SRB-02	0.004175	0.0001912	-0.0096746	0.0084643	0.0134469	0.0002253	59.42796	0.2226425	58.17956	0.226581	97.90129	0.1497596	349.3059	1.236782	1.42E-14	8.44E-13	0.003672	7.00E-06	11/11/2016	20.79	1.0024
9328-01B	PCB-SRB-02	0.0033326	0.0001262	-0.0092589	0.0042155	0.0135146	0.0001768	115.9989	0.2922443	115.0017	0.293536	99.14168	0.0739309	635.5146	1.3672	2.43E-14	2.82E-12	0.003672	7.00E-06	11/11/2016	21.79	1.0024

		36Ar/	36/39	37Ar/	37/39	38Ar/	38/39	40Ar/	40/39	40Ar*/	40*/39		%Ar40*	Age	Age Ma	Ar39	Ar40		J	Run	Run	Ar40
Run ID	Sample	39Ar	Error 1s	39Ar	Error 1s	39Ar	Error 1s	39Ar	Error 1s	39Ar	Error 1s	%Ar40*	Error 1s	Ma	Error 1s	Moles	Moles	J	Error 1s	Date	Hour	Disc
9328-01C	PCB-SRB-02	0.0033558	0.0002085	0.0117834	0.0079353	0.0130823	0.0002274	128.2741	0.4531312	127.2733	0.454878	99.21963	0.0870658	691.7848	2.053618	1.40E-14	1.80E-12	0.003672	7.00E-06	11/11/2016	22.75	1.0024
9328-01D	PCB-SRB-02	0.0037539	0.0004013	-0.0053853	0.0177423	0.014601	0.0004076	128.6798	0.6079908	127.5575	0.6153814	99.12882	0.1440877	693.0675	2.776262	6.05E-15	7.78E-13	0.003672	7.00E-06	11/11/2016	23.71	1.0024
9328-01E	PCB-SRB-02	0.0035816	0.0004551	0.0102089	0.02424	0.0148887	0.0005101	126.7475	1.38548	125.6792	1.380891	99.15708	0.1647062	684.5735	6.259218	4.62E-15	5.86E-13	0.003672	7.00E-06	11/12/2016	0.72	1.0024
9328-01F	PCB-SRB-02	0.0042423	0.0023448	0.0012224	0.0469636	0.0138767	0.0009797	126.829	2.270849	125.5619	2.354855	99.00147	0.5636296	684.0417	10.67709	2.49E-15	3.16E-13	0.003672	7.00E-06	11/12/2016	1.68	1.0024
9328-01G	PCB-SRB-02	-0.000387	0.0022904	0.0153103	0.0720516	0.0125784	0.0014322	125.1958	1.476831	125.3131	1.628785	100.0932	0.5589586	682.9133	7.389656	1.70E-15	2.12E-13	0.003672	7.00E-06	11/12/2016	2.69	1.0024
9328-01H	PCB-SRB-02	-0.0040191	0.0041906	-0.0725726	0.1011243	0.0135957	0.0016987	122.8812	2.768633	124.0688	3.062186	100.9721	1.039842	677.2593	13.93648	1.26E-15	1.55E-13	0.003672	7.00E-06	11/12/2016	3.76	1.0024
9328-01I	PCB-SRB-02	0.0082229	0.0021975	-0.2105144	0.1182032	0.0165508	0.0023591	130.1511	2.130254	127.6608	2.190303	98.10148	0.5413639	693.5335	9.87889	9.61E-16	1.25E-13	0.003672	7.00E-06	11/12/2016	4.78	1.0024
9328-01J	PCB-SRB-02	0.0025825	0.002427	-0.1054249	0.0930855	0.0170006	0.0017124	126.078	2.694345	125.2893	2.773836	99.38233	0.6074727	682.8056	12.58541	1.38E-15	1.74E-13	0.003672	7.00E-06	11/12/2016	5.82	1.0024
9328-01K	PCB-SRB-02	0.005751	0.0020607	-0.0348878	0.1343966	0.0168057	0.002027	129.1383	2.330442	127.4151	2.380626	98.66856	0.5187214	692.4248	10.7439	9.56E-16	1.24E-13	0.003672	7.00E-06	11/12/2016	6.97	1.0024
9328-01L	PCB-SRB-02	0.0022689	0.0026388	-0.0164206	0.1558559	0.0153505	0.0027007	127.8441	2.443243	127.1634	2.555108	99.46933	0.6759741	691.2889	11.53861	7.65E-16	9.78E-14	0.003672	7.00E-06	11/12/2016	7.96	1.0024
9328-01M	PCB-SRB-02	0.1360764	0.165965	-7.005848	9.042715	0.2671534	0.2436345	357.8029	289.8432	315.1335	256.7311	88.50121	10.52025	1386.97	788.4093	1.57E-17	5.62E-15	0.003672	7.00E-06	11/12/2016	9.05	1.0024
9328-01N	PCB-SRB-02	0.1881372	0.0941603	-1.747387	3.857656	0.1555615	0.0870979	168.8188	61.3552	112.3882	45.47548	66.65395	12.48713	623.3	213.2497	3.03E-17	5.12E-15	0.003672	7.00E-06	11/12/2016	10.11	1.0024
9328-01O	PCB-SRB-02	0.3301042	0.4123071	-6.441674	14.62134	-0.0022747	0.1881102	287.9841	311.7416	188.0885	211.8306	65.60305	21.56429	947.3564	830.0228	9.74E-18	2.80E-15	0.003672	7.00E-06	11/12/2016	11.21	1.0024
9328-02A	PCB-SRB-02	0.0036153	0.0003643	0.0728819	0.0233291	0.0135234	0.0004414	66.27938	0.3868477	65.20811	0.396494	98.37995	0.1896833	387.2687	2.119178	5.73E-15	3.80E-13	0.003672	7.00E-06	11/12/2016	16.40	1.0024
9328-02B	PCB-SRB-02	0.0023676	0.0004339	0.09878	0.0309216	0.0134267	0.0006216	112.4076	0.7785844	111.7152	0.7850034	99.37794	0.1540147	620.1414	3.687594	4.29E-15	4.82E-13	0.003672	7.00E-06	11/12/2016	17.34	1.0024
9328-02C	PCB-SRB-02	0.003113	0.00042	0.0575342	0.0278195	0.0126579	0.0005708	126.3171	0.8242068	125.3962	0.8283438	99.26768	0.1527705	683.2906	3.757338	4.73E-15	5.98E-13	0.003672	7.00E-06	11/12/2016	18.33	1.0024
9328-02D	PCB-SRB-02	0.0007377	0.0010163	0.0497088	0.0400966	0.012042	0.0008214	125.8026	0.8593282	125.5896	0.9101435	99.82791	0.2696695	684.1676	4.126372	3.26E-15	4.10E-13	0.003672	7.00E-06	11/12/2016	19.37	1.0024
9328-02E	PCB-SRB-02	0.0035075	0.0010476	0.2324047	0.0772775	0.0146559	0.0014091	128.84	1.813228	127.8305	1.826629	99.20117	0.2828413	694.2989	8.235118	1.62E-15	2.09E-13	0.003672	7.00E-06	11/12/2016	20.32	1.0024
9328-02F	PCB-SRB-02	0.0005796	0.0017634	0.2226278	0.1096603	0.0107015	0.0019338	126.2192	2.477553	126.0817	2.531567	99.87631	1.599053	686.3972	11.46334	1.21E-15	1.53E-13	0.003672	7.00E-06	11/12/2016	21.38	1.0024
9328-02G	PCB-SRB-02	0.0012235	0.002948	0.1905758	0.0975012	0.0137618	0.00187	126.4774	4.366661	126.1427	4.443874	99.72284	0.7197982	686.6734	20.11949	1.31E-15	1.66E-13	0.003672	7.00E-06	11/12/2016	22.47	1.0024
9328-02H	PCB-SRB-02	-0.003114	0.0018828	0.0175474	0.0728587	0.0131271	0.0015125	123.5718	3.235964	124.5037	3.308361	100.7536	0.4726288	679.2375	15.04036	1.62E-15	2.00E-13	0.003672	7.00E-06	11/12/2016	23.55	1.0024
9328-02I	PCB-SRB-02	0.0068474	0.0021006	-0.0181721	0.1205068	0.0142885	0.0023824	124.2164	4.35184	122.1684	4.325561	98.3531	0.5353015	668.5894	19.78113	9.69E-16	1.20E-13	0.003672	7.00E-06	11/13/2016	0.62	1.0024
9328-02J	PCB-SRB-02	0.0005583	0.0044864	0.390936	0.2981638	0.023173	0.0050742	125.1707	4.75615	125.068	4.939097	99.8916	1.122083	681.8013	22.42207	4.18E-16	5.23E-14	0.003672	7.00E-06	11/13/2016	1.63	1.0024
9328-02K	PCB-SRB-02	-0.0023146	0.0133667	0.8781036	0.7803311	0.0106693	0.0125547	123.2853	10.65241	124.1181	11.45037	100.6151	3.293489	677.4837	52.10593	1.59E-16	1.96E-14	0.003672	7.00E-06	11/13/2016	2.71	1.0024
9328-02L	PCB-SRB-02	-0.4711128	0.8500146	21.27629	39.67093	0.0861356	0.2941928	281.6226	488.2848	430.2507	760.4176	150.53	25.70496	1709.802	1952.587	7.47E-18	2.10E-15	0.003672	7.00E-06	11/13/2016	3.84	1.0024
9328-02M	PCB-SRB-02	-0.4853371	0.8732755	-32.3884	58.83497	0.4751354	0.8661909	274.1849	473.8864	407.5329	692.5625	151.9613	27.14975	1650.503	1837.774	6.96E-18	1.91E-15	0.003672	7.00E-06	11/13/2016	4.90	1.0024
9328-02N	PCB-SRB-02	-1.674346	8.496881	8.76692	70.4582	-0.6464955	3.364901	595.3362	3007.444	1102.547	5609.028	184.0758	41.69735	2920.985	7360.011	2.38E-18	1.42E-15	0.003672	7.00E-06	11/13/2016	5.94	1.0024
9328-02O	PCB-SRB-02	-0.0582478	0.0311403	0.1207886	2.219173	0.0030909	0.0331923	35.38371	6.810074	52.78721	13.31583	149.176	25.21928	319.6293	73.88935	5.83E-17	2.06E-15	0.003672	7.00E-06	11/13/2016	7.03	1.0024